TEXTURAL AND CHEMICAL RELATIONS AMONG SPINEL-SAPPHIRINE-GARNET-ORTHOPYROXENE, SALT HILL EMERY MINE, CORTLANDT COMPLEX, N.Y.

By

Amy Mechel Johnson

Thesis submitted to the faculty of

Virginia Polytechnic Institute and State University

in partial fulfillment of the requirements for the degree of

MASTER OF SCIENCE

in

Geological Sciences

_____
Robert J. Tracy, Chair

_____
James S. Beard

_____
Michael F. Hochella, Jr.

_____
Patty L. Kitchin

August, 1998
Blacksburg, Virginia

TEXTURAL AND CHEMICAL RELATIONS AMONG SPINEL-SAPPHIRINE-GARNET-ORTHOPYROXENE, SALT HILL EMERY MINE, CORTLANDT COMPLEX, N.Y.

By

Amy Mechel Johnson

Dr. Robert J. Tracy, Chairman

(ABSTRACT)

Very high temperature (>900 °C) contact metamorphism and metasomatism of aluminous schist xenoliths in the mafic to ultramafic Cortlandt Complex, New York, resulted in formation of bodies of unusual Fe- and Al-oxide-rich rock called emery. During contact heating, disequilibrium thermal decomposition of the protolith schists in one closely examined xenolith produced two end-member materials: a quartzo-feldspathic water-undersaturated melt which partitioned much of the silica and calcium and all of the alkalis of the original schist; and a highly aluminous fine-grained emery residuum which contained spinel, magnetite, ilmenohematite, sillimanite, and sporadically corundum. During cooling, melt within the xenoliths was injected as cm-scale veinlets into the silica-poor solid residuum. Local increase in silica activity resulted in progressive silication reactions of spinel-rich residuum to several silicates. A simple model of progressive silication would require that reactions should occur from lower to higher silica content of product silicates in stages, e.g., spinel sapphirine (Si/O=0.10), sapphirine garnet (0.25), garnet orthopyroxene (0.28), rather than directly from spinel to higher-silica minerals which would overstep intermediate reaction steps. However, observed reaction textures indicate the latter more complex behavior in which spinel may have reaction rims of, or occur as inclusions within, any of the three silicate minerals.

Statistical analysis of several samples has shown the mode to be the spinel-orthopyroxene reaction rim boundary although orthopyroxene is the highest-silica product mineral, based on Si/O ratio. Chi-square test results are significant and show that the

textural relations observed among spinel, sapphirine, garnet, and orthopyroxene are dependent. Increased silica activity therefore cannot be the only factor controlling the reaction sequence.

Microprobe data has been collected in an attempt to correlate mineral compositions with the different textural occurrences. The effects of local equilibria appear to be the dominant factors in the overstepping of sequential reactions. Qualitative activity-activity diagrams proved useful for examining the effects of bulk composition on the relative stabilities of spinel and the three silicates, including variations in Fe/(Fe+Mg), bulk Mn and Zn contents, and minor local variation in oxygen fugacity. Matrix spinel compositions (i.e., those not modified by reaction to silicates) fall into two groups: a more magnesian one containing spinels with average Fe/(Fe+Mg) (Fe#) of 0.49 and a less magnesian one, average Fe# of 0.67. With regard to this bulk compositional effect, the more magnesian composition should reduce garnet stability due to the strong fractionation of Fe into garnet, thus favoring the reaction of spinel to orthopyroxene within silica-rich areas. In more aluminous areas, spinel will react to form sapphirine, then garnet, then possibly orthopyroxene. A less magnesian composition would expand the stability of garnet at the expense of sapphirine and, to a lesser extent, orthopyroxene.

Zinc has a subtle effect on mineral stabilities. Because Zn is strongly partitioned into spinel, higher zinc contents (concentrations in some spinels are as high as 14.9 mol% gahnite) may expand the stability of that mineral considerably. Consequently, spinel stability may increase relative to the three silicates, but this may be quite variable due to variable reaction stoichiometry and different reaction-boundary slopes in the activity-activity diagram. In general, spinels with the highest Zn content occur next to orthopyroxene (ave. 4.9 mol% gahnite in spinels) for which the stability appears to be only slightly affected by this increase in Zn. The greatest decrease in silicate stability is observed in sapphirine. Spinels adjacent to sapphirine contain no more than 1.3 mol% gahnite.

The effects of manganese and oxygen fugacity were also examined. Mn increases the stability of garnet due to strong partitioning of Mn into this mineral. It can be inferred using statistical and chemical data that this has some bearing on textural relations in garnet-bearing samples, but the lack of obvious Mn fractionation by other minerals examined makes it impossible to interpret the effects of Mn in the garnet-free samples. Calculated ferric-ferrous ratios in analyzed minerals were examined in an attempt to study the effect of oxygen fugacity on the stabilities of minerals. In the more magnesian compositions, which may correlate with slightly higher fO_2 during reactions, spinels should react to form sapphirine, then possibly garnet or orthopyroxene with further silica activity increase. In lower-fO_2 environments (perhaps those with higher bulk Fe#), spinel should react directly to form orthopyroxene. The coexistence of magnetite and ilmenohematite dictates T-fO_2 conditions very nearly at those of the Hematite-Magnetite buffer. Minor fO_2 variations that might have had an effect on silicate-forming reactions would only be recorded by small variations in magnetite and ilmenohematite solid solutions (ulvospinel and ilmenite contents, respectively). These data were not acquired in this study, however, so no definite conclusions could be made.

ACKNOWLEDGEMENTS

It is actually very hard to sum up all of the people that have influenced you during the most challenging time of your life, much less those who have led you to this time and encouraged you to set your goals and achieve them. This in no way can actually mention every person that deserves thanks, but it is a bold attempt.

My thanks go to all of my committee members for their help. Thank you Bob Tracy for introducing me to this project and agreeing to advise a chemist on the ins and outs of metamorphic petrology. Mike Hochella and Jim Beard are also thanked for their input at various stages of project development. Also thanks go to Patty Kitchen for sharing her statistical knowledge and insuring that the statistical portion was presented correctly.

Statistical Consulting, specifically Walt Pirie and George Terrell, helped immensely in guiding me to specific statistical tests and assuring me that my thoughts were correct. Thanks to Rick Law for the use of his petrographic microscope with mechanical stage used for the statistical data collection. Todd Solberg set up analyses and ran calibration, as well as helped with data collection on the electron microprobe at Virginia Tech. He also spent many hours with me at the SEM. Special thanks to Larry Taylor and Alan Patchen at the University of Tennessee, Knoxville for allowing me to use the probe lab at UT and having everything set up for that 24 hours.

Of course there are those people who were there before this even started. Thanks Mom and Dad for believing in me, even when you couldn't believe your daughter was going to be a scientist. Thanks for the good food and the rest from the madness of grad school, and sometimes even Blacksburg, which many times was needed. Lara Montgomery- together since high school, through college, and still moving on. Through your experiences, I knew I could make it. Tara Rose-remember the New River and thanks for those late night phone calls. It's your turn next.

Cheers to the people who got me away from my work, sometimes a little more than I should have- VPI Cave Club. It was always comforting to know that I would have a

break on Friday nights for the Ton-80, meeting, and the ever popular speleoseminar, not to mention the weekly cave trip that kept me sane (although many thought I was insane) and the Bat Ranch Parties. I will always be proud to be a member of this group.

Three years of guys and gals in 4060- Adam, Eddie, Eric, Jay, Jeane, Luca, Maria, Paige, Peter, Russ, Wil, Zhaung. We tried to get some work done in there, but at least we had fun. Thanks Paige Baldassaro for listening to my ramblings and teaching me how to cook, when you weren't busy cooking for all of us yourself. I would have starved without you. Nancy Brauer, those D&D nights were so fun and I always looked forward to them. Jeane Jerz, thanks for the late evenings after boxing aerobics. Kelly Rose, your love of geology kept me going when mine was lacking. And Carl Bern- for three years you've been there and words can't express how much you mean to me.

TABLE OF CONTENTS

LIST OF FIGURES

LIST OF TABLES

INTRODUCTION

Emery is an old mining and petrologic term for very fine-grained and very high-grade contact-metamorphosed aluminous rocks, and is essentially synonymous with the term aluminous hornfels. Emery rock contains a mixture of corundum, Fe-Ti oxides and aluminous spinel and may contain varying amounts of aluminous silicates, such as sillimanite or sapphirine. Rocks of the Salt Hill emery deposit, Cortlandt Complex, New York, contain many complex chemical and textural relationships that appear to reflect disequilibrium, which most likely occurred during rapid heating, and local equilibration upon cooling on scales as small as sub-thin section. These emeries occur within numerous aluminous schist xenoliths surrounded by variably contaminated mafic igneous rocks, and problems in attainment of equilibrium probably relate to rapid contact-metamorphic heating and cooling. Tracy and McLellan (1985) was the first study to describe and emphasize the role of kinetic controls on local equilibrium within the emeries, although there are numerous earlier papers that described general petrogenetic relationships within this classic emery occurrence (Friedman, 1956; Barker, 1964; Caporuscio and Morse, 1978; Bender et al., 1984). The present study was intended to examine some of the reaction relations in the emeries in greater detail, specifically the nature of the reaction of spinel to either sapphirine, garnet, or orthopyroxene during the silication process that accompanied cooling following peak contact metamorphism.

The Salt Hill emery deposit in the southeastern part of the Cortlandt Complex consists of many xenoliths, screens and curtains of Manhattan schist adjacent to the outer contact of the youngest pluton of a composite mafic to ultramafic intrusion of alkali-basaltic magma. At the present level of exposure of the intrusion, pressure at the time of intrusion – 430 Ma (Bender et al., 1984) - was roughly 7 kbar (Ratcliffe et al., 1983). The emery xenoliths were heated to near-magmatic temperatures upon incorporation into the magma. Caporuscio and Morse (1978) estimated approximately 800-900 ˚C, whereas Tracy and McLellan (1985) argued for T in excess of 1000 °C. Temperature this high is reflected by

apparent disequilibrium melting and absence of hydrous phases within xenoliths. Tracy (1994) has reported quartzofeldspathic veinlets in emery xenoliths that contain ternary feldspars which crystallized at temperatures at least as high as 1050 ˚C.

A disequilibrium mineral breakdown process apparently occurred in place of normal prograde mineral reactions due to the rapid heating to unusually high temperatures. In particular, pelitic schist of the Manhattan Schist Formation underwent a fundamental segregation into two fractions, a strongly water-undersaturated silica-feldspar melt containing much of the SiO_2 and virtually all of the alkalis present in the protolith schist, and a solid, refractory aluminous residuum containing spinel, Fe-Ti oxides, sillimanite and sporadic corundum and in some cases extremely calcic plagioclase. Sillimanite appears to have been the only non-melt silicate present at this stage in development of most emeries. The emeries thus are a more completely developed natural example of the disequilibrium experimental textures observed by Brearly (1987). During cooling, the mobilized silica-rich melt was injected into the solid residuum as mm- to cm-scale veinlets, causing local increases in silica activity. Increasing silica activity in turn produced stable and metastable mineral associations involving spinel with the secondary (but still very high-T) silicates sapphirine, garnet, and orthopyroxene. Some of the molten mobilizate was lost from the xenoliths to the surrounding, partially solidifed mafic to ultramafic igneous material to produce an unusual hybrid monzonorite lithology. This monzonorite is found adjacent to xenolith swarms and as a border phase a few hundred meters wide along the external contact of the igneous complex in its southeastern quadrant.

Spatial (textural) arrangements of the silicate mineral phases in emery generally indicate that local increase in silica activity resulted in progressive silication reactions of spinel to sapphirine, garnet and orthopyroxene in this order, but numerous exceptions occur. In a simplest model, increase in silica content of product minerals sapphirine (Si/O = 0.10) to garnet (0.25) to orthopyroxene (0.28) implies that reactions forming these phases should occur from lower to higher silica content in stages rather than directly from

spinel to higher-silica minerals, thus overstepping intermediate reactions. Figure 1 illustrates some of the possible chemographic relationships among these minerals with increasing silication that might be preserved texturally as reaction rims. However, most of the possible reaction-rim relationships are not observed, suggesting a more complex set of controls on reaction sequence than simple silication. For example, variations in original bulk composition (particularly, subtle variation in Fe/Mg) reflecting pre-contact metamorphic mineral assemblages produced different reaction sequences and general textural relations with progressive silication (Tracy and McLellan, 1985). Compositional differences of minor components (e.g., Mn, Zn) within spinels reacting with introduced silica may have produced different reaction sequences and textural relations. Subtle local variations in oxygen fugacity may also have had significant effects because of the variable ferric iron contents of the different silicates. In the Salt Hill emeries, interface-controlled reaction rims of sapphirine, garnet, or even orthopyroxene in direct contact with spinel are common. Diffusion was obviously very limited based on the scale of these reaction rims.

This study consists of three parts. First, a statistical analysis of the different textural relationships (e.g., sapphirine-spinel, garnet-spinel, orthopyroxene-spinel contacts) was performed to determine how commonly the skips in predicted reaction sequences occur. Fluctuations from homogeneity were deemed significant by statistical tests. As input data for the statistical analysis, mineral grain-contact relationships were counted using the petrographic microscope to determine if skips in reaction sequences are significant or simply a result of sampling error inherant in the sampling procedure. Establishment of the statistics of grain-contact relationships as indicating a sequence not predicted by simple silication prompted the examination of chemical compositions as controls of the documented reaction paths.

Chemical compositions of each mineral along the different types of grain boundaries were then analyzed by electron microprobe to determine the underlying chemical controls of observed textural behavior. Based on the findings of Tracy and

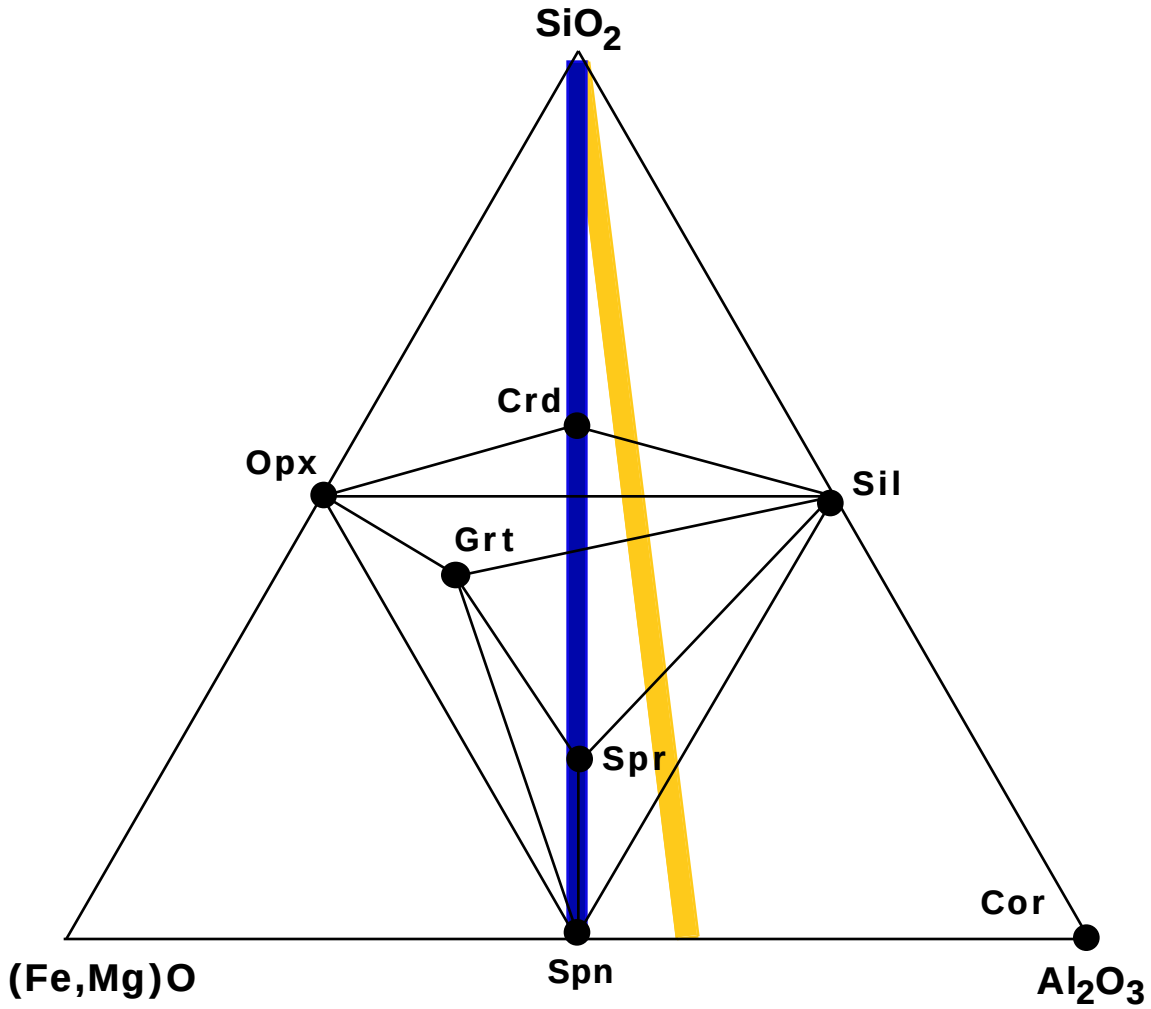

Figure 1. Ternary diagram showing possible reaction sequences with increasing silica. FeO and MgO have been combined into a single "ferromagnesian" component to simplify the graphical portrayal. Original mineral assemblages within the host material (spinel-corundum (yellow) vs. corundum-free (blue) matrix) produced different reaction pathways with increasing silication. Subtly differing bulk compositions along with varying compositions of the original spinels reacting with introduced silica produce different mineral associations.

McLellan (1985), subtly more magnesian centimeter- to meter-scale lithologic units within the examined xenolith contain different mineral assemblages than less magnesian units. In particular, the more magnesian emeries contain greater amounts of sapphirine and orthopyroxene and less garnet. These observed variations in emery compositions probably reflect original bulk compositional variations within schist protoliths, and apparently play a

subtle but important role in controlling the sequence of silicate mineral formation in emery. This paper presents a model for the mechanism by which these compositional differences control reaction sequences.

Finally, a discussion of the effect of oxygen fugacity and suggestions for further study will be presented. Henson (1986) noted that oxygen fugacity is an important intensive variable that controls spinel and sapphirine stability in high-temperature, regionally metamorphosed granulite-facies aluminous rocks. In higher-fO_2 environments, such as those found in the hematite-bearing Salt Hill emeries, different reaction sequences may occur, causing observed gaps in reaction sequences.

GEOLOGIC SETTING

The Cortlandt Complex near Peekskill, Westchester County, New York, is a roughly 45-50 km^2 composite intrusion of six mafic to ultramafic plutons located about 60 km north of New York City. These six plutons are distinguished by crosscutting relations, internal structure, post-emplacement deformation, mineralogy and chemistry (Ratcliffe et al., 1983). Age of intrusion has been estimated at 430-440 million years (Ratcliffe et al., 1983) from isotopic data. The intrusion postdates both metamorphism and deformation of the Taconic Orogeny (estimated peak at 450-455 Ma – Hames et al., 1991) by about 15-20 Ma and therefore cuts the steeply tilted (nearly vertical) Barrovian regional metamorphic isograd surfaces (chlorite to sillimanite grade) formed by this event. Any effects of the subsequent Acadian Orogeny (at roughly 390 Ma) are weak and are probably restricted to formation of minor shear zones and associated recrystallization.

Country rocks of the Cortlandt Complex comprise regionally metamorphosed Cambrian and Ordovician schists, marbles and amphibolites of the Manhattan Prong which were complexly folded during and after Taconic metamorphism. The complex is immediately surrounded by the Inwood Marble, which crops out along about 4 km of the

southern border, and the Manhattan Schist (incorporating both pelitic schist and amphibolite), which encircles much of the rest of the complex and is described in the next section. The Salt Hill emery deposit is located in the southeastern section of the complex within pluton VI (Figure 2). Alkalic basalt parental magma which is now represented by fractionally crystallized layered mafic to ultramafic igneous rocks (Bender et al., 1984) intruded the folded country rocks and produced an unusually significant amount of pluton-country rock physical and chemical interaction, including development of many xenoliths of both schist and marble. The Salt Hill emery deposit is located in a concentrated swarm of such xenoliths of Manhattan Schist.

As an aside, another emery deposit area in the Cortlandt Complex was economically exploited many years ago and occurs in the northeastern quadrant at Emery Hill (Figure 2). These emeries, although superficially mineralogically similar to the Salt Hill emeries in some respects, have a rather different origin. Although the contact relationships presented in older references are not entirely clear and the former emery deposit is no longer accessible to geological observation, historical references to this deposit suggest that it consisted not of xenoliths but of true, uninterrupted contact aureole, likely as a window through the flat-lying basal contact of the Complex. Consistent with this model, mineral assemblages in the Emery Hill emery are not nearly as high-temperature as those at Salt Hill (for example, at Emery Hill no sapphirine is known and staurolite and kyanite are common).

Additional information on the petrology and structure of the Cortlandt Complex and the surrounding rocks (including emeries) can be found in Friedman (1956), Barker (1964), Caporuscio and Morse (1978), Domenick and Basu (1982), Ratcliffe et al.(1983), and Waldron (1986). Numerous older (late nineteenth and early twentieth century) references exist as well but are of mostly historical interest; a relatively complete list of older (pre-1950) references can be found in Friedman (1956).

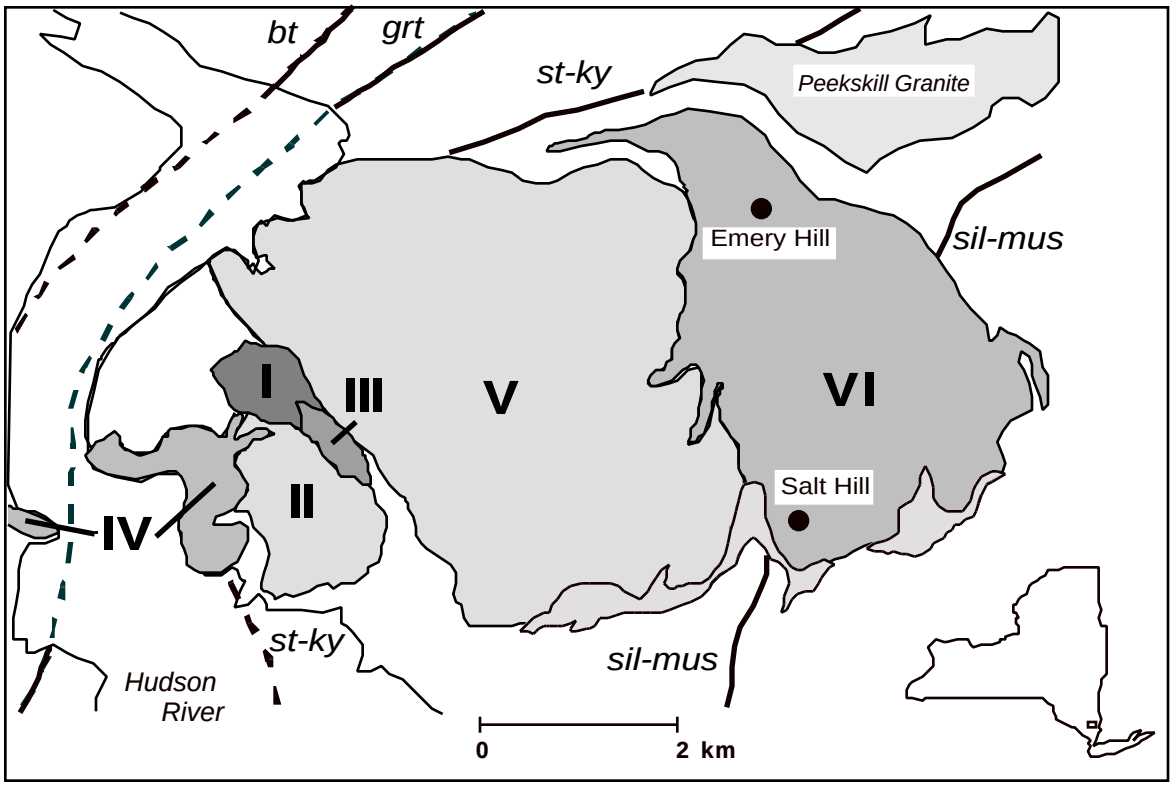

Figure 2. Generalized map of the Cortlandt Complex with inset (based on mapping by Ratcliffe, 1978-1982). The numbers denote the order of emplacement as defined by Ratcliffe et al. (1983). It includes locations of the Salt Hill and Emery Hill deposits, two areas where two different types of emeries exist. The complex is surrounded primarily by the Manhattan Schist.

PETROLOGY

Emery is a term for a rare, highly aluminous type of contact metamorphic rock which in the US has only been reported from Virginia, Massachusetts, North Carolina, Pennsylvania, and New York. The term emery has been used for material exploited as an abrasive, and implies the presence of corundum. Emery is therefore a highly aluminous material and virtually synonymous with the term “buchite,” but this report will continue to refer to this material as emery. Buchite is defined in the AGI Glossary of Geology as "a vitrified hornfels produced by fusion of an argillaceous rock by intense local thermal metamorphism" and classic buchites are typically associated with volcanic phenomena such

as lavas and shallow feeder dikes. Although the Salt Hill emeries had obviously been melted, their depth (>20 km) allowed such slow cooling that internal melts crystallized rather than being quenched to the glass typical of classic near-surface buchites.

Based on his work and earlier reports, Friedman (1956) defined two types of emeries found within the Cortlandt Complex: black emery and grey emery. The black emery contains green Al-spinel (hereafter simply referred to as spinel), magnetite and corundum, with a limited silicate content (typically only quartz veinlets, sillimanite, and rare sapphirine) and is essentially restricted to the Salt Hill emery deposit. Grey emery is found in association with the black emery at Salt Hill and is typically formed from it. In addition to spinel and magnetite, grey emery contains increased amounts of quartz, sillimanite, and sapphirine, plus one or more of the minerals orthopyroxene, cordierite, and garnet.

Friedman also proposed several possible explanations for formation of these deposits: magmatic segregation, absorption of xenoliths and contact metamorphism with accompanying metasomatism. His preferred explanation was that emanations released from the magma passed through the schist in advance of the approaching magmatic front, causing much of the metamorphism and metasomatism that formed the emeries. Aluminum and iron concentrations increase within the margins of xenoliths and in the contact aureole close to the contact with the igneous rock, indicating movement of magmatic components into the former schist and loss of easily mobilized schist components, particularly alkalis and silica, from the schist. Friedman also noted that the xenoliths may also contain scattered quartzose inclusions, orthoclase inclusions and emery-rich inclusions surrounded by orthoclase. His explanation of emery formation as a largely metasomatic effect was essentially correct, but deficient in lacking detailed discussion of mechanism. Both reaction mechanisms and processes of mass transfer that are consistent with Friedman's overall conclusions can be filled in from more recent investigations, as discussed below.

The Manhattan Schist Formation which borders much of the complex is dominantly pelitic in composition, although it is highly variable in texture and bulk composition. Volumetrically dominant pelitic units within the Manhattan Schist are separated by relatively common thin amphibolite and granulite layers of probable volcanic or volcaniclastic origin. Pelites contain varying proportions of quartz, muscovite, biotite and plagioclase, and typically also contain one or more of the minerals chlorite, garnet, microcline, staurolite, sillimanite, kyanite, ilmenite, and magnetite, depending upon exact bulk composition and metamorphic grade. Regional metamorphic grade of country rocks varies from biotite zone in the western part of the Complex near the Hudson River to sillimanite-muscovite zone along the southeastern border (near Salt Hill). Adjacent to the igneous contact quartz and muscovite decrease in favor of sillimanite, magnetite and garnet (Barker, 1964). Based on observation of Manhattan Schist pelitic units outside the contact aureole but near Salt Hill, the protolith rocks in emery xenoliths probably were quartz-rich plagioclase-sillimanite-muscovite-biotite-garnet schists with or without Fe-Ti oxides and staurolite.

The igneous host rock to emery xenoliths in Pluton VI of the Cortlandt Complex is a layered olivine pyroxenite containing calcic clinopyroxene (60 modal %), orthopyroxene (<10 to as much as 35 %), olivine (up to 35 %), and sporadic interstitial kaersutite (<5%) with associated plagioclase, biotite, magnetite, ilmenite, pyrite, and pyrrhotite (Ratcliffe et al., 1983). Pluton VI is a dominantly ultramafic layered cumulate with a very minor proportion of felsic rocks, especially hornblende gabbro. Based on major and trace element compositions and phase relations, Bender et al. (1984) proposed an origin for the cumulates as fractional crystallization and gravitational settling products of a parental mildly alkalic basaltic magma. The parental magma is probably well represented by coarse kaersutite gabbros in several of the smaller, older, less fractionated or contaminated western plutons of the Complex (Bender et al., 1984). In general, however, the Complex shows significant physical and chemical interaction with the country rocks. Strong interaction was probably enhanced by the very deep level of the intrusion (discussed

below), as well as by the elevated temperature of the country rocks at the time of intrusion. The best estimate for the time of intrusion (430-440 Ma – Ratcliffe et al., 1983) puts it at only 10-20 Ma younger than Taconic regional metamorphism. At a nominal post-metamorphic cooling rate of 5 °C/m.y., the sillimanite-muscovite zone country rocks would still have been at roughly 500 to 550 °C at the time of intrusion. The present erosion level of the plutons represents a depth of 20-25 km, based on thermobarometric estimates of 6.5 – 7 kbar for both Emery Hill emeries and adjacent country rocks (Tracy and McLellan, 1985; Waldron, 1986). The unusually deep crustal level for this type of layered, fractionated mafic pluton implies that post-intrusion cooling of both igneous rocks and emery xenoliths would have been much slower than typically observed. Certain textural features of the emeries, particularly the widespread distribution of quartzofeldspathic veinlets and extensive development of the secondary silicates sapphirine, garnet, orthopyroxene and cordierite, probably have resulted from the slow cooling which distinguishes the emeries from other described buchites (Turner, 1968; Benimoff and Sclar, 1984; van Bergen and Barton, 1984; Grapes, 1986).

Petrologic studies of the emery in the petrologic "modern era" (post-1960 and especially after the introduction of the electron microprobe about 1963) are limited in number. Barker (1964) was the first investigation of the emeries to provide systematic description of mineral associations (Barker mistakenly assumed that most or all associations were mineral assemblages in the technical thermodynamic sense) and to portray the phase relationships graphically. Unfortunately, Barker's work was done just before the microprobe era and his study lacks the detailed chemical analytical data that would have enhanced the phase equilibrium analysis. The study of Caporuscio and Morse (1978) used microprobe analyses in their emery study which focussed on the question of stability of sapphirine + quartz and on comparison of emery petrology with that of sapphirine-bearing regional metamorphic granulites.

The study of Tracy and McLellan (1985) was centered on the mineral assemblages within the emeries and how they reflected the unusual thermal history of these rocks. They described the kinetics of the emery-forming process, particularly reaction kinetics and occurrence of localized scales of equilibrium. They examined samples collected in a traverse across a single aluminous xenolith exposed in the Salt Hill quarry. Their samples contained black emery (spinel-magnetite-ilmenohematite-sillimanite) or what they called "emery matrix" with varying degrees of reaction of this matrix with injected siliceous veinlets to produce the secondary silicates sapphirine, garnet, orthopyroxene and cordierite. They showed that overall mineral associations within the rocks of this Salt Hill emery xenolith probably reflect variations in original bulk chemistry, as well as the availability of silica. Individual samples from the traverse that showed no obvious microscopic differences nevertheless contained quite different associations of secondary silicates. Reasoning that the most likely significant chemical variable controlling associations was bulk Fe/(Fe+Mg), they further inferred: (1) that the only emery matrix mineral that reflected this variable was aluminous spinel; and (2) that the Fe/(Fe+Mg) (Fe#) of spinel was an accurate monitor of this ratio in the bulk composition of the present emery and probably also of the protolith.

By tabulating mean matrix spinel compositions within a group of samples, they found two distinct and consistent populations and concluded that iron and magnesium content varied in layers that represented essentially two pre-existing lithologic units. Tracy and McLellan's two compositional groups were a less magnesian group with a matrix spinel Fe# of about 0.60, and a more magnesian group with an Fe# of about 0.50 (Figure 3.). It is likely that the pre-contact metamorphic schists varied most strongly in garnet content, with the less magnesian group having substantially more garnet than the other and probably more staurolite as well. (Similar variation in garnet content and mineral assemblage from layer to layer within single outcrops is commonly observed in regional metamorphic terrains with the Manhattan Schist being no exception.) Samples within the

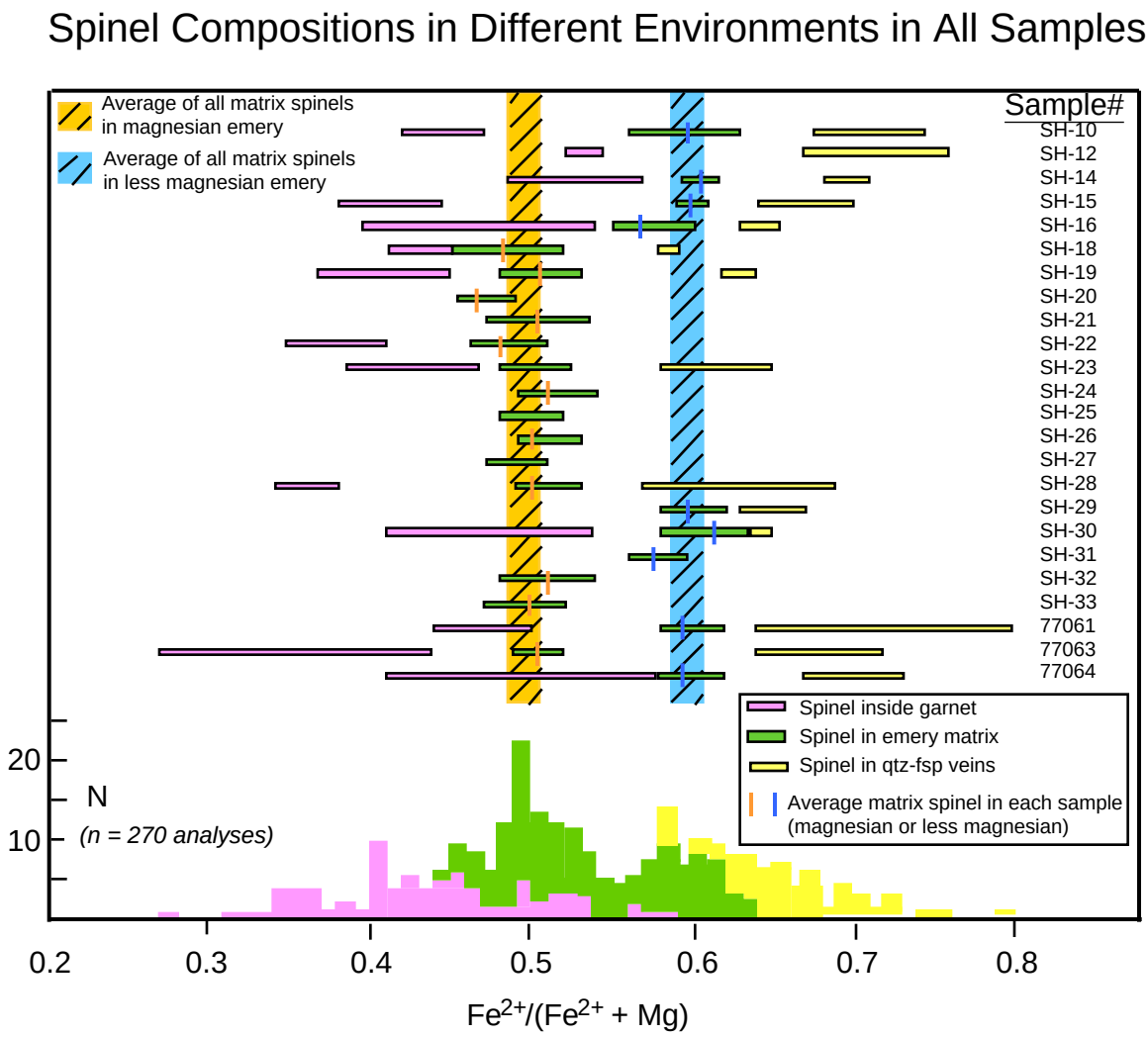

Figure 3. Spinel composition in different environments in all samples (from Tracy and McLellan, 1985). Spinel compositions as inclusions within garnet (pink, left side of diagram), as matrix (green, middle), and within quartz veins (yellow, right) are shown. Notice the wide range of spinel compositions within single samples, for example, 77063. Matrix spinel compositions were used to distinguish compositional groupings: a more magnesian group with Fe# of about 0.49 (yellow bar) and a less magnesian group with spinel Fe# of 0.60 (blue bar). Spinel inclusions within garnet always have a lower Fe# than those within the matrix.

more magnesian group typically contain the mineral association (and probable assemblage) sillimanite-spinel-magnetite-ilmenohematite-sapphirine-hypersthene +/- cordierite +/- corundum +/- garnet. Samples of the less magnesian group contain sillimanite-spinel-magnetite- ilmenohematite- garnet +/- hypersthene +/- corundum.

The areas of fine-grained aluminous matrix 1-10 cm thick are interspersed with coarser-grained quartz-feldspar veinlets and lenses (1-2 cm thick), containing quartz with feldspars: typically both orthoclase and plagioclase, or rarely a single ternary feldspar microperthite. One of these ternary feldspars has a composition that indicates a minimum temperature of crystallization as a single feldspar of 1050 °C (Tracy, 1994). The veinlets are very quartz-rich, probably reflecting disequilibrium melting of original quartzose schist protoliths at temperatures greatly in excess of ternary (qtz-plg-kfs) minimum or eutectic temperatures. The abundance of quartz in veinlets has produced an odd texture: large, rounded quartz crystals form a nearly grain-supported network with feldspars restricted to occurring as triangular interstitial patches that are commonly optically continuous over a scale of a centimeter or more.

Except for an early generation of sapphirine (as discussed below) the silicates present in each of the aluminous emery assemblages are generally products of interface-controlled reactions between silica and either spinel or one of the lower-Si silicates formed from silica and spinel. However, this simple picture is complicated somewhat by the occurrence of secondary silicates as apparent thin reaction rims along interfaces that demonstrably could not have produced such product minerals with the chemical components locally available (e.g., thin aluminous orthopyroxene or sapphirine rims between magnetite and quartz). The interface-controlled reactions apparently occurred during recrystallization after the melt veinlets were introduced, following an initial episode of silica diffusion from melt veinlets into aluminous matrix. This first stage of reaction produced small euhedral sapphirine crystals uniformly distributed through spinel - Fe-Ti oxide – sillimanite matrix adjacent to veinlets. The sapphirine may rarely also be found as intergrowths with matrix sillimanite. Extensive monomineralic reaction rim development, as noted above, indicates that not only silica but other components as well were diffusing, including Al_2O_3, FeO and MgO.

The model for secondary silicate development suggested by Tracy and McLellan (1985) involved local elevation of silica activity by outward diffusion of silica from the quartzofeldspathic segregations, driven by a strong chemical potential gradient for SiO_2. They did not specify the precise diffusion mechanism, but it is likely to have been intergranular surface diffusion. Because the emeries are essentially completely anhydrous rocks and intergranular aqueous film at the high temperature of emery formation must have been minimal or absent, diffusion of silica and other components can be assumed to have occurred as dry molecular surface diffusion. In the case of silica, the diffusing molecular entity would likely have been a minimally hydrated silica complex, given the high T and very low H_2O activity. Normally at typical metamorphic temperatures (400 to 700 °C) such diffusion of silica would be extremely slow relative to the more typical diffusion of silica complexes through intergranular aqueous fluid or film, but at the high temperature of emery formation even dry diffusion of silica was probably relatively rapid.

In any case, as silica activity rose locally (adjacent to veinlets), the simple model suggests reaction to form secondary silicates from spinel (and possibly other matrix minerals, as reaction stoichiometry might require) when silica activity rose to appropriate levels. The lowest-silica mineral is sapphirine (modeled as $[Fe,Mg]_4Al_8Si_2O_{20}$) with an Si/O ratio of 0.10, so it would be predicted to be the first silicate to appear as silica activity increased. Indeed, sapphirine is observed to appear in black emery matrix at some distance (as much as several cm) from veinlets. The other silicates (in order of increasing silica content) that would be predicted are garnet ($[Fe,Mg]_3Al_2Si_3O_{12}$ – Si/O = 0.25), cordierite ($[Fe,Mg]_2Al_4Si_5O_{18}$ – Si/O = 0.277) and aluminous orthopyroxene ($[Fe,Mg]_{1.75}Al_{0.5}Si_{1.75}O_6$ – Si/O = 0.28).

This simple model, however, requires some modification when the increase in silica activity is considered in conjunction with activities of Al_2O_3 and a combined component (Fe,Mg)O (Figure 1, above) (this combined component can be assumed to act as a single chemical component thermodynamically as long as no change in bulk Fe/Mg ratios occurs

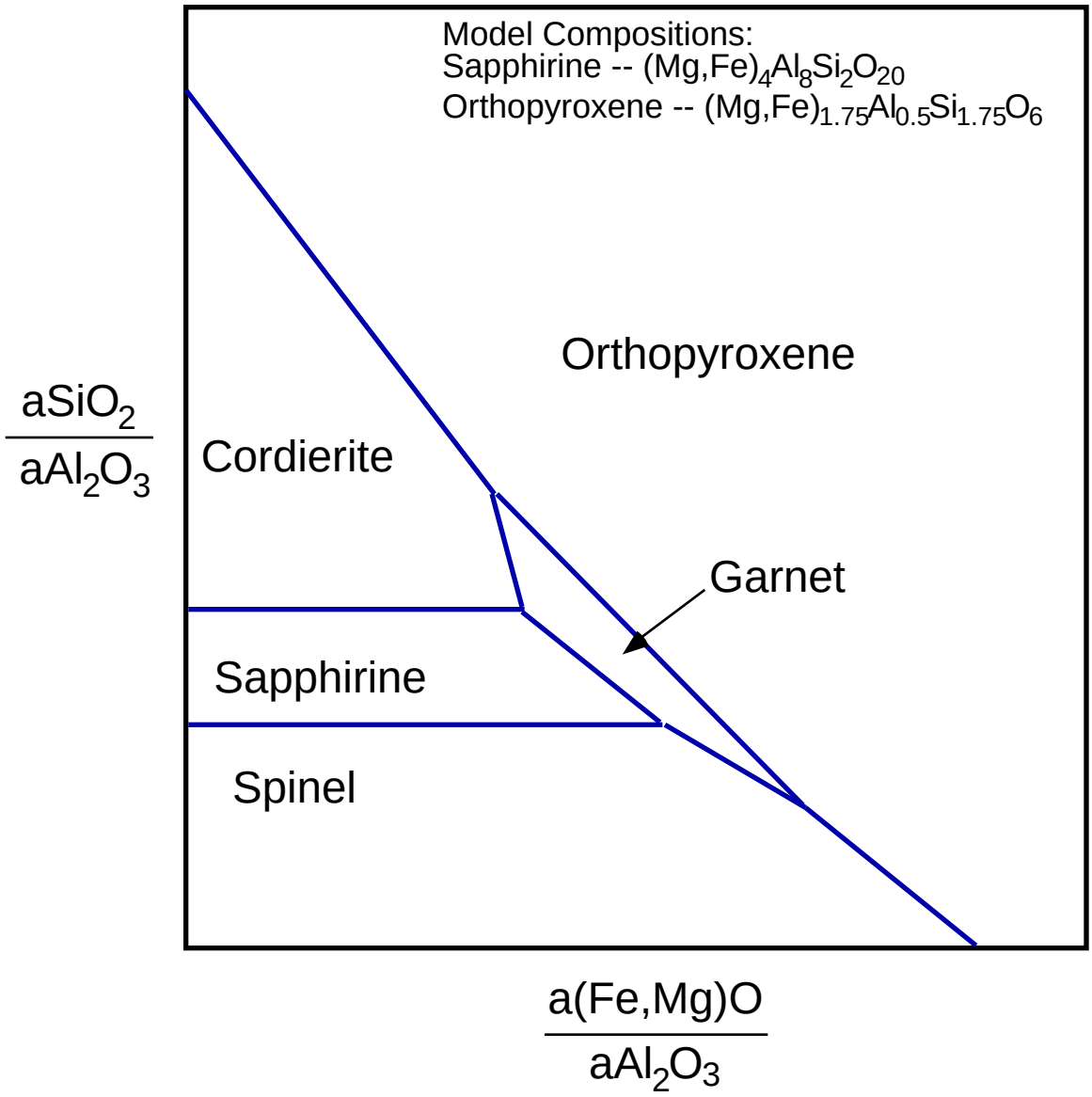

Figure 4. $a(Fe,Mg)O/aAl_2O_3$ vs. $aSiO_2/aAl_2O_3$ diagram. The activities are normalized to alumina. The diagram predicts that cordierite will not form directly from spinel. Also notice that in more aluminous areas spinel will react to form sapphirine, then garnet. It is only within the least aluminous areas that spinel will react directly to form orthopyroxene.

during the reaction process). All components are shown in an activity-activity diagram in Figure 4. This diagram is normalized to alumina activity, so that silica activity increase for various bulk compositions can be illustrated as vertical paths at various values of $a(Fe,Mg)O/aAl_2O_3$. Note that the relative rarity of cordierite compared to other silicates

may be explained by its restriction to bulk compositions with low ratios of a(Fe,Mg)O to aAl_2O_3 (i.e., the most aluminous local bulk compositions). In addition, the activity diagram predicts that cordierite should never form directly from spinel. Also note that this diagram predicts that direct reaction of spinel to various silicates is controlled by the relative alumina concentration in the bulk composition: in alumina-rich compositions spinel should react directly to sapphirine. In progressively less aluminous compositions, the sequences would be spinel to garnet and only in the least aluminous compositions should spinel react directly to orthopyroxene. This diagram is key to understanding the sequence of silicate-forming reactions and its implications will be discussed in detail in the Discussion section below.

DESCRIPTIONS AND TEXTURES OF SAMPLES STUDIED

Six thin sections from the suite of samples studied by Tracy and McLellan (1985) were chosen for this study based on mineral assemblage (Table 1) and inferred original bulk chemistry of each sample (more or less magnesian, based on spinel Fe#, as discussed above). Samples SH-10, SH-14, SH-21, SH-22, and SH-25 came from the emery xenolith traverse, whereas sample 77063 was taken from a large loose block near the traverse (and is assumed to be essentially the same material as the other samples).

Table 1.

Mineral Associations

Sample	**spl**	**spr**	**grt**	**opx**
77063 (Mg)	X	X	X	X
SH-10 (Fe)	X		X	X
SH-14 (Fe)	X		X	X
SH-21 (Mg)	X	X		X
SH-22 (Mg)	X	X	X	
SH-25 (Mg)	X	X	X	X

There are a variety of textures associated with the reaction sequences of spinel with silica that produced the silicates sapphirine, garnet and orthopyroxene. Most textures include spinel surrounded by one of the three silicates. Spinel may be found as one of many inclusions within the silicates or it can be surrounded by a reaction rim of the silicate produced. Most silicates are anhedral or subhedral, containing many spinel inclusions, but some like sapphirine can form elongate laths around the spinel. These textures are illustrated in the SEM back-scattered electron images shown in Figure 5. Most samples are very fine-grained, on the order of 100-300 µm average grain size. Spinels in thin sections are translucent and green in color, indicating spinel-hercynite solid solution with generally very low concentrations of other spinel components (gahnite is one exception which occurs in greater concentration in several spinels, as noted below). Spinel grains are anhedral and are found in a number of textural settings in each sample: as annealed textures within the matrix, as inclusions in sapphirine, garnet, or orthopyroxene crystals, as separate grains rimmed by one or more silicates, and as separate small grains within quartzofeldspathic veins or segregations.

"Black emery" matrix typically shows a very well developed classic annealing texture, with both spinels and Fe-Ti oxides having straight or curvilinear grain boundaries that meet in 120-degree triple junctions. The predicted first step in the reaction sequence of silica plus spinel is the appearance of sapphirine, producing spinel-sapphirine grain boundaries. Sapphirine has grown within aluminous matrix as elongated blocky crystals and also as elongate laths surrounding and including small spinels. These laths may also

Figure 5. (succeeding pages) SEM backscattered images illustrating complex mineral associations found in the emery of the Salt Hill deposit. (a and b) The "expected" spinel-sapphirine grain boundary. Sapphirine surrounds spinel as elongate laths. Garnet typically occurs as thin reaction rims (c), but also as anhedral grains surrounding spinel inclusions (d). (e) Orthopyroxenes containing spinel inclusions are also anhedral. (f) An example of other mineral associations is the common orthopyroxene reaction rims around sapphirine.

Figure 5. a

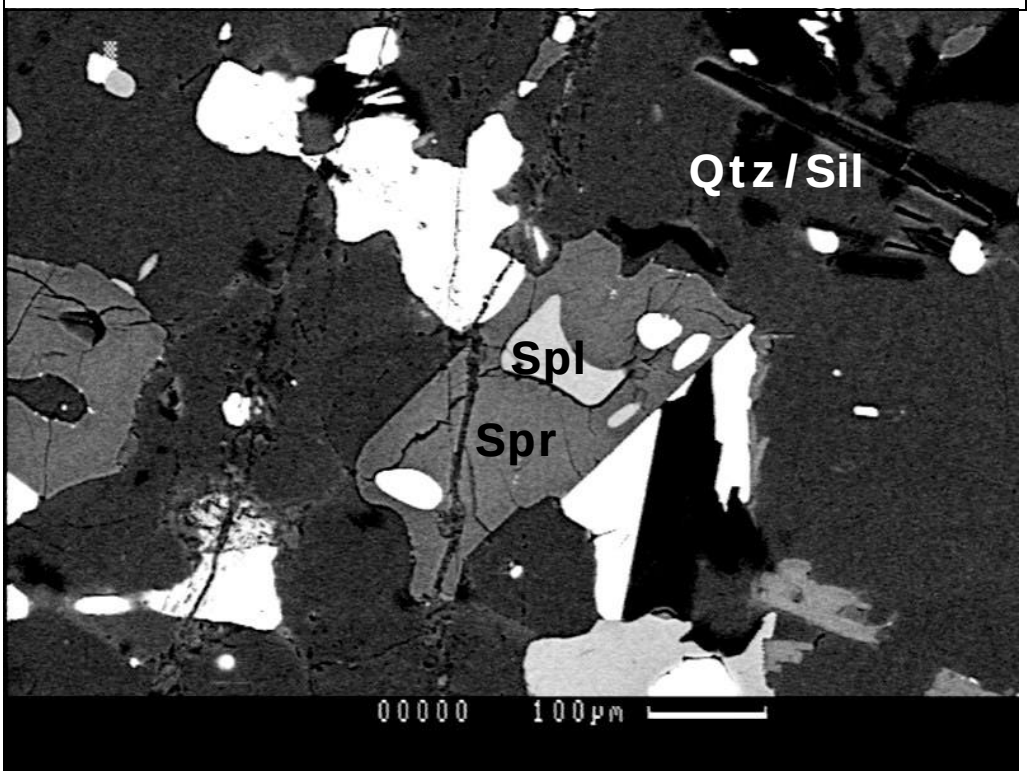

Figure 5. b

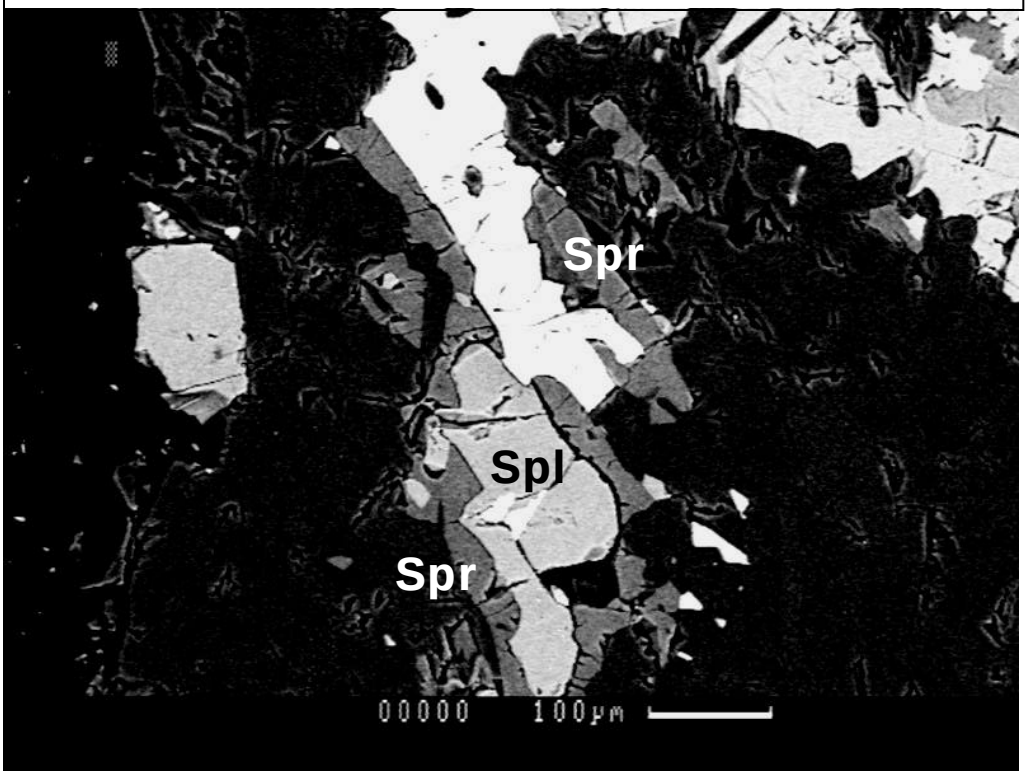

Figure 5. c

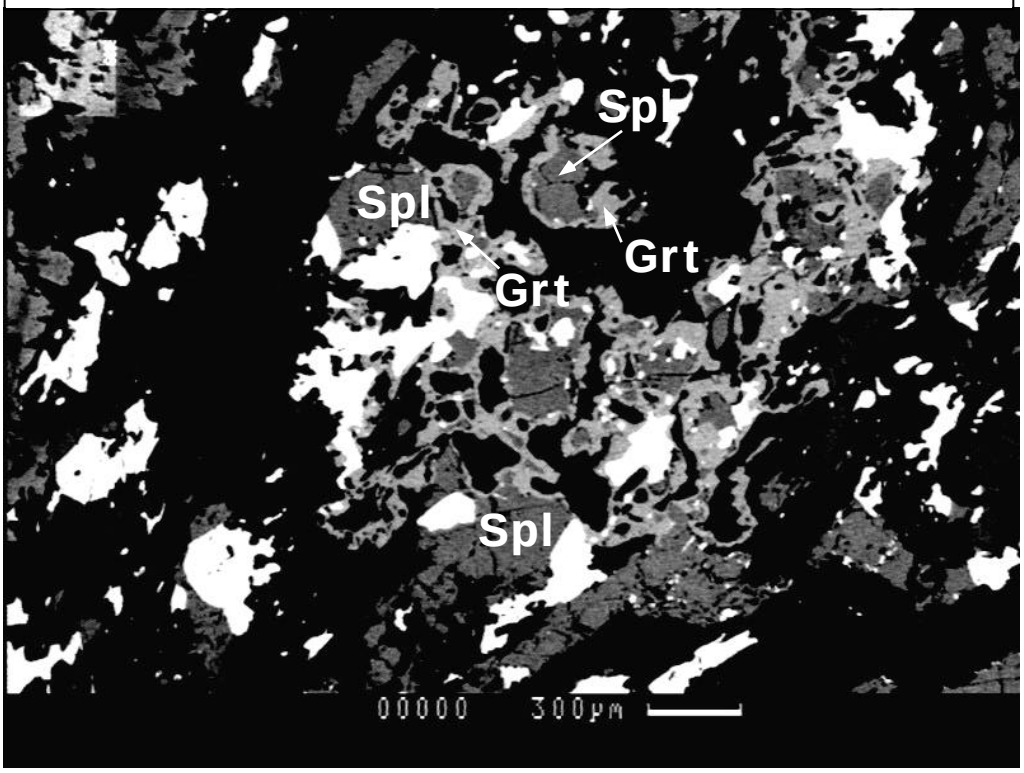

Figure 5. d

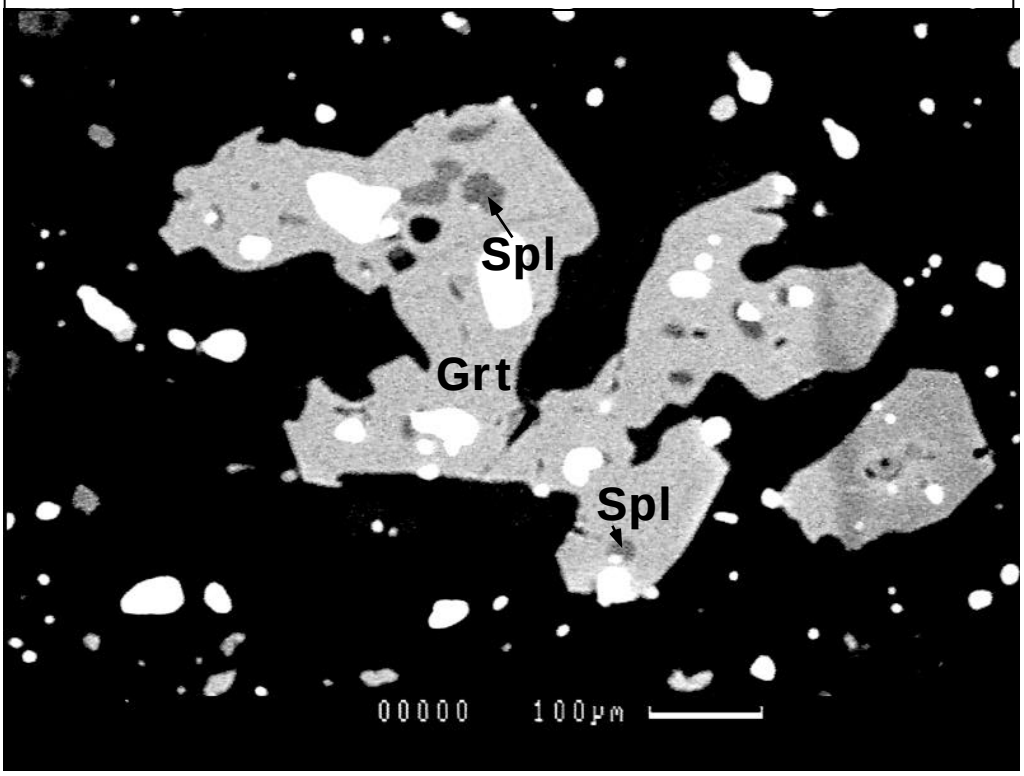

Figure 5. e

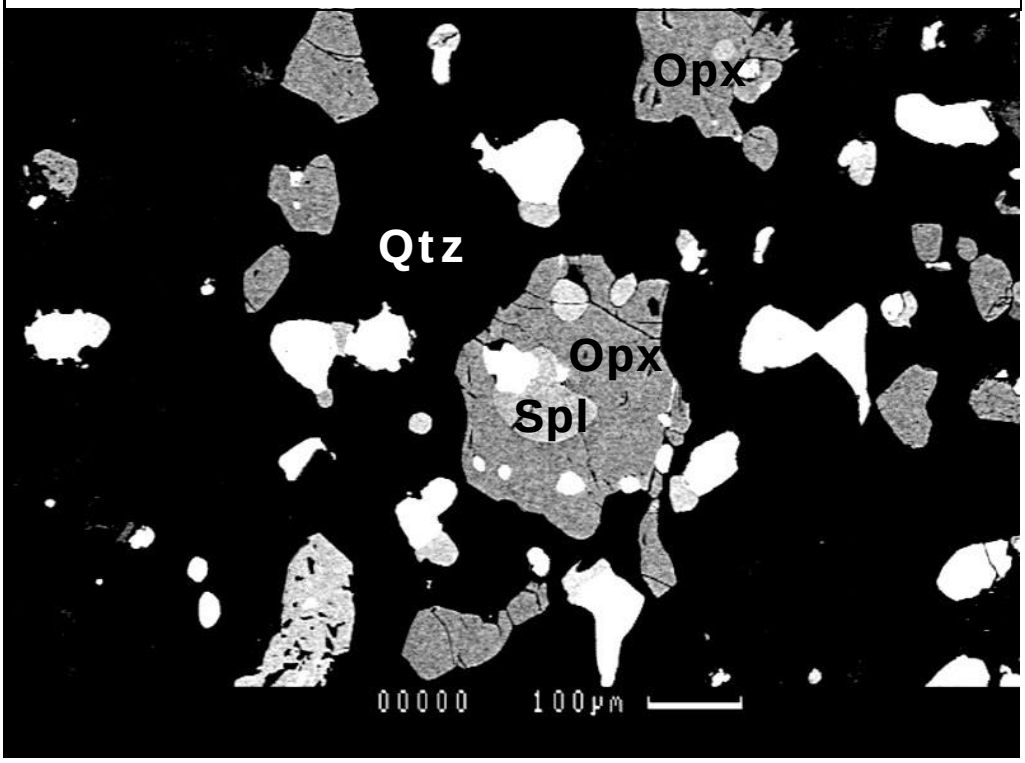

Figure 5. f

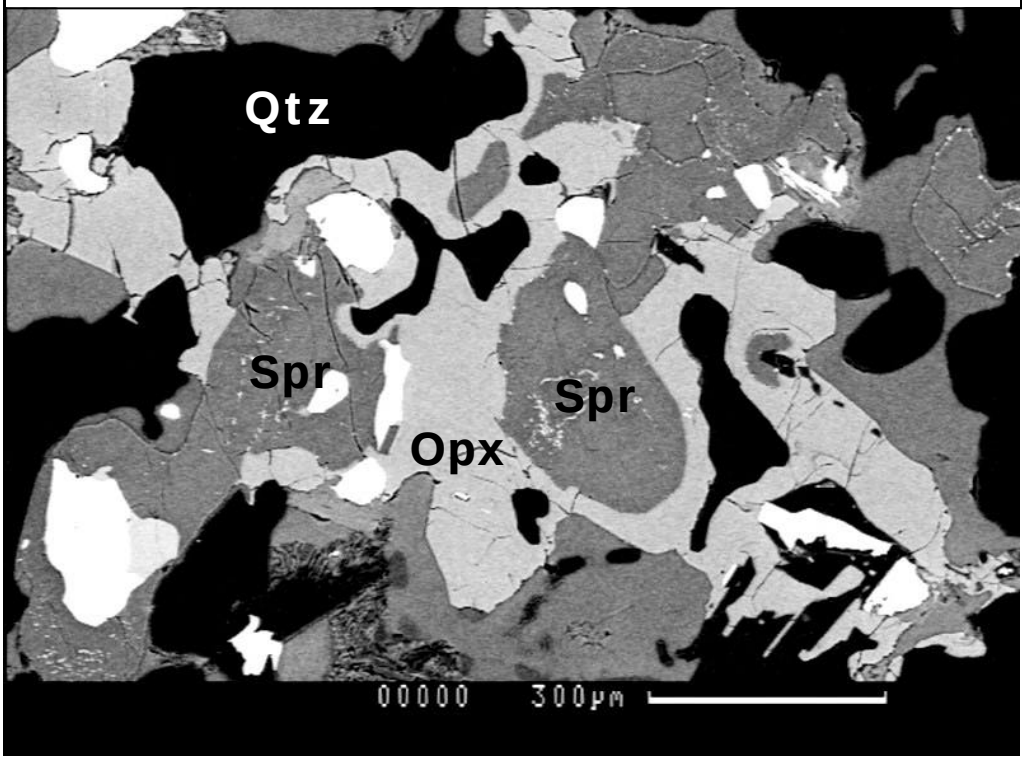

form complex patterns around the spinels as the crystals intergrow. However, anhedral grains of sapphirine also appear interspersed with spinels of similar shape in annealed textures. In thin section, sapphirines are pleochroic from light blue or colorless to medium or dark blue.

Garnet typically occurs as thin reaction rims of uniform thickness around spinels or, less commonly, Fe-Ti oxides, but also is seen as anhedral grains containing small rounded spinel inclusions. The tendency to anhedral behavior is so strong that garnet is virtually never seen as the subhedral to euhedral grains so typical of lower-grade metamorphic rocks. Garnets within the xenolith are not chemically zoned and are mainly almandine-pyrope solid solutions with low spessartine and grossular (typically less than 10 mol% total sps + grs). Pyrope contents may approach 50 mol% and are much higher than typical non-eclogite metamorphic garnets, reflecting the high T and P of origin.

Orthopyroxenes surrounding spinels are typically anhedral and very fine-grained. Orthopyroxene as thin, uniform reaction rims surrounding spinel (or rarely other minerals) is also quite common. In fact, such thin continuous uniform rims may form on a polycrystalline substrate such as aluminous matrix borders of quartzofeldspathic veins or segregations without any noticeable change in either thickness or chemical composition regardless of which mineral (spinel, magnetite, ilmenohematite or sillimanite) they locally surround. Orthopyroxenes in thin section are pleochroic from pale green or blue-green to reddish pink, and on occasion even pink to pale yellow. Strong pleochroism may reflect an unusually significant ferric iron content that is indicated by charge balance calculations of microprobe analyses (see below) and undoubtedly reflects the locally high oxygen fugacity of the emeries (roughly on the Hematite-Magnetite buffer).

Another common textural relationship involving orthopyroxene is the occurrence of reaction rims around sapphirine. Sapphirines in this instance are mainly anhedral or resorbed with the orthopyroxene rims coalescing and causing complex patterns around the

sapphirines. Larger orthopyroxene grains may also contain inclusions of sapphirine as well as spinel.

STATISTICAL METHODS

In order to determine the proportion of occurrences of each type of mineral grain-to-grain contact within samples from the Salt Hill emery, six thin sections were chosen based on observed mineral assemblages (Table 1, above) and inferred original chemistry of each sample (more or less magnesian, based on Fe# of matrix spinel). The samples were chosen in an attempt to produce a representative sampling of the Salt Hill emeries. Four of these samples are from the more magnesian group (denoted M) and two are from the less magnesian group (denoted F). The occurrences, by thin section, of minerals examined in this study are presented in Table 1 (above). Statistical analysis was done on sample 77063 along with the others and the results from this sample are included in the more magnesian sample group, despite the fact that this sample is technically not from the xenolith traverse of Tracy and McLellan (1985). It is emphasized that results from 77063 should not be used in the study of this particular xenolith without caution, and are only used as comparison, although the material in 77063 is probably closely related to the xenolith. Therefore, more magnesian group analyses are separated into two groups: with and without 77063.

The number of occurrences of each mineral studied and the frequency of grain boundary contacts were found by making point counts of the selected thin sections. The 40x objective lens on an Olympus research petrographic microscope (0.45 mm field of view) was used to count the mineral associations. This magnification was chosen to allow the smallest area to be studied without duplication of grains and grain boundary counts, and to assure that the fields of view did not overlap. This required a 0.6 mm mechanical stage interval. Mineral contacts and minerals counted were spl-spr, spl-grt, spl-opx, spl-spr-grt, spl-spr-opx, spl-grt-opx, spr, grt, and opx. The mineral associations were counted if that

mineral grain boundary was within the field of view. Single minerals (spr, grt, opx) were counted when that mineral was within the field of view, but not in contact with another mineral of interest. Counting continued until 500 total counts were reached or until the area of the thin section was covered.

For each thin section, the mode, which is the most abundant occurrence, and variation ratio were found. Variation ratio provides a measure of the distribution of the number of occurrences of each mineral assemblage. The variation ratio was calculated using the formula $\mathbf{v = 1 - (f/N)}$ where f is the number of occurrences of the mode and N is the total number of counts in the sample. The more even the distribution, the closer v is to 1. A variation ratio of zero means the mode is the only occurrence. Totals were calculated for the more magnesian compositions (M), with and without 77063, for the less magnesian compositions (F), and for the entire sample population. The statistical analysis was done for these groups, as well.

To determine degree of homogeneity throughout the sample population, contingency tables were made and expected values calculated. Expected values for homogeneity were calculated using $\mathbf{(H*B)/N}$, where H is the row total, B is the column total and N is the table total. Comparisons of the observed versus expected values give clues to independence with respect to location and mineral assemblage. Fluctuations from homogeneity must be tested to determine if these differences are statistically significant. The null hypothesis is that the differences from observed to expected values are the result of sampling fluctuations or are independent. If this is not true, then these differences can be assumed to be statistically significant, or dependent. The Chi-square test was used to test the hypothesis. The equation used to conduct this test is

$$\mathbf{X^2 = \sum[(O_{i,j} - E_{i,j})^2/E_{i,j}]}$$

where $O_{i,j}$ is the observed value for that row and column and $E_{i,j}$ is the expected value for the row and column calculated within the contingency table as described above. The level of significance used is alpha = 0.05. The degrees of freedom vary with the table tested, but

can be found by the equation **df = (r-1) * (c-1)** where r is the number of rows in the table and c is the number of columns. The Chi-square test was also used on tables containing expected values of zero. These rows were removed and the test was run on those as well.

STATISTICAL DATA/OBSERVATIONS

Occurrences of the mineral assemblages are given in Appendix I and presented in the bar graphs (Figures 6-11). Numbers within the graphs show the total number of counts taken in each thin section. The spinel - orthopyroxene grain boundary was the most abundant of the assemblages found in four of the six samples: SH-10 (397), SH-14 (46), SH-21 (186) and SH-25 (148). The remaining samples show spinel-garnet as the mode: SH-22 (226), and 77063 (188). Three of the six samples (SH-21, SH-22, SH-25) showed the second highest occurrence as spinel-sapphirine. The less magnesian samples contained spinel-garnet as the second most-frequent occurrence. Sample 77063 had spinel-orthopyroxene as the second most-frequent occurrence.

The data for mode and variation ratios are given in Table 2. All sample groups (more magnesian without sample 77063, less magnesian, and total sample group) contain the spinel-orthopyroxene grain boundary as the main occurrence. When sample 77063 is included with the magnesian sample group, the mode is the spinel-garnet grain boundary. The less magnesian samples produced a variation ratio of 0.26, whereas all other groups produced variation ratios of 0.65 - 0.76.

Contingency tables for the expected values of the mineral assemblages are located in Appendix I. There are four tables, each processed for the different original compositions of the host rocks and the total number of samples. Numbers printed in bold type are those that have lower expected than observed values.

The Chi-square test gave the results shown in Table 3. m is the minimum value for chi-square for the samples to be dependent, or significant. Chi-square values for all groups

are much higher than the m indicates they need to be to be. For the total number of samples, the chi-square value is 2272.055. This is much greater than m of 55.758, which is the minimum value for chi-square test to be significant.

Table 2.

Mode and Variation Ratios for the Salt Hill Emery Deposit Samples		
More Magnesian Sample Totals		
With sample 77063		
• Mode		Spinel - Garnet (414 occurrences)
• Variation Ratio	0.76	
Without 77063		
• Mode		Spinel - Orthopyroxene (334 occurrences)
• Variation Ratio	0.73	
Less Magnesian Sample Totals		
• Mode		Spinel - Orthopyroxene (443 occurrences)
• Variation Ratio	0.26	
Total samples		
• Mode		Spinel - Orthopyroxene (812 occurrences)
• Variation Ratio	0.65	

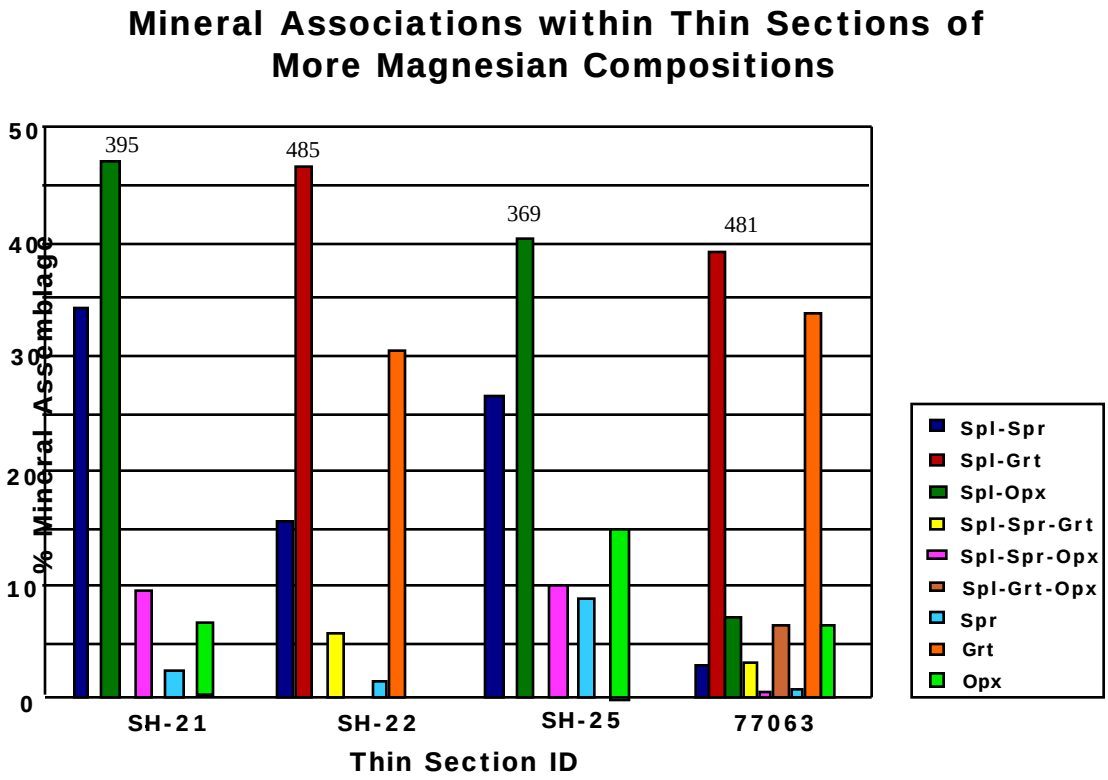

Figure 6. Mineral associations within thin sections of more magnesian compositions. Spinel-garnet and spinel-orthopyroxene occur the most often in these thin sections. Spinel-sapphirine fluctuates from about 3% to about 34% of the occurrences within this sample group. Numbers on the graph denote the number of counts for that thin section.

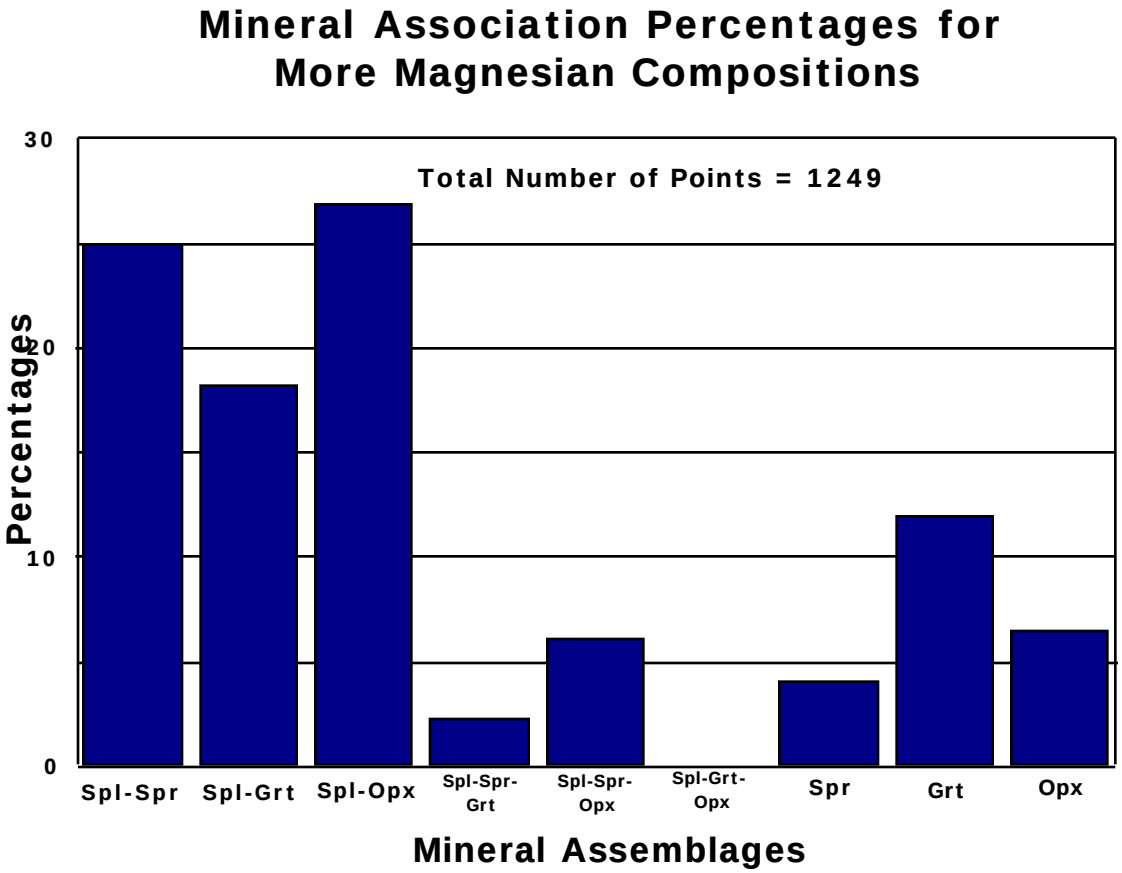

Figure 7. Total mineral association percentages for more magnesian compositions. This does not include sample 77063, because it may come from a rock located outside the Salt Hill xenolith. The most abundant relationship is spinel-orthopyroxene.

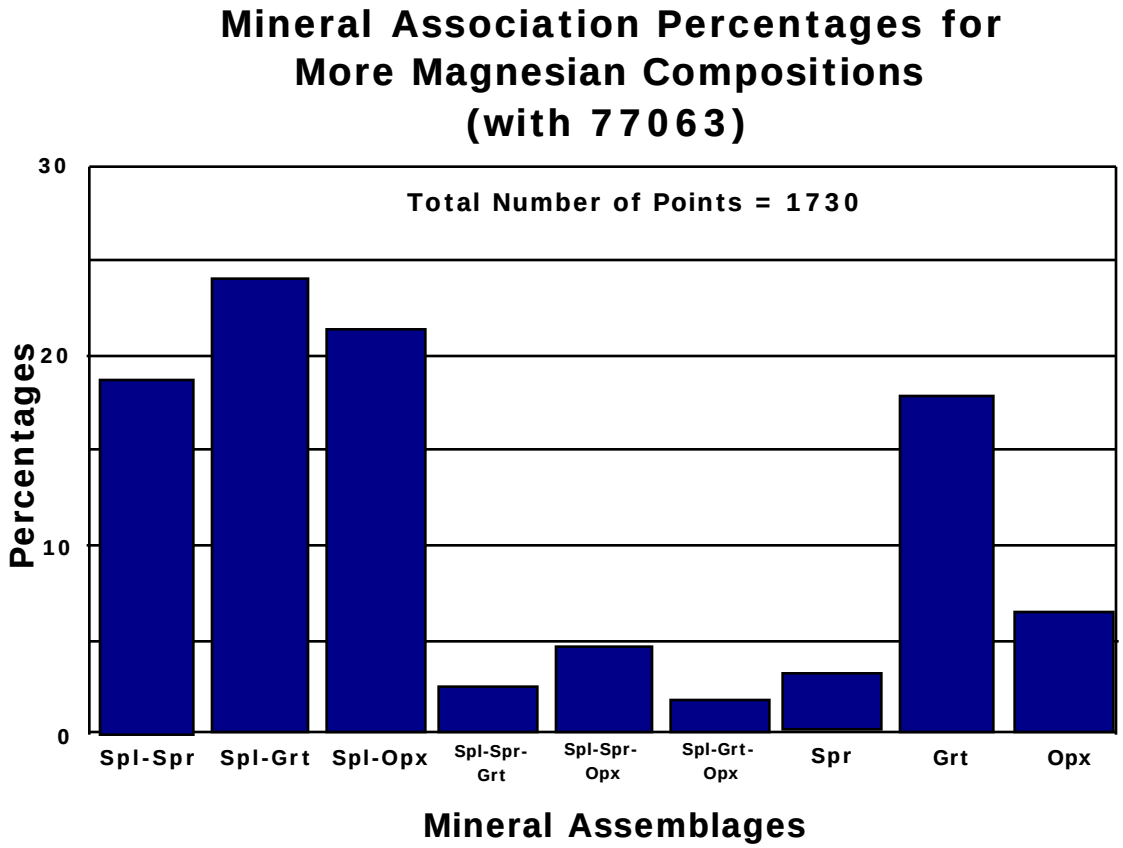

Figure 8. Total mineral association percentages for more magnesian compositions with 77063. Notice how the association that occurs most often has changed from spinel-orthopyroxene (Figure 7.) to spinel-garnet with the addition of sample 77063.

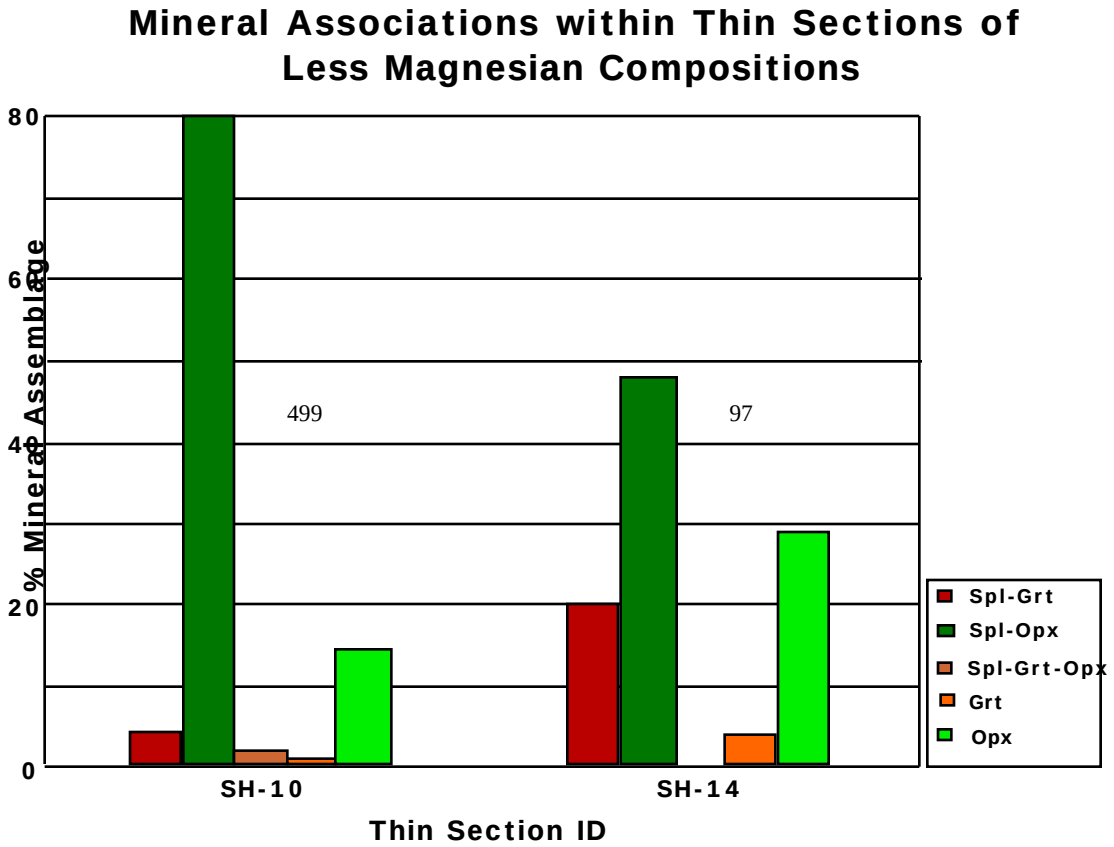

Figure 9. Mineral associations within less magnesian compositions. Spinel-orthopyroxene occurs the greatest percentage. The spinel-sapphirine grain boundary does not occur. Numbers on the graph denote the number of counts for that thin section.

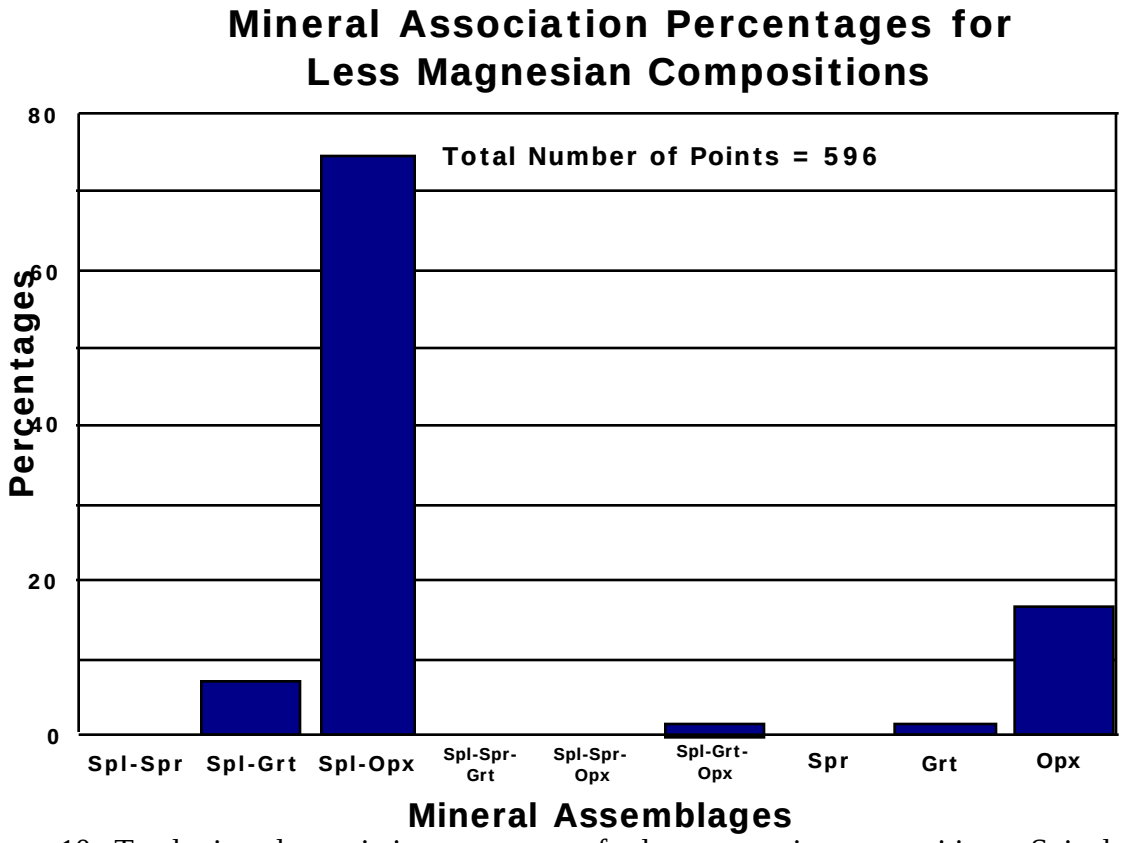

Figure 10. Total mineral association percentages for less magnesian compositions. Spinel-orthopyroxene is the mode.

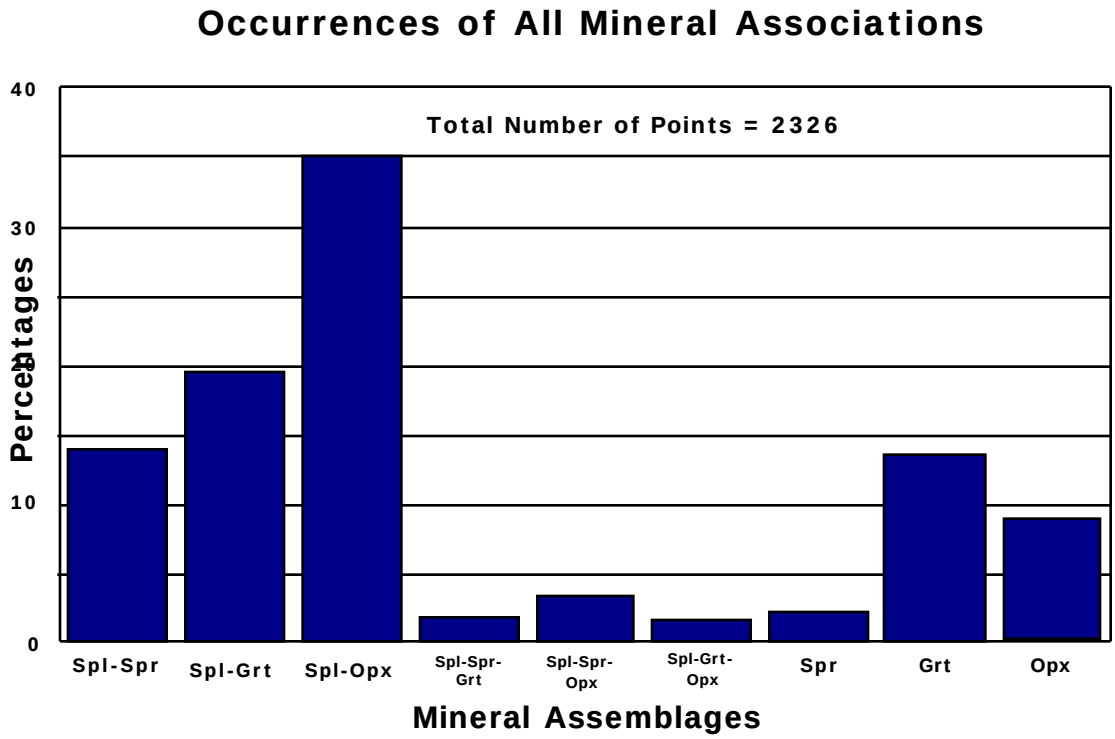

Figure 11. Total mineral associations for all samples. The spinel-orthopyroxene grain boundary is the mode.

Table 3.

Chi-square test Results

df = Degrees of Freedom
m = Minimum results of chi-square needed to determine significance

More Magnesian Samples

With sample 77063 (df = 24)

- chi-square = 1366.257
- m = 36.415

Without 77063(df = 14)

- chi-square = 1024.724
- m = 23.685

Less Magnesian Samples

(df = 4)

- chi-square = 60.914
- m = 9.488

Total samples

(df = 40)

- chi-square = 2272.055
- m = 55.758

CHEMICAL ANALYTICAL METHODS

Following statistical measurements, chemical compositions of spinels, sapphirines, garnets, and orthopyroxenes were analyzed using the CAMECA SX-50 electron microprobes at Virginia Tech and the University of Tennessee, Knoxville, to examine possible correlations of chemistry with textural relationships. Analyses for the following oxides were performed: SiO_2, TiO_2, Al_2O_3, MgO, CaO, MnO, FeO, ZnO, Na_2O, K_2O. At Virginia Tech, beam conditions were 15 kv accelerating potential and 20 nA sample current. Beam conditions at the University of Tennessee were 15 kv and 30 nA. Standard Cameca software (Quantiview) ZAF-type corrections were used for online data reduction

(Goldstein, et al., 1992). Mineral compositions were collected in spot mode as close to grain boundaries as possible to provide the most accurate composition-texture correlation.

Analytical data (as wt% oxides) were then converted to mineral structural formulas through use of a set of Excel spreadsheet recalculation templates for each mineral. Where appropriate (spinel, sapphirine, orthopyroxene), recalculation templates included an estimate of Fe^{3+}/Fe^{2+} ratio based on a charge-balance calculation and an assumption of cation-anion stoichiometry (Finger, 1972). The bases for recalculation were: spinel – 3 cations, 4 oxygens; garnet – 12 oxygens; sapphirine – 10 cations, 20 oxygens; orthopyroxene – 4 cations, 6 oxygens. Graphs for spinel compositional distributions were made using Cricket Graph. Plots were also done using ACF-Triplot software for all minerals. On each plot the data were separated into more and less magnesian groups, just as in the statistical analysis.

CHEMICAL ANALYTICAL DATA/OBSERVATIONS

Compositions of the minerals differed according to bulk chemistries and adjacent minerals. Data used for this study can be found in Appendices II-IV. In more magnesian samples, spinels were found adjacent to all three of the silicate minerals sapphirine, garnet and orthopyroxene. Spinels in the more magnesian samples vary in composition according to which mineral they abut. Adjacent to sapphirine, spinels contain an average of 47.9 mol% Hercynite ($FeAl_2O_4$), 48.7 mol% Spinel ($MgAl_2O_4$), 0.9 mol% Gahnite ($ZnAl_2O_4$), and 1.9 mol% Magnetite ($FeFe^{3+}{}_2O_4$). Spinels adjacent to garnet have a mean composition of 36.8 mol% Hercynite, 56.7 mol% Spinel, 3.7 mol% Gahnite and 2.4 mol% Magnetite. Spinels adjacent to orthopyroxene average 47.5 mol% Hercynite, 44.4 mol% Spinel, 4.9 mol% Gahnite and 2.1 mol% Magnetite, and may have as much as 14.9 mol% Gahnite.

In less magnesian samples where spinel contacts only garnet and orthopyroxene, different spinel compositions occur adjacent to each mineral. Spinels adjacent to garnet contain 49.9 mol% Hercynite, 44.8 mol% Spinel, 2.4 mol% Gahnite and 2.7 mol%

Magnetite. Spinels adjacent to orthopyroxene contain 61.9 mol% Hercynite, 31.3 mol% Spinel, 1.9 mol% Gahnite and 4.1 mol% Magnetite, and may contain up to 7.1 mol% Magnetite. Ranges of spinel compositions are given in Table 4.

Variations of gahnite component within spinels are shown in the graph in Figure 12. As stated above, some spinels contain a significant amount of zinc. Less magnesian bulk compositions have a narrow range of ZnO, which lies within less than 2 wt% ZnO. In the more magnesian compositions, spinels adjacent to sapphirine have similarly low ZnO, but a wider range of compositions occurs in spinels next to garnet (0.32-2.66 wt% ZnO). Spinels adjacent to orthopyroxenes actually show a bimodal behavior, which also occurs to a lesser extent in the spinel-garnet association. The highest concentrations of ZnO were found in sample 77063, whereas lower concentrations exist in other thin sections of more magnesian composition in each case. ZnO concentrations within spinel are tabulated in Table 5.

Table 4.

Spinel compositions (Mol%) according to bulk chemistry and adjacent mineral

	Her	**Spl**	**Gah**	**Mag**
More magnesian samples				
Spl-Spr	38.1-53.9	43.7-58.2	0.6-1.3	0.7-3.0
Spl-Grt	31.6-44.3	52.3-60.3	0.6-5.3	1.3-3.2
Spl-Opx	37.8-51.4	40.6-49.3	1.0-14.9	0.2-3.6
Less magnesian samples				
Spl-Grt	47.7-52.8	41.7-47.9	1.9-2.8	1.3-3.7
Spl-Opx	55.0-69.6	23.3-35.5	1.5-3.1	1.9-7.1

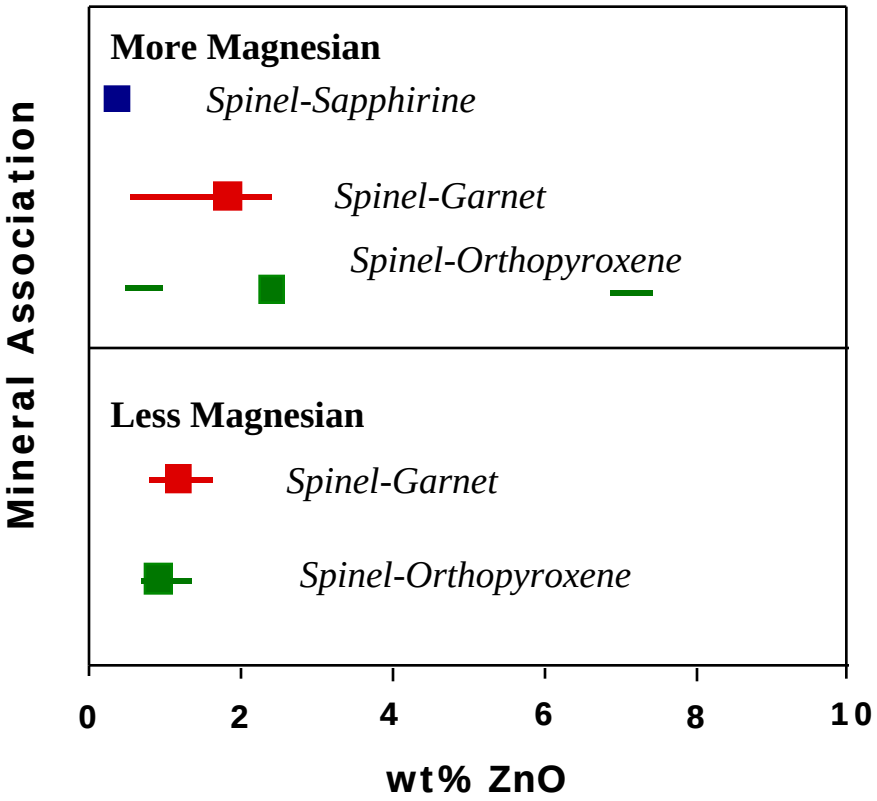

Figure 12. Spinel ZnO contents. Spinels next to sapphirines have the lowest zinc. Spinels next to garnets and orthopyroxenes have increasing amounts of zinc. The bimodality of spinels next to orthopyroxene in the more magnesian samples is attributed to the chemical difference between samples 77063 and SH-21. Greater concentration of ZnO is found in sample 77063. The higher-Zn end of the range of spinels next to garnet in this sample group is also from 77063. This sample also contains the lowest percentage of the spinel-sapphirine grain boundary.

Table 5.

Average Weight Percent ZnO in Spinels by Sample Number

Spinels-Sapphirines

Sample No.	wt % ZnO
SH-22	0.36
SH-21	0.52

Spinels-Garnets

More Magnesian		Less magnesian	
Sample No.	wt % ZnO	Sample No.	wt % ZnO
SH-22	0.35	SH-14	1.18
77063	2.56		

Spinels-Orthopyroxenes

More Magnesian		Less magnesian	
Sample No.	wt % ZnO	Sample No.	wt % ZnO
77063	6.92	SH-14	1.00
SH-21	0.61	SH-10	0.84

Manganese contents of spinels were also studied in an attempt to explain preference between spinel-garnet and spinel-orthopyroxene grain boundaries. Spinels next to garnets contain an average of 0.07 wt% MnO and those next to orthopyroxene 0.23 wt% MnO in less magnesian samples. In more magnesian samples spinels contain an average of 0.11 wt% MnO next to garnet and 0.42 wt% MnO next to orthopyroxene.

Spinels generally contain less than 5 wt% Fe_2O_3 (Figure 13.). In more magnesian bulk compositions, the spinel-garnet association has an average spinel composition slightly higher in Fe_2O_3 than the other two assemblages. The spinel-orthopyroxene assemblage shows a greater range of spinel compositions. In the less magnesian bulk compositions, spinels next to garnet and orthopyroxene are very similar in ferric iron concentration, except for a single spinel analysis, which has 6.78 wt% Fe_2O_3. Relative ferric iron contents may also be shown by using ferric/ferrous ratios (Figure 14). Spinels adjacent to garnet in the less magnesian samples have a lower average ferric/ferrous ratio than in the other two assemblages. One outlier occurs within ferric/ferrous ratios in the spinel-

orthopyroxene assemblage in each bulk composition group (0.99 in the more magnesian and 0.81 in the less magnesian). Within the spinel sampled, there are inclusions of Fe-Ti oxides not exposed at the surface, but probably within the analytical volume of the probe spot. The analysis of this grain may have been slightly affected by these inclusions causing the higher ferric iron content.

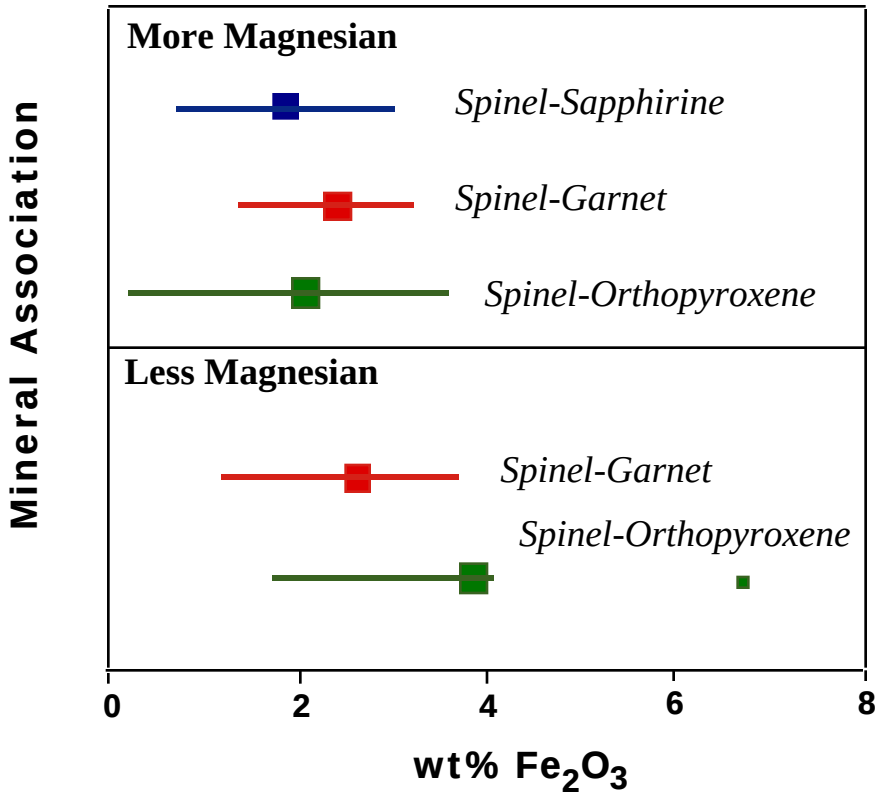

Figure 13. Ferric iron content of spinels based on calculated wt% Fe_2O_3. Ferric iron content is generally less than 5 wt%. The outlier is apparently caused by an area of Fe-Ti oxide inclusions not exposed at the surface of the section, but which may have been within the analytical volume of the probe spot.

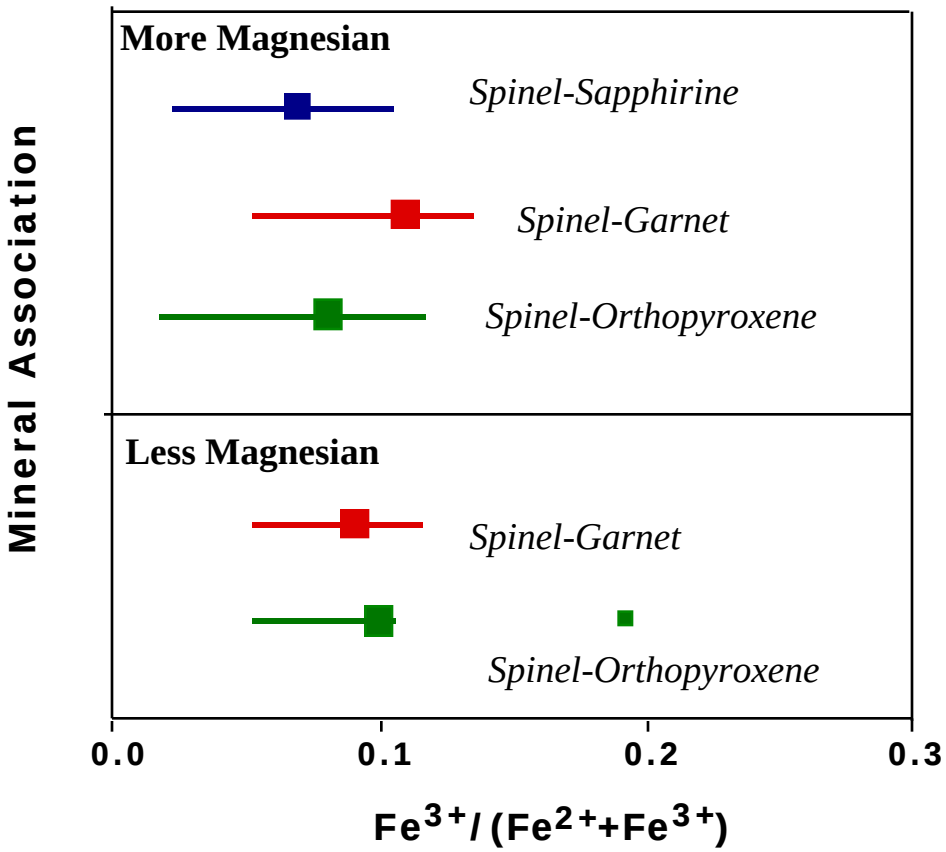

Figure 14. Ferric iron content of spinels shown in terms of ferric/ferrous ratios. Spinels next to garnet in the more magnesian samples have a slightly higher ratio of ferric iron to total iron. However, these changes are very small and therefore probably not significant.

Sapphirine only occurs within more magnesian samples and contains about 3wt% calculated Fe_2O_3 on average. This contrasts with approximately 10 wt% FeO, indicating that roughly 25% of total iron in sapphirine is ferric. According to the formula basis of 10 cations and 20 oxygens, sapphirine analyses fall close to the model composition of $(Fe^{2+}, Mg)_4Al_8Si_2O_{20}$, assuming that Fe^{3+} replaces Al.

Garnets within more magnesian samples contain 41.7-55.2 mol% Almandine and 37.8-49.7 Mol% Pyrope with less than 10% total Grossular and Spessartine. Spessartine component is approximately 4.5 mol% in more magnesian samples. Garnets within the less magnesian samples contain 57.9-66.1 mol% Almandine and 27.5-36.5 mol% Pyrope with less than 6% total Grossular and Spessartine. Spessartine averages 2.2 mol% in less magnesian samples.

Orthopyroxene also occurs in both more and less magnesian sample groups and consists mostly of enstatite (50.2 mol% in the more magnesian group and 45.9 mol% in the less magnesian) and ferrosilite (21.2 mol% in the more magnesian and 26.4 mol% in the less magnesian). Approximately 10 wt% Al_2O_3 is present in the orthopyroxenes which are unusually aluminous (reflecting both the highly aluminous environment and the high temperature). Tschermak component occurs in relatively high concentrations within both groups of samples. Total Fe- and Mg- Tschermak contents are 17.3 and 19.1 mol% for more and less magnesian samples, respectively. Estimated ferri-Tschermak substitution also occurs, but to a lesser extent: 9.1 mol% in the more magnesian and 7.1 mol% in the less magnesian.

Fe# [$Fe^{2+}/(Fe^{2+}+Mg)$] of spinel varies with which mineral is adjacent. Spinels adjacent to sapphirine have an Fe# range of 0.41-0.56 (range of Fe# of adjacent sapphirine is 0.23-0.27). Spinel inclusions within garnets are significantly more magnesian due to reaction partitioning, and have Fe# from 0.36-0.47 (the enclosing adjacent garnets have Fe# from 0.46-0.58). Orthopyroxenes with Fe# of 0.27-0.33 contain spinel inclusions with Fe# from 0.48-0.56. Within less magnesian samples, variations also occur. Spinels adjacent to garnets have a range of Fe# from 0.51-0.57. Spinels adjacent to orthopyroxenes show a range of Fe# from 0.64-0.76. Fe# for garnet in these samples has a range of 0.61-0.67 and for orthopyroxenes the range is 0.36-0.39. The results for spinel compositions are shown in Figure 15.

Table 6 lists Fe# for the spinels and immediately adjacent silicates (shown graphically in Figures 16 a and b). Variations in composition occur not only between the more and less magnesian bulk compositional groups and different adjacent minerals, but also, in some instances, between different samples within the same bulk chemical group and even in different areas of the same section regardless of adjacent mineral. For example, for spinels next to garnet in more magnesian samples, the spinel Fe# for areas in thin section SH-22 is 0.47. In sample 77063 there are two separate compositions in area 8

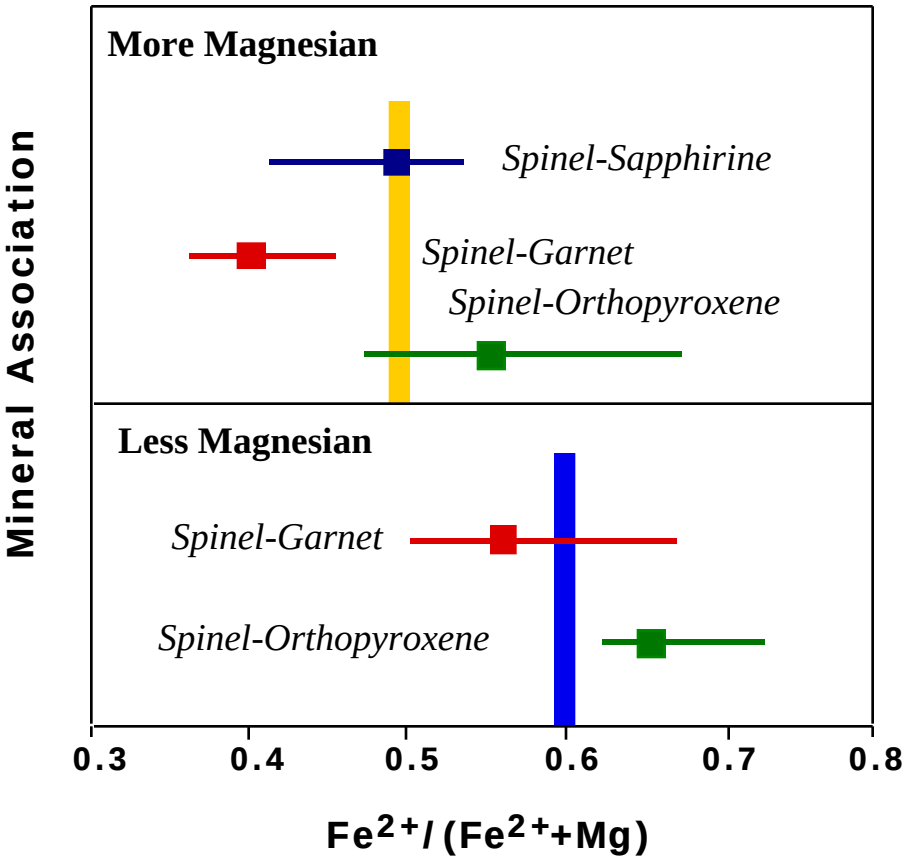

Figure 15. Fe#'s in spinels next to sapphirines, garnets, and orthopyroxenes in more and less magnesian samples. Spinels that occur next to garnet have a lower Fe# than those next to sapphirine or orthopyroxene. The vertical bars denote the average matrix spinel composition as found by Tracy and McLellan (1985).

Table 6.

Spinel and Adjacent Silicate Fe#'s

Spinels-Sapphirines

Spinels Sample #	Fe#	Sapphirines Sample #	Fe#
SH-22	0.50	SH-22	0.24
SH-21	0.52	SH-21	0.26

Spinels-Garnets

More Magnesian Samples

Spinels Sample #	Fe#	Garnets Sample #	Fe#
SH-22	0.47	SH-22	0.58
77063	0.38	77063	0.48
Area 2	0.37	Area 2	0.48
Area 8	0.41	Area 8	0.49

Less Magnesian Samples

Spinels Sample #	Fe#	Garnets Sample #	Fe#
SH-14	0.54	SH-14	0.64
Area 2	0.57	Area 2	0.66
Area 5	0.52	Area 5	0.63

Spinels-Orthopyroxenes

More Magnesian Samples

Spinels Sample #	Fe#	Orthopyroxenes Sample #	Fe#
SH-21	0.54	SH-21	0.31
77063	0.51	77063	0.27

Less Magnesian Samples

Spinels Sample #	Fe#	Orthopyroxenes Sample #	Fe#
SH-10	0.66	SH-10	0.39
SH-14	0.70	SH-14	0.38

the Fe# is 0.41, however, in area 2 the Fe# is 0.37. Fe# in garnet also changes from 0.58 in sample SH-22 to an average of 0.48 in sample 77063. Garnet Fe# does not illustrate as drastic a change within the same samples as Fe# within spinels. This can also be observed in spinels and garnets in less magnesian samples. These variations are not found within the spinels next to sapphirines or orthopyroxenes in their respective bulk compositions.

Figures 16a and b. illustrate the compositional relationships of all minerals in the Al_2O_3-FeO-MgO ternary chemographic diagram and emphasize the differences between minerals of the two bulk chemical groups in this compositional space. The "tielines" shown for these samples are actually projected tieplanes in three dimensions with the fourth apex being silica increasing vertically. The spinel-orthopyroxene tielines are located at higher silica contents than spinel-garnet tielines. The apparent crossing of these tielines is

More Magnesian Compositions

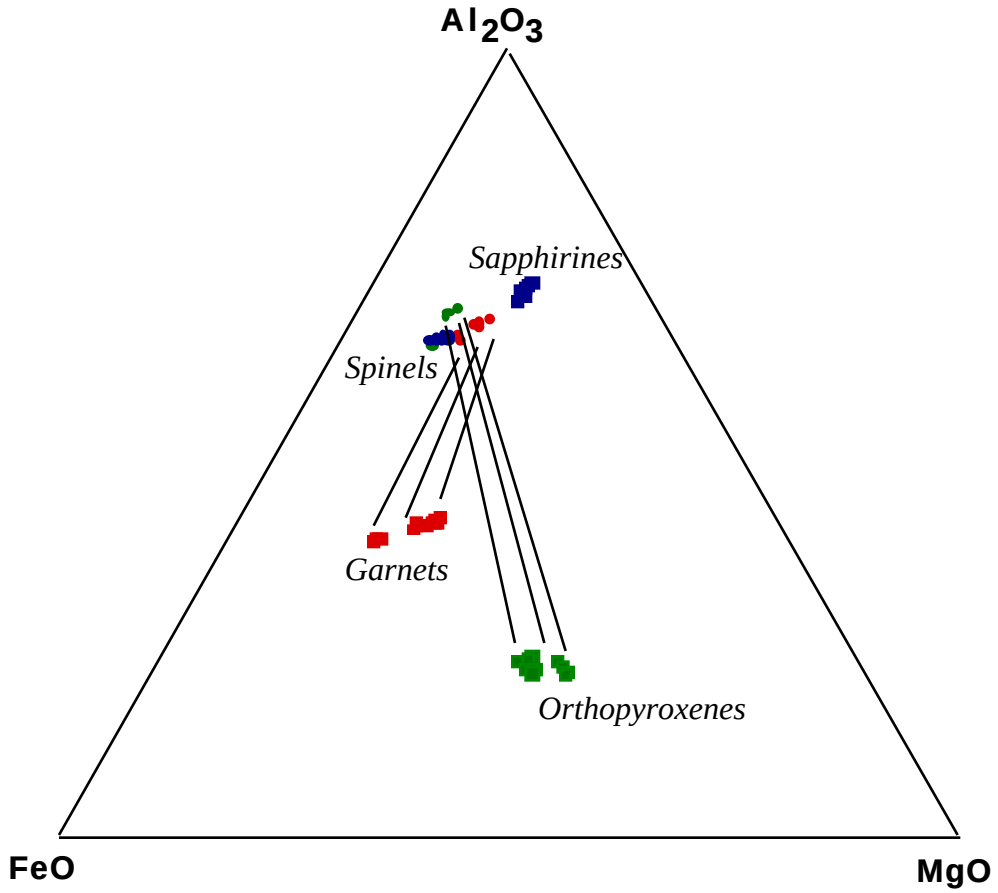

Figure 16.a. FeO-MgO-Al_2O_3 ternary plot of spinels, sapphirines, garnets, and orthopyroxenes in more magnesian samples. Garnet has a higher Fe# than the other silicates. Among silicates the decreasing order of $Fe^{2+}/(Fe^{2+}+Mg^{2+})$ is garnet>orthopyroxene>sapphirine, which agrees with Harley (1984) and Henson (1986). Fe# is based on Fe^{2+} calculated from probe analyses based on stoichiometry and charge balance.

Less Magnesian Compositions

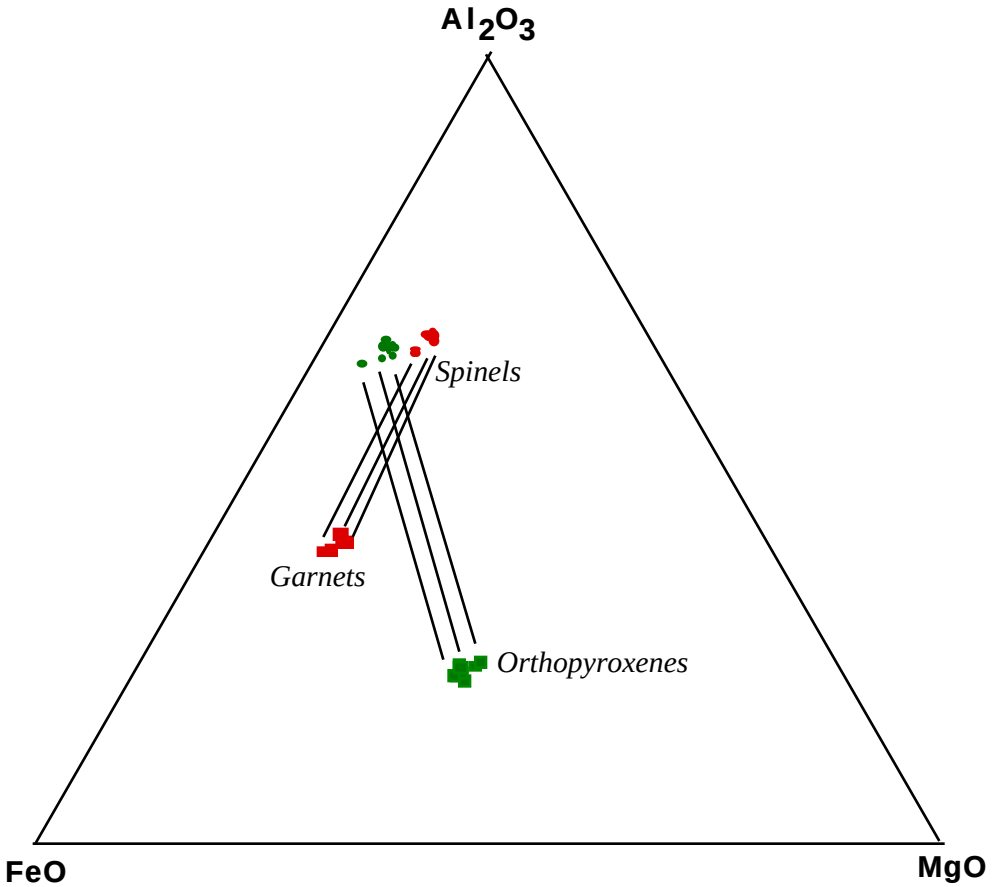

Figure 16.b. FeO-MgO-Al_2O_3 ternary plot of spinels, sapphirines, garnets, and orthopyroxenes in less magnesian samples. The chemical relationships among the minerals are the same as those within 16.a. However, these samples contain no sapphirine and the compositions are shifted toward the FeO corner of the diagram.

actually not occurring because they occupy different areas in tetrahedral space. Samples from the less magnesian compositional group show a shift toward the FeO corner of the diagram, indicating generally higher Fe# of minerals within these samples. Spinel compositions group together in much the same way within each sample group: spinels next to orthopyroxene have higher Fe# than those adjacent to garnet, and spinel inclusions in garnet are more magnesian (due to the reaction partitioning effect). Garnet has higher Fe#

than either orthopyroxene or the adjacent spinel. Orthopyroxene is more magnesian than all other minerals except for sapphirine (16a).

INTERPRETATIONS AND DISCUSSION

Statistical Analysis

Within the Salt Hill emery samples examined in detail, spinel-orthopyroxene is the most abundant grain boundary relationship. In four of the six samples studied, SH-10, SH-14, SH-21, and SH-25, this relationship was found to be the most frequent. The other two samples, SH-22 and 77063, have spinel-garnet as the most frequent grain boundary. Sample 77063 should not be included in total statistics for the emeries, but, as will be shown in later sections, it can however be used as a comparison to show different chemical environments where these different grain boundary relationships occur. The low variation ratio in less magnesian samples indicates that spinel-orthopyroxene is close to being the only occurrence and this can be seen in the bar graphs presented earlier. Other individual thin sections and the total section count shows that the mode is not the only occurrence, however, but the distribution is not even. More magnesian samples show a more even distribution than less magnesian ones. The mode also is not the same within all samples (the mode is spinel-garnet in samples SH-22 and 77063 and SH-22 does not even contain orthopyroxene). The total number of samples gives an uneven distribution of mineral assemblages, but again the occurrence most often observed is spinel-orthopyroxene.

Of the reaction steps observed within the samples (spl-->spr, spl-->grt, spl-->opx), it is interesting to note that the most frequent occurrence is that of spinel-orthopyroxene. This is the occurrence that represents the reaction requiring the greatest amount of introduced silica to occur, as shown in the reaction steps observed. The spinel-sapphirine and sapphirine-garnet steps have both apparently been bypassed in favor of this mineral grain boundary, using the simplest silica activity model.

In the calculated contingency tables, the spinel-orthopyroxene grain boundary relationship is almost always higher than the expected value for this relationship. Only sections SH-22 and 77063 show observed values for spinel-orthopyroxene lower than the expected values. In addition, lower-than-expected values for the spinel-sapphirine boundary are actually observed in less magnesian samples (0 occurrences). All of the more magnesian samples, excluding 77063, have higher observed values of spinel-sapphirine than expected. 77063, in contrast with the less magnesian samples, does contain the spinel-sapphirine grain boundary, however the observed value is less than the expected value for that mineral relationship.

The remarkably high values for the chi-square test show that the fluctuations within the contingency tables from observed to expected are statistically significant and the mineral associations and locations are dependent on each other. These data fluctuations are not sampling error, but illustrate that the textural relations among spinel, sapphirine, garnet, and orthopyroxene observed in these sections are statistically significant. Textural aberrations from model-predicted behavior thus require petrogenetic explanation based on chemical arguments.

Mineral Chemistry

The effect of Fe-Mg Ratios and Bulk Composition

The total range of spinel compositions can be attributed to two things: original bulk composition and adjacent mineral. The original compositions inferred by Tracy and McLellan (1985) were based on matrix spinel compositions (see Introduction). Unreacted spinels located in the matrix should therefore retain compositions most closely reflecting the original bulk compositions. As spinel reacted with diffused silica to form silicate reaction rims, the product mineral or minerals should have incorporated cations from the spinel as it formed. $Fe^{2+}/(Fe^{2+}+Mg)$ ratios increase in the order cordierite, sapphirine, orthopyroxene, spinel, garnet (Harley, 1984; Henson, 1986). Therefore, garnet forming directly from

spinel will tend to fractionate the ferrous iron from spinels. Orthopyroxene and sapphirine do not incorporate Fe^{2+} as strongly as garnet does. The garnet-orthopyroxene assemblage has even been used in numerous studies as a granulite-facies geothermobarometer because of the strong Fe-Mg partitioning (Harley, 1984). Sapphirine is the most magnesian mineral and therefore does not fractionate as much Fe^{2+} as garnet does. Because garnet incorporates a greater proportion of ferrous iron than either sapphirine or orthopyroxene does, the more magnesian, reaction-depleted spinels are located adjacent to garnet.

Stability fields of solid-solution ferromagnesian minerals in activity-activity space shift in response to changes in bulk composition, i.e., to original (protolith) Fe/Mg ratios, because of the Fe-Mg partitioning between the silicates and spinel during reaction. Figure 17 is the same qualitative activity-activity diagram (slopes, however, are correct, based on model compositions of participating phases shown in the figure) shown above (Figure 4, above) that indicates the relative shifts in mineral stability due to bulk chemistry and resulting mineral chemistry (more magnesian or less magnesian compositional types). For example, due to the strong fractionation of Fe^{2+} into garnet during the garnet-spinel reaction, the stability field of garnet in the less magnesian environment will expand. In other words, as the more Fe-rich mineral, garnet is stabilized relative to spinel in these Fe-richer compositions and the spinel-garnet phase boundary therefore moves into the spinel field. Because garnet is the most Fe-rich mineral of all those discussed here, phase boundaries between garnet and the other silicates similarly move so as to expand the garnet field. The extent of shift of each boundary is a function of the extent of Fe-Mg partitioning: the greater this partitioning (e.g., between garnet and cordierite), the greater the shift. The analytical data of Tracy and McLellan (1985) and this study illustrate that in each of the two bulk chemical environments spinels next to garnet show lower Fe# (average 0.41 in the more magnesian samples and 0.54 in the less magnesian samples) than do spinels next to sapphirine (average Fe# = 0.51) or orthopyroxene (average Fe# = 0.53 in the more magnesian samples and 0.68 in the less magnesian samples). The average Fe# in garnet is

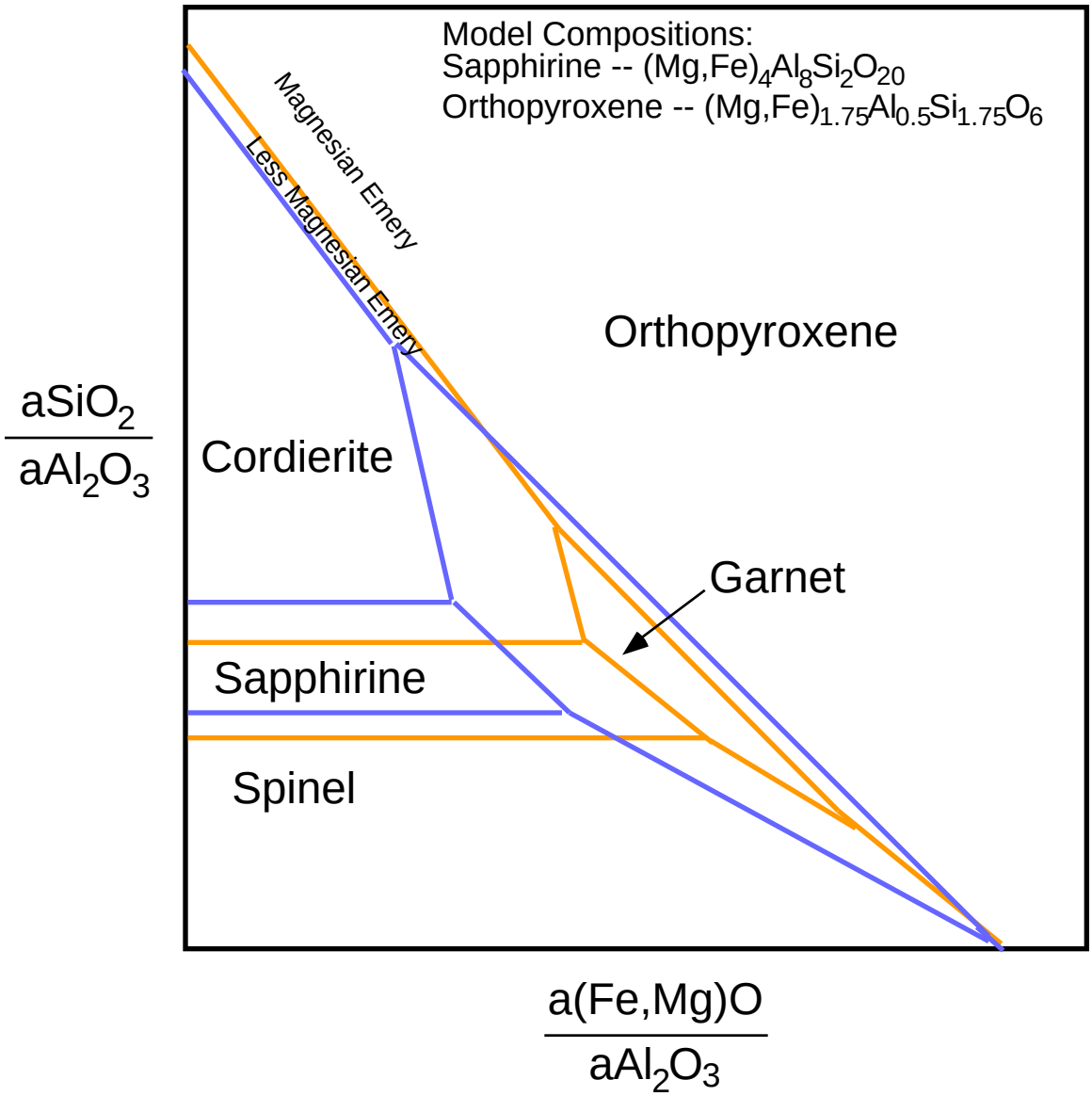

Figure 17. a(Fe,Mg)O/aAl_2O_3 vs. aSiO_2/aAl_2O_3 diagram illustrating the change in stability fields in more and less magnesian samples. As the Fe# increases, the stability of garnet increases, favoring its occurrence. The stability field of sapphirine in these environments decreases, presenting one possible explanation for the absence of sapphirine in less magnesian samples. In more magnesian environments, the stability field of garnet decreases in favor of sapphirine or orthopyroxene. See text for discussion.

0.51 (more magnesian samples) and 0.64 (less magnesian samples), compared with 0.25 in sapphirine (only in more magnesian samples) and in orthopyroxene 0.30 (more magnesian samples) and 0.38 (less magnesian).

The stability field of sapphirine also shifts between the more- and less-magnesian environments . Sapphirine stability, with specific regard to the sapphirine-garnet boundary, will expand in more magnesian samples because of the relatively strong partitioning of Mg into sapphirine relative to garnet. Also in this more magnesian environment, the stability field of spinel relative to sapphirine shrinks because of the strong partitioning of Fe into spinel relative to sapphirine. This shifts this boundary to relatively lower a(SiO_2) positions. Studies done on the stability of sapphirine by Seifert (1974) and Ackermand et al. (1987) confirm this. These earlier studies showed that rocks containing sapphirine were found in more magnesian environments and that sapphirine stability apparently decreased with increasing activity of FeO. Seifert (1974) stated that sapphirine is favored in more magnesian environments and does not occur in more ferrous ones. Similarly, the stability of cordierite decreases, but even more strongly, in less magnesian environments because cordierite is typically the most magnesian phase in an assemblage. In these less magnesian environments, therefore, the stability field of sapphirine will expand relative to cordierite (Henson, 1986). Analytical data of this study confirms Henson's observation. Fe# of spinels adjacent to sapphirine and of those adjacent to orthopyroxene are essentially the same but each is higher than spinel found adjacent to garnet. The stability field of orthopyroxene slightly expands toward lower a(SiO_2) in the less magnesian environment, specifically along the cordierite-orthopyroxene phase boundary and the spinel-orthopyroxene phase boundary. Orthopyroxene Fe# is typically intermediate between those of sapphirine and garnet.

Although silicate phase equilibrium behavior shows chemical evidence of the above relationships, other relationships are occur. The spinel-garnet grain boundary actually has a higher frequency in more magnesian samples (about 17%) compared to <10% in less

magnesian samples. Sample SH-21 does not even contain garnet. The relative change (decrease) in sapphirine stability is apparent in the less magnesian samples in the absence of sapphirine, as also noted by Seifert (1974) and Ackermand et al. (1987). In less magnesian samples the spinel-orthopyroxene grain boundary is the most common. This can be attributed in part to the slight expansion of orthopyroxene stability along the spinel-orthopyroxene phase boundary (Figure 17) within the less magnesian environment.

The effect of Zinc

When ZnO is added to the system, there are resulting shifts in the topology of the activity diagram, particularly strong shifts in the stability of spinel relative to the silicates because of the very strong partitioning of ZnO into spinel relative to all other minerals. Figure 18 shows the qualitative activity diagram seen above but modified to show the postulated relative effect as ZnO is added to the more magnesian system. Because of its bonding-orbital hybridization, Zn^{2+} strongly prefers medium to large crystallographic sites with tetrahedral coordination such as those in staurolite, spinel and sphalerite, and rarely is found in significant concentration in minerals lacking such sites, like sapphirine, garnet or orthopyroxene (Holdaway et al., 1986). The stability field of spinel will therefore expand with respect to all the silicates when ZnO is added to the system, but the slopes of the boundaries between each of the silicates will not change. The result is that in samples containing more zinc locally, the stability field of sapphirine will shrink more than those of either garnet or orthopyroxene, due to the horizontal orientation of the spinel-sapphirine boundary in the activity diagram (Figure 18). Therefore, in such Zn-rich environments the reaction from spinel to garnet, then to orthopyroxene, is favored, depending upon relative activities of (Fe,Mg)O and Al_2O_3. In more silica-rich environments, spinel will react directly to form orthopyroxene.

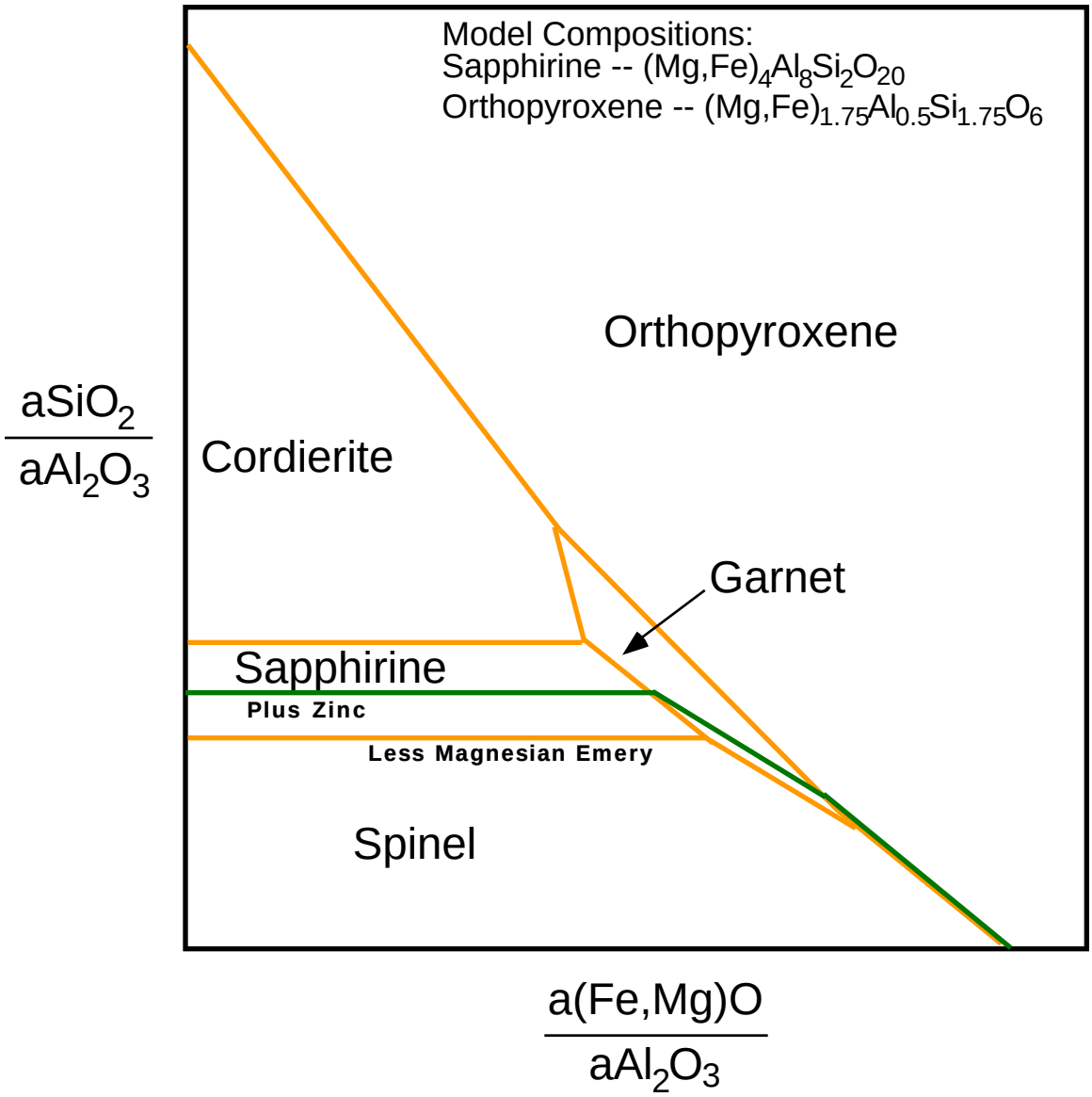

Figure 18. The effect of zinc on the $a(Fe,Mg)O/aAl_2O_3$ vs. $aSiO_2/aAl_2O_3$ diagram. According to LeChâtelier's Principle, the stability field of spinel should increase as zinc is added to the system. This activity diagram shows the qualitative effect of this increase in stability in more magnesian environments. The stability field of sapphirine decreases more than that of the other silicates. Garnet stability decreases somewhat, but the stability field of orthopyroxene actually increases slightly in the direction of lower a(Fe,MgO).

According to analytical data reported in this study, spinels located next to sapphirine have the lowest zinc concentration of all spinels (0.6-1.3 mol% Gahnite), consistent with the sapphirine stability relationships described just above. Spinels adjacent to garnet show an increased zinc concentration, as do those adjacent to orthopyroxenes. Spinels adjacent to orthopyroxene show the highest zinc, as seen in sample 77063 where in one local mineral association the Gahnite concentration is 14.9 mol%. The stability fields of garnet and orthopyroxene appear to be only slightly affected by increased zinc concentration. The highest-Zn sample, 77063 (approximately 2 wt% ZnO in spinels adjacent to garnet and 7 wt% ZnO in spinels adjacent to orthopyroxene), actually contains the least sapphirine of all the more magnesian samples.

The source of higher zinc contents in some of the emery samples cannot be unequivocally demonstrated, but almost certainly is inherited from the schist protolith. Some pelitic schists (particularly those with larger modal contents of staurolite) have been shown to have higher Zn contents that are apparently a product of a greater contribution of Zn-bearing detrital minerals in the sedimentary environment of the protolith shale. Continuing this speculation, the emery xenolith could thus be considered to have a further subdivision of bulk compositional types in which the more magnesian group could be subdivided into low- and high-Zn types which have subtle but observable effects on phase relations.

The effect of Manganese

Even a small amount of manganese will expand the stability of garnet, due to the strong partitioning of Mn into garnet. In fact, Spear and Cheney (1989) expanded upon this well known phenomenon and suggested that garnet only occurs in normal pelites because of stabilization due to inclusion of minor manganese (and to a lesser extent calcium). Their paper included a proposed petrogenetic grid for the Mn-KFMASH system in which they indicated that in the reaction sequence chloritoid + biotite = garnet + chlorite,

Mn caused product minerals garnet + chlorite to form at much lower temperatures than pure almandine-pyrope garnets in the same system. In fact, they went so far as to conclude that pure Fe-Mg garnets are metastable compared to other ferromagnesian phases within pelites at all possible metamorphic conditions.

According to the statistics of the present study, two samples of the more magnesian group have spinel-garnet as the mode for grain-boundary types. Two of this group of samples have spinel-orthopyroxene as the mode and do not even contain garnet. The mode in the two less magnesian samples is spinel-orthopyroxene, but these samples also contain the spinel-garnet grain boundary type, although at a much lower percentage than spinel-orthopyroxene. The average spessartine component in garnet in the samples containing spinel-garnet as the mode is approximately 2.5 mol% greater than in the less magnesian samples containing less garnet. Examination of the compositions of spinels indicated that MnO contents of spinels adjacent to garnet were depleted due to Mn fractionation into garnet. (Less magnesian samples contain spinels with an average of 0.07 wt% MnO next to garnet and 0.23 wt% MnO next to orthopyroxene. More magnesian samples contain 0.11 wt% MnO in spinels next to garnet and 0.42 wt% MnO in spinels next to orthopyroxene.) However, because of the variety of possible variables that might affect Mn contents (e.g., unusually high temperature compared to a normal metamorphic temperature range of 450˚C to 700°C, an anomalously high pyrope content in garnet), it is not possible at this point to conclude anything definite about the effect of manganese in emery compared to its effect in normal pelitic schists.

The effect of Oxygen Fugacity

Because of solid solution toward Fe^{3+}-bearing end members in several of the minerals in the emery samples (e.g., spinel, orthopyroxene, sapphirine), it is possible that minor variations in oxygen fugacity (fO_2) may have had an effect on the assemblages that involve any of these minerals (Henson, 1986). Such variations could obviously also have

caused shifts in a key bulk chemical parameter of this study, Fe#. For example, it is possible that the more magnesian bulk compositions represent not environments originally richer in Mg, as proposed by Tracy and McLellan (1985), but ones locally higher in fO_2, because Fe^{2+} would have been oxidized to Fe^{3+} and thus lowered in calculation of Fe#. In the less magnesian environments, the Fe# would be higher because of the increase in Fe^{2+} in the less oxidized environments.

To illustrate how this may have affected mineral assemblages in the Salt Hill emeries, notice that on the activity diagrams presented in sections above that the spinel-orthopyroxene boundary is located on the far right of the diagram. The bulk a(Mg,Fe)O/a Al_2O_3 would have been higher in the lower fO_2 environments, where a greater proportion of iron is in the Fe^{2+} state. The higher the ratio a(Mg,Fe)O/a Al_2O_3, therefore, the more likely that spinel would react directly to orthopyroxene upon silication. Greater conversion of Fe^{2+} in the system to Fe^{3+} would lower the activity ratio and therefore favor direct reactions of spinel to garnet or spinel to sapphirine in higher-fO_2 environments.

Henson (1986) pointed out that when the coexisting phases cordierite, sapphirine, hypersthene, garnet, spinel, sillimanite and quartz are present in a system, increasing fO_2 from the FMQ to HM buffers produces topologic inversions of reaction sequence in P-T space (Figure 19.). At low fO_2, spinel-sapphirine-quartz coexist at temperatures greater than 1000˚C. Increasing fO_2 increases the stability field of spinel (based on the greater solubility of Fe^{3+} in spinel than sapphirine). Caporuscio and Morse (1978) found the fO_2 of the Salt Hill emeries to be very near the hematite-magnetite buffer. At 1000˚C, log fO_2 would be approximately equal to -5 along this buffer (Figure 20, modified from Buddington and Lindsley, 1964). However, the solid solution toward ilmenite in rhombohedral oxide in the emery (roughly 30mol% ilm in the hem-ilm solid solution) would shift the actual fO_2 from HM to a slightly lower value, but probably not more than a few tenths of a log unit at most.

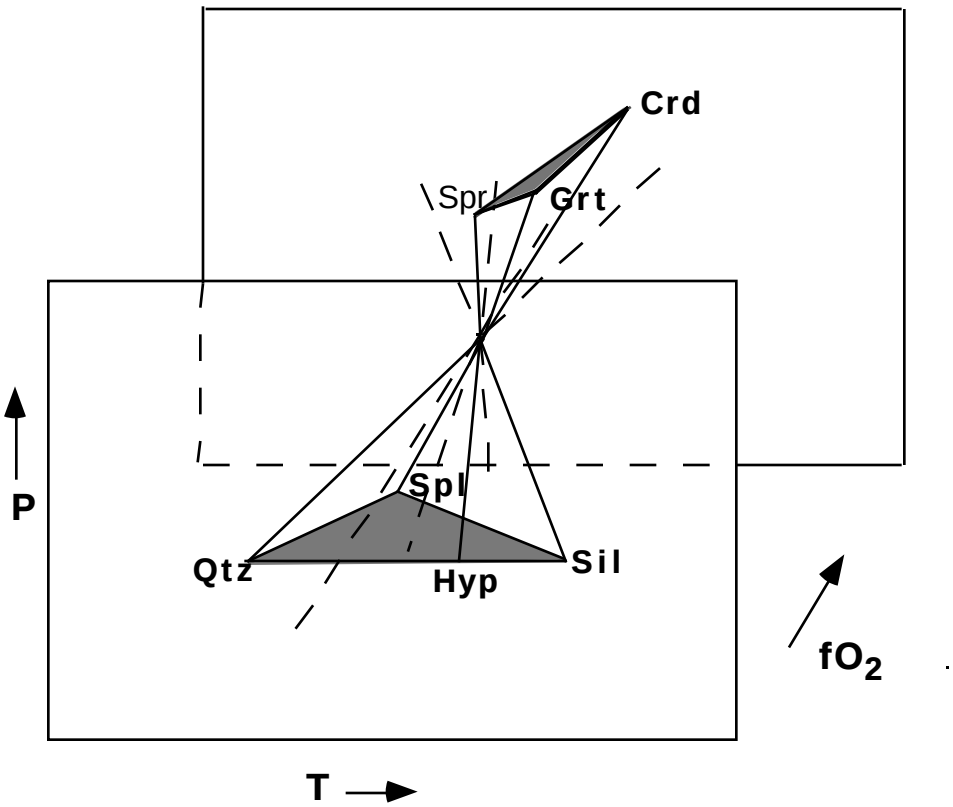

Figure 19. Three dimensional view of phase relations in P-T-fO_2 space (from Henson, 1986). Note change in topology of P-T sections as a function of fO_2. At low fO_2 the invariant points [Hyp][Spl][Sil] and [Qtz] (hypersthene, spinel, sillimanite, and quartz) are stable. At high fO_2 [Spr][Grt] and [Crd] (sapphirine, garnet, and cordierite) are stable. Stable portions are shown as heavy lines, metastable extensions are dashed. All phases in the system stably coexist at an invariant point at a unique P, T, and fO_2.

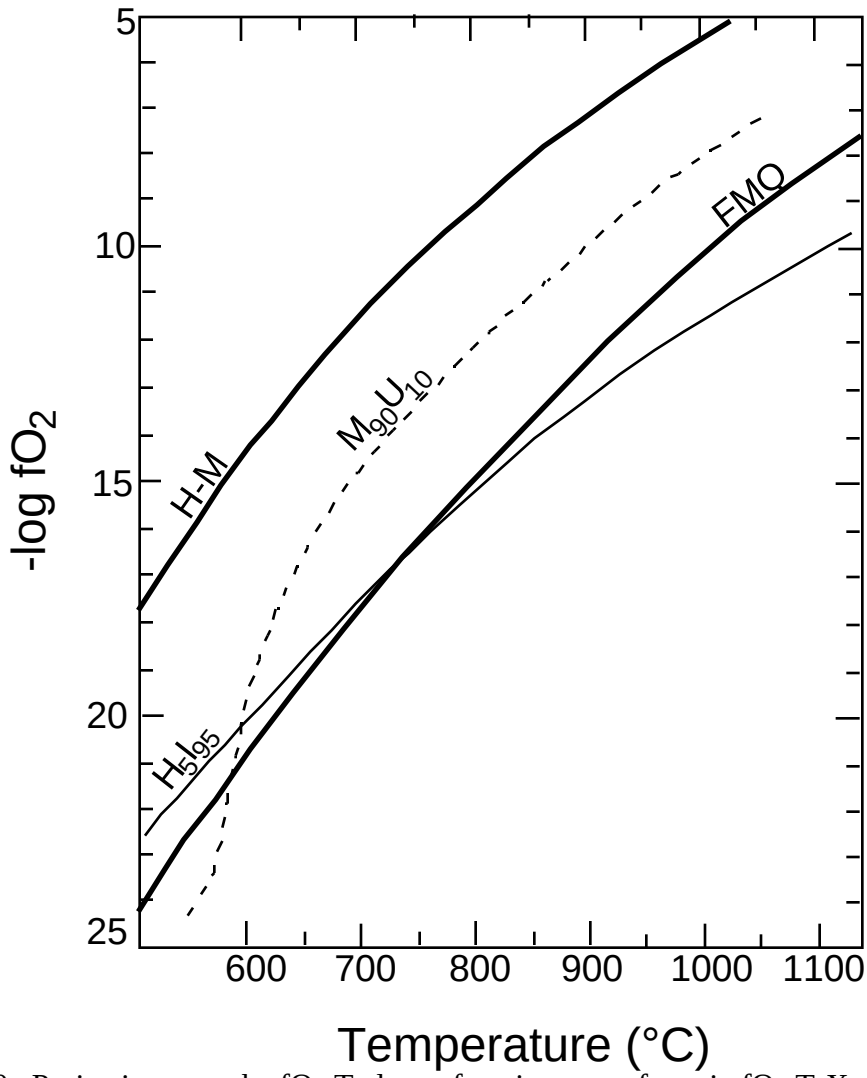

Figure 20. Projection onto the fO_2-T plane of conjugate surfaces in fO_2-T-X space. Compositions are in mole percent. The Salt Hill emeries are at approximately 1100°C and log fO_2 of -5 if they lie on the hematite-magnetite buffer. Lower oxygen fugacity conditions for the emeries would be indicated by higher ilmenite and ulvospinel in solid solution with hematite and magnetite. See text for discussion. (Adapted from Buddington and Lindsley, 1964).

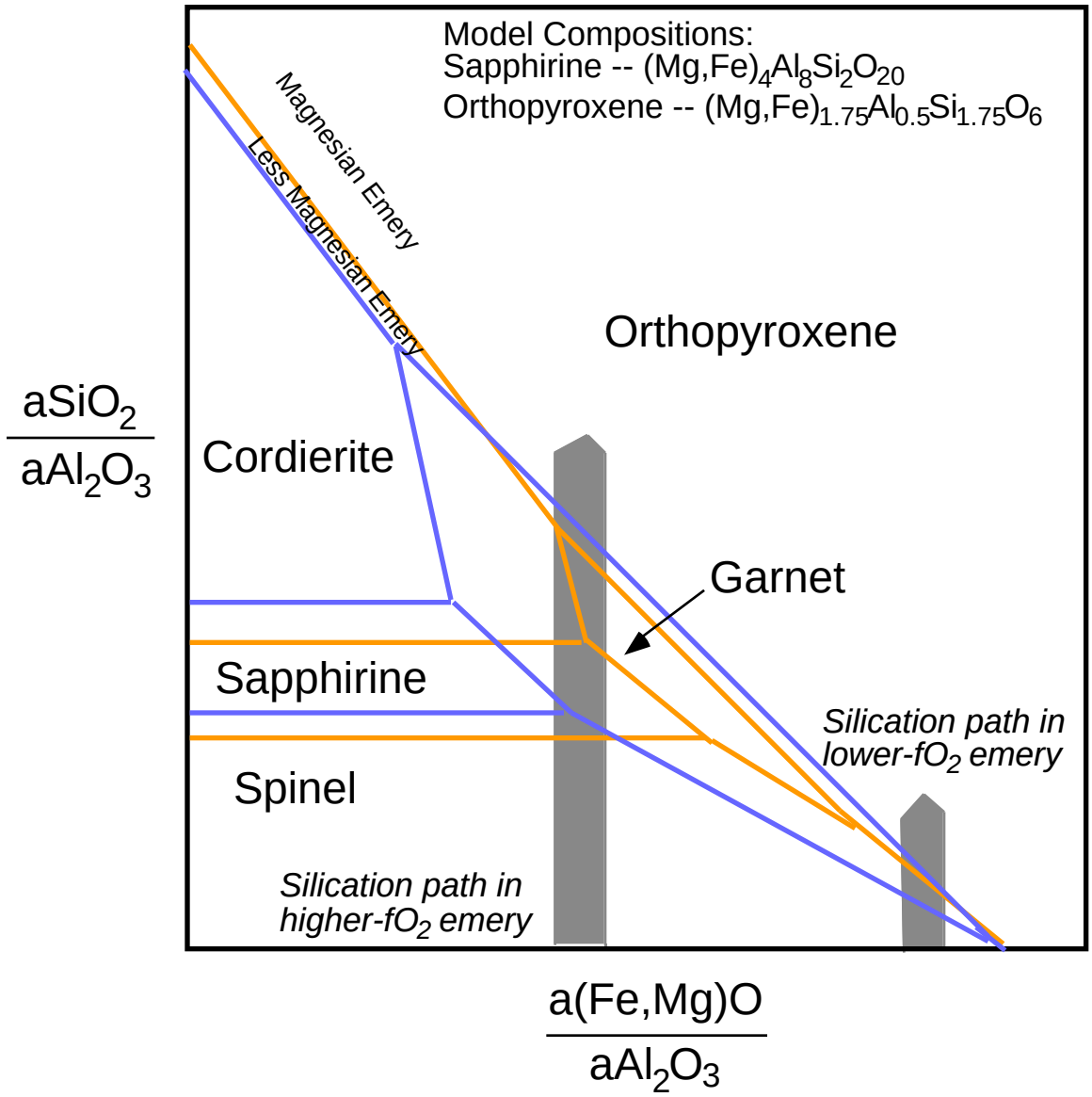

Figure 21. The possible effect of oxygen fugacity. The activity diagram predicts that in lower fO_2 environments spinel will react directly to orthopyroxene because of the increase in activity of (Fe,MgO), which is caused by an abundance of Fe^{2+}. As the fO_2 increases and Fe^{2+} is oxidized to Fe^{3+} the reaction will move to the left as the a(Fe,Mg)O decreases in favor of the reaction of spinel to sapphirine.

The above discussion of the effects of oxygen fugacity on this system is consistent with the textural observations. Sapphirine, for example, only occurs in more magnesian environments (this study and Seifert, 1974). Spinels next to sapphirine have an upper limit of Fe# at 0.56 and the highest Fe# within sapphirine is 0.27. It also is the silicate which incorporates the most Fe^{3+} in its structure. The amount of Fe^{3+} is simply dictated by the bulk composition and thus should decrease in lower-fO_2 environments. In less magnesian environments, spinel-orthopyroxene boundaries occur far more frequently than spinel-garnet and sapphirine does not occur at all. Here, the fO_2 is probably lower because the Fe# is higher (although this is by no means guaranteed). In such environments, the a(Fe, Mg)O/a Al_2O_3 is higher and shifts the vertical silication path (and thus the reaction sequence) to the right on the activity-activity diagrams (Figure 21.).

One means to constrain the possible effects of oxygen fugacity is to examine the ferric/ferrous ratio [$Fe^{3+}/(Fe^{3+}+Fe^{2+})$] within spinels. It should be noted, however, that this ratio must be viewed with some caution because it is based on calculated rather than strictly analytical values (although error associated with the calculation of ferric iron in microprobe analyses of spinel is undoubtedly less than that for silicates), and is also a function of temperature, pressure, and bulk composition, as well as fO_2. Within the Salt Hill emery, variations in spinel ferric/ferrous ratios are not significant or systematic enough to base any conclusions on. It can only be concluded that these spinel-bearing assemblages formed within essentially the same fO_2 range. The reaction of spinel to an adjacent silicate minerals therefore might or might not have been significantly affected by oxygen fugacity.

This conclusion is obviously a bit speculative and further work should be done. For example, chemical compositions of the ilmenohematites within the emeries could show greater variation as a result of minor fO_2 shifts at high temperature than the spinel $Fe^{3+}/(Fe^{3+}+Fe^{2+})$ ratio does. However, this analysis is complicated by the extensive post-formation exsolution of the ilmenohematite solid solution into ilmenite-rich and hematite-

rich lamellae, requiring sophisticated integration of spot microprobe analyses to approximate the bulk compositions of original high-T grains.

SUGGESTIONS FOR FURTHER STUDY

Despite the constraints of the data of this study on the details of the formation of the Salt Hill emery deposit, there are still questions to be addressed. The effects of zinc and manganese on sapphirine stability have been superficially examined, but more specifically targeted analytical data is required to make firm conclusions about the roles of these minor components on the formation of orthopyroxene *versus* garnet or sapphirine during silication of spinel. Although the preliminary data on the effects of Mn in this study are limited by the lack of garnet within key samples of the more magnesian group, variations in Mn do not appear to explain the predominance of orthopyroxene in four out of six samples.

Oxygen fugacity almost certainly had an effect on the phase relationships, but without further statistical and chemical analysis (probably including very detailed integrative mineral modal analysis of ilmenohematite by point counting), the actual effect of fO_2 on the relative stabilities of the oxide-silicate assemblages cannot be specified. Additional work is required to specify relatively accurate values for P and T. Some investigation of P-T location of reactions and other equilibria was attempted using the thermodynamic database computer program, TWEEQU (Berman, 1991). Unfortunately the reaction sequences observed in the emeries are not amenable to study using this software due to unavailability of well constrained thermochemical data on key mineral solid solutions, notably sapphirine and aluminous orthopyroxene.

In summary, although data collected in this study leave gaps in explaining the emery-forming process, it can be stated with some certainty that a simple progressive-silication model alone (such as Friedman's "spinel-silica reaction succession" , 1956: spinel reacting directly to sapphirine, sapphirine to garnet and garnet to orthopyroxene) cannot explain the reaction textures observed in the Salt Hill emeries. Bulk composition,

specifically Fe#, has an obvious effect on the phase equilibria, with increased stability of garnet in Fe^{2+}-richer compositions and decreased stability of sapphirine in these less magnesian environments. The effect of Zn appears to be to decrease the stabilities of both sapphirine and garnet relative to spinel, while having less effect on that of orthopyroxene, but the issue clearly needs further examination. The effect of Mn is a similarly promising possible solution for the somewhat sporadic presence of garnet, but Mn cannot yet be pinned down as the culprit in samples with dominance of spinel reacting to garnet.

SUMMARY

Special, non-random mineral textural associations within the examined xenolith of the Salt Hill emery deposit have proven to be statistically significant. Correlations of these textures with chemical compositions of the minerals have been attempted. Despite an operating hypothesis that the silicate minerals formed as a result of silication of a highly aluminous protolith, the dominant mode in most samples is the spinel-orthopyroxene boundary, which is not expected because it apparently oversteps several intermediate reaction steps and requires the largest increase in activity of silica to produce. Contingency table analysis and a high chi-square test value further illustrate that the mineral grain boundary relations counted are significant. Silica activity therefore cannot be the only variable involved in controlling reactions and producing these different grain boundary relationships: some other variable or variables must be involved.

The data illustrate that one of the variables controlling the reaction of spinel to each of the three silicates is Fe# ($Fe^{2+}/(Fe^{2+}+Mg^{2+})$). As the proportion of ferrous iron increases, the stability field of garnet (as shown in activity diagrams) expands due to the preferential fractionation of Fe^{2+} into garnet relative to the other silicates. Consequently, spinels located adjacent to garnet (or especially small spinel inclusions within garnets) show lower Fe# than those adjacent to the other silicates due to strong Fe depletion during garnet formation. Garnet formed in place of sapphirine as the first product of spinel

silication in compositions higher in Fe#. The stability of garnet in high-Fe# environments especially expanded at the expense of sapphirine, so sapphirine formed almost exclusively in the more magnesian environments. The general distinction between the range of Fe# that supports spinel to sapphirine and that which supports spinel to garnet must clearly be a complex function of variables, but fortunately in the Salt Hill emeries, the shift in behavior falls conveniently right between the two principal compositional types observed. Sapphirine does not even form in the less magnesian compositions, which has also been found by Seifert (1974) and Ackermand, et al. (1987), in regional metamorphic granulite facies rocks.

The effects of minor components on the phase equilibria may be significant. Zn expands the stability field of spinel since none of the silicates can incorporate it to any extent (as indicated by the microprobe data). This increased spinel stability affects (decreases) sapphirine stability more than those of garnet or orthopyroxene, thus requiring a greater increase in silica activity for sapphirine to form directly from spinel in local environments higher in Zn. In fact, the data shows that in sample 77063, where zinc is found in the greatest concentration, the modal percentage of sapphirine is much lower than in the other more magnesian samples. Orthopyroxene occurs in samples with the highest Zn, emphasizing that Zn barely affects its stability field.

The effect of Mn was also examined. Garnet stability should expand as manganese content within the rock increases, thus causing spinel to react directly to garnet instead of to orthopyroxene. Spear and Cheney (1989) suggested that in normal pelites, garnet should not even form unless Mn is present in the bulk composition. Although garnets within more magnesian samples contain slightly more Mn (average 4.5 mol% spessartine) than those within the less magnesian samples (average 2.2 mol% spessartine), there is not, at this time, enough data to conclude that there is no garnet at all in two samples of the more magnesian group because the Mn concentration is too low.

Control of phase relations by fO_2 was also examined, but not enough information had been collected to allow accurate determination of the effect of this intensive parameter. Further study of the compositions of Fe-Ti oxide minerals magnetite and ilmenohematite is required to constrain fO_2 conditions precisely, although it is clear that the substantial modal proportions of magnetite (virtually pure Fe_3O_4) and ilmenohematite (Ilm30Hem70) point to fO_2 conditions very close to the Hematite-Magnetite buffer. It is plausible that subtle local changes in oxygen fugacity below the HM buffer (within a few tenths of a log unit in fO_2) may have caused (or at least contributed to) the observed divergence from an expected reaction sequence.

The conclusions of this study explain why sapphirine does not appear, or its stability is decreased in environments with increasing iron and zinc contents, but it cannot yet be proven why garnet formed instead of orthopyroxene or vice versa. Further work is required to determine this, including more targeted study of the effects of oxygen fugacity and the minor components such as Zn and Mn, and more specific constraint on temperature and pressure of the observed silicate-forming reactions.

REFERENCES

Ackermand, D., Herd, R.K., Reinhardt, M., and Windley, B.F., 1987. Sapphirine parageneses from the Caraiba complex, Bahai, Brazil: the influence of Fe^{2+}-Fe^{3+} distribution on the stability of sapphirine in natural assemblages: Journal of Metamorphic Geology, v. 5, pp. 323-339.

Barker, F., 1964. Reaction between mafic magmas and pelitic schist, Cortlandt, New York: American Journal of Science, v. 262, pp. 614-634.

Bender, J.F., Hanson, G.N., and Bence, A.E., 1984. Cortlandt Complex: differentiation and contamination in plutons of alkali basalt affinity: American Journal of Science, v. 284, pp. 1-57.

Benimoff, A.I. and Sclar, C.B., 1984. Coexisting silicic and mafic melts resulting from marginal fusion of a xenolith of Lockatong Argillite in the Palisades Sill, Graniteville, Staten Island, New York: American Mineralogist, v. 69, pp. 1005-1014.

Berman, R.G., 1991. Thermobarometry using multiequilibrium calculations: a new technique with petrologic applications: Canadian Mineralogist, v. 29, pp. 833-855.

Brearly, A.J., 1987. An experimental and kinetic study of the breakdown of aluminous biotite at 800°C: reaction microstructures and mineral chemistry: Bulletin de Mineralogie, v. 110, pp. 513-532.

Budding ton, A.F., and Lindsley, D.H., 1964. Iron-titanium oxide minerals and synthetic equivalents: Journal of Petrology, v. 5, pp. 310-357.

Caporuscio, F.A., and Morse, S.A., 1978. Occurrence of sapphirine plus quartz at Peekskill, New York: American Journal of Science, v. 278, pp. 1334-1342.

Cheeney, R.F., 1983. Statistical Methods in Geology, Ch. 1,3. London: George Allen & Unwin.

Domenick, M.A., and Basu, A.R., 1982. Age and origin of the Cortlandt Complex New York: Implications from Sm-Nd data: Contributions to Mineralogy and Petrology, v. 79, pp. 290-294.

Finger, L.W., 1972. The uncertainty in the calculated ferric iron content of a microprobe analysis: Year Book- Carnegie Institution of Washington, v. 71, pp. 600-603.

Friedman, G.M. 1956. The origin of spinel-emery deposits with particular reference to those of the Cortlandt Complex, New York: New York State Museum Bulletin 351, 68p.

Ghiorso, M.S., and Carmichael, I.S.E., 1981. A FORTRAN IV computer program for evaluating temperatures and oxygen fugacitites from the compositions of coexisting iron-titanium oxides: Computers and Geosciences, v. 7, pp. 123-129.

Grapes, R.H., 1986. Melting and thermal reconstitution of pelitic xenoliths, Wehr Volcano, East Eifel, West Germany: Journal of Petrology, v. 27, pp. 343-396.

Goldstein, J.L., Romig, A.D. Jr., Newbury, D.E., Lyman, C.E., Echlin, P., Fiori, C., Joy, D.C., and Lifshin, E., 1992. Scanning electron microscopy and x-ray microanalysis, a text for biologists, materials scientists, and geologists. Ch. 9, pp. 417-436. New York: Plenum Press.

Hames, W.E., Tracy, R.J., Ratcliffe, N.M., and Sutter, J.F., 1991. Petrologic, structural, and geochronologic characteristics of the Acadian metamorphic overprint on the Taconide zone in part of Western New England: American Journal of Science, v. 291, pp.887-913.

Harley, S.L., 1984. An experimental study of the partitioning of Fe and Mg between garnet and orthopyroxene: Contributions to Mineralogy and Petrology, v. 86, pp. 359-373.

Henson, B.J., 1986. Theoretical phase relations involving cordierite and garnet revisited: the influence of oxygen fugacity on the stability of sapphirine and spinel in the system Mg-Fe-Al-Si-O: Contributions to Mineralogy and Petrology, v. 92, pp. 362-367.

Holdaway, M.J., Dutrow, B.L., and Shore, P., 1986. A model for the crystal chemistry of staurolite: American Mineralogist, v. 71, pp. 1142-1159.

Ratcliffe, N.M., Bender, J.F., and Tracy, R.J., 1983. Tectonic setting, chemical petrology and petrogenesis of the Cortlandt Complex and related igneous rocks of southeastern New York State: Northeastern Section Geological Society of America Meeting Guidebook Field Trip 1.

Seifert, F., 1974. Stability of sapphirine: a study of the aluminous part of the system $MgO-Al_2O_3-SiO_2-H_2O$: Journal of Geology, v. 82, pp. 173-204.

Spear, F.S., and Cheney, J.T., 1989. A petrogenetic grid for pelitic schists in the system $SiO_2-Al_2O_3-FeO-MgO-K_2-H_2O$: Contributions to Mineralogy and Petrology, v. 101, pp. 1189-1201.

Tracy, R.J., 1994. Disequilibrium melting of pelitic schist xenoliths in mafic magma and formation of quartzofeldspathic microveins in aluminous residuum: Supplement to EOS, Transactions of the 1994 Spring Meeting, Baltimore, Maryland, pp.364.

Tracy, R.J., and McLellan, E.L., 1985. A natural example of the kinetic controls of compositional and textural equilibrium: in Metamorphic Reactions: Kinetics, textures, and deformation, Advances in Physical Geochemistry, v.4., pp.118-137.

van Bergen, M.J., and Barton, M., 1984. Complex interaction of aluminous metasedimentary xenoliths and siliceous magma; an example from Mt. Amiata (Central Italy): Contributions to Mineralogy and Petrology, v. 86, pp. 374-385.

Waldron, Kim, 1986. High pressure contact metamorphism in the aureole of the Cortlandt Complex, Southeast New York: PhD. Dissertation, Yale University, New Haven Connecticut, pp. 1-11.

APPENDICES

Appendix I Statistical data and Contingency Tables.

Observed Values for all Samples

	SH-21(M)	SH-22(M)	SH-25(M)	77063(M)	SH-10(F)	SH-14(F)	Total
Spl-Spr	135	76	98	14	0	0	323
Spl-Garnet	0	226	0	188	21	19	454
Spl-Opx	186	0	148	35	397	46	812
Spl-Spr-Grt	0	27	0	15	0	0	42
Spl-Spr-Opx	38	0	37	3	0	0	78
Spl-Grt-Opx	0	0	0	31	8	0	39
Spr	10	8	32	3	0	0	53
Garnet	0	148	0	161	3	4	316
Opx	26	0	54	31	70	28	209
Total	395	485	369	481	499	97	2326

Contingency Table Showing Expected Values for All Samples
Values shown in bold face are expected values lower than observed values. Values in parentheses are observed values.

Total Samples	SH-21(M)	SH-22(M)	SH-25(M)	77063(M)	SH-10(F)	SH14(F)	Total
Spl-Spr	54.85 (135)	67.35 (76)	51.24 (98)	66.79 (14)	69.29 (0)	13.47 (0)	323
Spl-Grt	77.1 (0	94.66 (226)	72.02 (0)	93.88 (188)	97.40 (21)	18.93 (19)	454
Spl-Opx	137.89 (186)	169.3 (0	128.82 (148)	167.92 (35)	174.20 (397)	33.86 (46)	812
Spl-Spr-Grt	7.13 (0	8.76 (27)	6.66 (0)	8.69 (15)	9.01 (0)	1.75 (0)	42
Spl-Spr-Opx	13.25 (38)	16.2 (0	12.37 (37)	16.13 (3)	16.73 (0)	3.25 (0)	78
Spl-Grt-Opx	6.62 (0	8.13 (0	6.19 (0)	8.06 (31)	8.37 (8)	1.63 (0)	39
Spr	9.00 (10)	11.0 (8	8.41 (32)	10.96 (3)	11.37 (0)	2.21 (0)	53
Grt	53.6 (0	65.89 (148)	50.13 (0)	65.35 (161)	67.79 (3)	13.18 (4)	316
Opx	35.4 (26	43.5 (0	33.16 (54)	43.22 (31)	44.84 (70)	8.72 (28)	209
Total	395.0	485.0	369.00	481.00	499.00	97.00	2326

Contingency Tables Separated into More and Less Magnesian Groups. Values shown in bold face are expected values lower than observed values. Values in parentheses are observed values.

More Magnesian Samples

Mg-rich samples	SH-21(M)	SH-22(M)	SH-25(M)	77063(M)	Total
Spl-Spr	73.75 (135)	90.55 (76)	68.89 (98)	89.81 (14)	323.
Spl-Grt	94.53 (0)	116.06 (226)	88.3 (0)	115.11 (188)	414.
Spl-Opx	84.25 (186)	103.45 (0)	78.71 (148)	102.59 (35)	369.
Spl-Spr-Grt	9.59 (0)	11.77 (27)	8.96 (0)	11.68 (15)	42.
Spl-Spr-Opx	17.81 (38)	21.87 (0)	16.64 (37)	21.69 (3)	78.
Spl-Grt-Opx	7.08 (0)	8.69 (0)	6.61 (0)	8.62 (31)	31.
Spr	12.10 (10)	14.86 (8)	11.30 (32)	14.74 (3)	53.
Grt	70.55 (0)	86.63 (148)	65.9 (0)	85.91 (161)	309.
Opx	25.34 (26)	31.12 (0)	23.68 (54)	30.86 (31)	111.
Total	395.00	485.00	369.0	481.00	1730.

Contingency Tables Separated into More and Less Magnesian Groups (cont.).
Values shown in bold face are expected values lower than observed values. Values in parentheses are observed values.

More Magnesian Samples without 77063

Mg-rich samples	SH-21(M)	SH-22(M)	SH-25(M)	Total
Spl-Spr	97.72 (135)	119.9 (76)	91.29 (98)	309.0
Spl-Grt	71.4 (0)	87.76 (226)	66.7 (0)	226.0
Spl-Opx	105.63 (186)	129.7 (0)	98.68 (148)	334.0
Spl-Spr-Grt	8.54 (0)	10.48 (27)	7.98 (0)	27.0
Spl-Spr-Opx	23.72 (38)	29.1 (0)	22.16 (37)	75.0
Spl-Grt-Opx	0.00 (0)	0.00 (0)	0.00 (0)	0.00
Spr	15.8 (10)	19.4 (8)	14.77 (32)	50.0
Grt	46.8 (0)	57.47 (148)	43.7 (0)	148.0
Opx	25.30 (26)	31.0 (0)	23.63 (54)	80.0
Total	395.0	485.0	369.0	1249.0

Contingency Tables Separated into More and Less Magnesian Groups (cont.).
Values shown in bold face are expected values lower than observed values. Values in parentheses are observed values.

Less Magnesian Samples

Fe-rich samples	SH-10(F)	SH-14(F)	Total
Spl-Spr	0 (0)	0 (0)	0
Spl-Grt	33.49 (21)	6.51 (19)	40
Spl-Opx	370.10 (397)	72.10 (46)	443
Spl-Spr-Grt	0 (0)	0 (0)	0
Spl-Spr-Opx	0 (0)	0 (0)	0
Spl-Grt-Opx	6.70 (8)	1.30 (0)	8
Spr	0 (0)	0 (0)	0
Grt	5.86 (3)	1.14 (4)	7
Opx	82.05 (70)	15.95 (28)	98
Total	499	97	596

Appendix II Spinel Templates.

Spinel Sept. 30, 1997 Revised 6/9/98

Sample No.	77sp8	14spg2-1	14spg2-2good	14spg2-3	14sp2-4
Analysis No.					
SiO2	0.37	0	0	0	0
TiO2	0.01	0.03	0.03	0.03	0
Al2O3	61.52	62.41	62.06	62.19	62.38
Cr2O3					
FeO*	20.29	27.21	27.82	27.91	26.88
MnO	0.43	0.14	0.15	0.08	0.12
MgO	10.93	10.73	10.56	11.02	10.56
ZnO	7.49	1.33	1.38	1.45	1.41
total	101.04	101.85	102.00	102.68	101.35
FeO	17.99	24.80	25.00	24.55	24.81
Fe2O3	2.56	2.68	3.13	3.73	2.30
TOTAL	101.30	102.12	102.31	103.05	101.58

Formulas on the basis of 24 cations/32 oxygens

Ti	0.002	0.005	0.005	0.005	0.000
Al	15.583	15.564	15.491	15.401	15.631
Cr	0.000	0.000	0.000	0.000	0.000
Fe3+	0.413	0.427	0.499	0.590	0.369
Fe2+	0.002	0.005	0.005	0.005	0.000
	16.000	16.000	16.000	16.000	16.000
Fe2+	3.232	4.383	4.424	4.309	4.410
Mn	0.078	0.025	0.027	0.014	0.022
Mg	3.501	3.384	3.334	3.451	3.347
Zn	1.189	0.208	0.216	0.225	0.221
	8.000	8.000	8.000	8.000	8.000
Mol% Her	37.79	52.06	52.12	50.12	52.83
Mol% Spn	43.77	42.30	41.67	43.14	41.83
Mol% Chr	0.00	0.00	0.00	0.00	0.00
Mol% Mag	2.58	2.67	3.12	3.69	2.30
Mol% Gah	14.86	2.60	2.70	2.81	2.77
Mol% Usp	0.02	0.06	0.06	0.06	0.00
Mol% Gax	0.98	0.31	0.34	0.18	0.27
Total	100.00	100.00	100.00	100.00	100.00
Fe2/(Fe2+Mg)	0.48	0.56	0.57	0.56	0.57
Mg/(Mg+Fe2)	0.52	0.44	0.43	0.44	0.43
Fe2/(Fe2+Fe3)	0.89	0.91	0.90	0.88	0.92
Fe3/R3+	0.03	0.03	0.03	0.04	0.02
Cr/R3+	0.00	0.00	0.00	0.00	0.00

Spinel

Sample No.	14sp1-2	14sp1-3	21sp3-1	21sp3-3	21sp3-4
Analysis No.					
SiO2	0	0	0	0	0
TiO2	0.04	0.03	0	0.01	0.08
Al2O3	59.64	60.66	63.54	62.32	62.42
Cr2O3					
FeO*	34.94	31.8	26.55	27.69	27.62
MnO	0.37	0.29	0.4	0.57	0.48
MgO	5.69	7.59	11.64	11.19	11.05
ZnO	1.34	1.56	0.73	0.69	0.55
total	102.02	101.93	102.86	102.47	102.20
FeO	31.91	29.00	24.17	24.43	24.84
Fe2O3	3.37	3.11	2.65	3.62	3.09
TOTAL	102.36	102.24	103.12	102.83	102.51

Formulas on the basis of 24 cations/32 oxygens

Ti	0.007	0.005	0.000	0.002	0.013
Al	15.431	15.483	15.586	15.425	15.487
Cr	0.000	0.000	0.000	0.000	0.000
Fe3+	0.556	0.507	0.414	0.572	0.488
Fe2+	0.007	0.005	0.000	0.002	0.013
	16.000	16.000	16.000	16.000	16.000
Fe2+	5.852	5.247	4.206	4.289	4.362
Mn	0.069	0.053	0.071	0.101	0.086
Mg	1.862	2.450	3.611	3.503	3.467
Zn	0.217	0.249	0.112	0.107	0.085
	8.000	8.000	8.000	8.000	8.000
Mol% Her	69.60	62.36	49.99	50.02	51.31
Mol% Spn	23.27	30.63	45.14	43.78	43.34
Mol% Chr	0.00	0.00	0.00	0.00	0.00
Mol% Mag	3.47	3.17	2.59	3.58	3.05
Mol% Gah	2.71	3.12	1.40	1.34	1.07
Mol% Usp	0.08	0.06	0.00	0.02	0.16
Mol% Gax	0.86	0.66	0.88	1.27	1.07
Total	100.00	100.00	100.00	100.00	100.00
Fe2/(Fe2+Mg)	0.76	0.68	0.54	0.55	0.56
Mg/(Mg+Fe2)	0.24	0.32	0.46	0.45	0.44
Fe2/(Fe2+Fe3)	0.91	0.91	0.91	0.88	0.90
Fe3/R3+	0.03	0.03	0.03	0.04	0.03
Cr/R3+	0.00	0.00	0.00	0.00	0.00

Spinel

Sample No.	21spg3-6	21sp3-9	22sp3-2	22sp3-4	22sp3-8
Analysis No.					
SiO2	0	0	0	0	0
TiO2	0.18	0.02	0.03	0.04	0.03
Al2O3	64.26	63.62	63.24	63.61	63.78
Cr2O3					
FeO*	23.97	26.2	24.07	24.37	24.47
MnO	0.5	0.47	0.15	0.14	0.18
MgO	12.78	11.83	13.57	13.74	13.63
ZnO	0.72	0.53	0.34	0.32	0.43
total	102.41	102.67	101.40	102.22	102.52
FeO	22.44	23.96	21.34	21.44	21.58
Fe2O3	1.70	2.49	3.03	3.26	3.21
TOTAL	102.58	102.92	101.70	102.55	102.84

Formulas on the basis of 24 cations/32 oxygens

Ti	0.028	0.003	0.005	0.006	0.005
Al	15.680	15.604	15.516	15.482	15.493
Cr	0.000	0.000	0.000	0.000	0.000
Fe3+	0.264	0.390	0.475	0.505	0.497
Fe2+	0.028	0.003	0.005	0.006	0.005
	16.000	16.000	16.000	16.000	16.000
Fe2+	3.858	4.166	3.711	3.697	3.716
Mn	0.088	0.083	0.026	0.024	0.031
Mg	3.944	3.669	4.211	4.229	4.187
Zn	0.110	0.081	0.052	0.049	0.065
	8.000	8.000	8.000	8.000	8.000
Mol% Her	46.23	49.60	43.36	42.98	43.28
Mol% Spn	49.30	45.87	52.63	52.87	52.34
Mol% Chr	0.00	0.00	0.00	0.00	0.00
Mol% Mag	1.65	2.44	2.97	3.16	3.11
Mol% Gah	1.38	1.02	0.65	0.61	0.82
Mol% Usp	0.35	0.04	0.06	0.08	0.06
Mol% Gax	1.10	1.04	0.33	0.31	0.39
Total	100.00	100.00	100.00	100.00	100.00
Fe2/(Fe2+Mg)	0.49	0.53	0.47	0.47	0.47
Mg/(Mg+Fe2)	0.51	0.47	0.53	0.53	0.53
Fe2/(Fe2+Fe3)	0.94	0.91	0.89	0.88	0.88
Fe3/R3+	0.02	0.02	0.03	0.03	0.03
Cr/R3+	0.00	0.00	0.00	0.00	0.00

Spinel

Sample No.	22spg3-9	22sp1b-2	22sp1b-4good	22sp1b-5	22sp1a-1
Analysis No.					
SiO2	0	0	0	0	0
TiO2	0.15	0.01	0	0.05	0.03
Al2O3	64.95	62.97	63.68	62.73	62.61
Cr2O3					
FeO*	22.74	24.06	23.97	25.09	25.1
MnO	0.09	0.26	0.17	0.14	0.23
MgO	13.9	12.63	12.95	12.07	12.68
ZnO	0.32	0.47	0.33	0.31	0.36
Total	102.15	100.40	101.10	100.39	101.01
FeO	21.50	22.15	22.21	23.27	22.38
Fe2O3	1.38	2.12	1.96	2.02	3.02
TOTAL	102.29	100.61	101.30	100.59	101.31

Formulas on the basis of 24 cations/32 oxygens

Ti	0.023	0.002	0.000	0.008	0.005
Al	15.741	15.661	15.692	15.662	15.513
Cr	0.000	0.000	0.000	0.000	0.000
Fe3+	0.212	0.336	0.308	0.322	0.478
Fe2+	0.023	0.002	0.000	0.008	0.005
	16.000	16.000	16.000	16.000	16.000
Fe2+	3.675	3.908	3.883	4.115	3.930
Mn	0.016	0.046	0.030	0.025	0.041
Mg	4.261	3.973	4.036	3.811	3.973
Zn	0.049	0.073	0.051	0.048	0.056
	8.000	8.000	8.000	8.000	8.000
Mol% Her	44.32	46.73	46.61	49.33	46.08
Mol% Spn	53.26	49.66	50.45	47.64	49.67
Mol% Chr	0.00	0.00	0.00	0.00	0.00
Mol% Mag	1.33	2.10	1.92	2.01	2.99
Mol% Gah	0.61	0.92	0.64	0.61	0.70
Mol% Usp	0.29	0.02	0.00	0.10	0.06
Mol% Gax	0.20	0.58	0.38	0.31	0.51
Total	100.00	100.00	100.00	100.00	100.00
Fe2/(Fe2+Mg)	0.46	0.50	0.49	0.52	0.50
Mg/(Mg+Fe2)	0.54	0.50	0.51	0.48	0.50
Fe2/(Fe2+Fe3)	0.95	0.92	0.93	0.93	0.89
Fe3/R3+	0.01	0.02	0.02	0.02	0.03
Cr/R3+	0.00	0.00	0.00	0.00	0.00

Spinel

Sample No.	22sp1a-3
Analysis No.	
SiO2	0
TiO2	0
Al2O3	62.76
Cr2O3	
FeO*	24.96
MnO	0.25
MgO	12.53
ZnO	0.31
Total	100.81
FeO	22.56
Fe2O3	2.66
TOTAL	101.08

Formulas on the basis of 24 cations/32 oxygens

Ti	0.000
Al	15.578
Cr	0.000
Fe3+	0.422
Fe2+	0.000
	16.000
Fe2+	3.974
Mn	0.045
Mg	3.933
Zn	0.048
	8.000
Mol% Her	47.04
Mol% Spn	49.17
Mol% Chr	0.00
Mol% Mag	2.64
Mol% Gah	0.60
Mol% Usp	0.00
Mol% Gax	0.56
Total	100.00
Fe2/(Fe2+Mg)	0.50
Mg/(Mg+Fe2)	0.50
Fe2/(Fe2+Fe3)	0.90
Fe3/R3+	0.03
Cr/R3+	0.00

Spinel	5/17/98		Revised 6/9/98		
Sample No.	SH10SP3A	SH10SP3B	SH10SP3C	SH10SP3D	SH10SP3E
Analysis No.					
SiO2	0.027	0.037	0.044	0.054	0.061
TiO2	0	0	0.01	0.02	0.011
Al2O3	58.124	58.407	56.184	57.16	57.467
Cr2O3	0.262	0.236	0.205	0.272	0.347
FeO*	30.783	30.7	32.78	32.012	31.882
MnO	0.283	0.249	0.182	0.291	0.304
MgO	8.065	8.273	8.507	7.215	7.331
ZnO	0.832	0.88	0.829	0.742	0.968
total	98.38	98.78	98.74	97.77	98.37
FeO	27.39	27.23	26.68	28.42	28.26
Fe2O3	3.78	3.86	6.78	3.99	4.03
TOTAL	98.75	99.17	99.42	98.17	98.77

Formulas on the basis of 24 cations/32 oxygens

Ti	0.000	0.000	0.002	0.003	0.002
Al	15.318	15.313	14.819	15.265	15.253
Cr	0.046	0.041	0.036	0.049	0.062
Fe3+	0.635	0.645	1.142	0.679	0.682
Fe2+	0.000	0.000	0.002	0.003	0.002
	16.000	16.000	16.000	16.000	16.000
Fe2+	5.121	5.065	4.991	5.383	5.320
Mn	0.054	0.047	0.034	0.056	0.058
Mg	2.688	2.743	2.838	2.437	2.461
Zn	0.137	0.145	0.137	0.124	0.161
	8.000	8.000	8.000	8.000	8.000
Mol% Her	59.75	59.02	55.00	62.70	61.83
Mol% Spn	33.60	34.29	35.47	30.46	30.76
Mol% Chr	0.29	0.26	0.23	0.30	0.39
Mol% Mag	3.97	4.03	7.14	4.25	4.26
Mol% Gah	1.72	1.81	1.71	1.55	2.01
Mol% Usp	0.00	0.00	0.02	0.04	0.02
Mol% Gax	0.67	0.59	0.43	0.70	0.72
Total	100.00	100.00	100.00	100.00	100.00
Fe2/(Fe2+Mg)	0.66	0.65	0.64	0.69	0.68
Mg/(Mg+Fe2)	0.34	0.35	0.36	0.31	0.32
Fe2/(Fe2+Fe3)	0.89	0.89	0.81	0.89	0.89
Fe3/R3+	0.04	0.04	0.07	0.04	0.04
Cr/R3+	0.00	0.00	0.00	0.00	0.00

Spinel

Sample No.	SH10SP3F	77SP11A	77SP11B	77SP11C	77SP8A	77SP8B
Analysis No.						
SiO2	0.038	0.035	0.027	0.022	0.021	0.031
TiO2	0.018	0.022	0.023	0	0.012	0.003
Al2O3	57.786	59.456	59.082	59.95	61.386	61.277
Cr2O3	0.331	0.162	0.183	0.191	0.133	0.172
FeO*	30.925	20.34	20.68	20.257	20.062	19.436
MnO	0.297	0.446	0.468	0.371	0.123	0.088
MgO	8.019	9.821	9.701	9.974	13.885	13.853
ZnO	0.774	6.788	6.566	6.818	2.546	2.416
total	98.19	97.07	96.73	97.58	98.17	97.28
FeO	27.39	18.82	19.02	18.86	17.50	17.38
Fe2O3	3.92	1.69	1.84	1.55	2.85	2.28
TOTAL	98.58	97.24	96.91	97.74	98.45	97.50

Formulas on the basis of 24 cations/32 oxygens

Ti	0.003	0.004	0.004	0.000	0.002	0.000
Al	15.274	15.680	15.649	15.707	15.514	15.599
Cr	0.059	0.029	0.033	0.034	0.023	0.029
Fe3+	0.662	0.284	0.311	0.260	0.459	0.371
Fe2+	0.003	0.004	0.004	0.000	0.002	0.000
	16.000	16.000	16.000	16.000	16.000	16.000
Fe2+	5.135	3.518	3.572	3.506	3.136	3.139
Mn	0.056	0.085	0.089	0.070	0.022	0.016
Mg	2.681	3.276	3.250	3.305	4.438	4.460
Zn	0.128	1.121	1.089	1.119	0.403	0.385
	8.000	8.000	8.000	8.000	8.000	8.000
Mol% Her	59.65	41.98	42.45	42.00	36.17	36.73
Mol% Spn	33.51	40.95	40.62	41.31	55.48	55.75
Mol% Chr	0.37	0.18	0.20	0.21	0.14	0.18
Mol% Mag	4.14	1.77	1.94	1.62	2.87	2.32
Mol% Gah	1.60	14.02	13.62	13.99	5.04	4.82
Mol% Usp	0.04	0.05	0.05	0.00	0.02	0.01
Mol% Gax	0.71	1.06	1.11	0.87	0.28	0.20
Total	100.00	100.00	100.00	100.00	100.00	100.00
Fe2/(Fe2+Mg)	0.66	0.52	0.52	0.51	0.41	0.41
Mg/(Mg+Fe2)	0.34	0.48	0.48	0.49	0.59	0.59
Fe2/(Fe2+Fe3)	0.89	0.93	0.92	0.93	0.87	0.89
Fe3/R3+	0.04	0.02	0.02	0.02	0.03	0.02
Cr/R3+	0.00	0.00	0.00	0.00	0.00	0.00

Spinel

Sample No.	77SP8C	77SP2A	77SP2B	77SP2C	77SP2D
Analysis No.					
SiO2	0.026	0.021	0.0265	0.0347	0.0244
TiO2	0.002	0.008	0.0019	0.024	0.0081
Al2O3	61.291	61.846	62.011	61.5767	62.0025
Cr2O3	0.136	0.11	0.1105	0.1448	0.1962
FeO*	19.685	17.932	17.5543	17.4486	17.4216
MnO	0.138	0.115	0.0643	0.1286	0.0958
MgO	13.885	15.191	15.0342	14.8632	14.8282
ZnO	2.372	2.511	2.6063	2.5293	2.6261
total	97.54	97.73	97.41	96.75	97.20
FeO	17.41	15.47	15.58	15.58	15.78
Fe2O3	2.53	2.74	2.20	2.08	1.83
TOTAL	97.79	98.01	97.63	96.96	97.39

Formulas on the basis of 24 cations/32 oxygens

Ti	0.000	0.001	0.000	0.004	0.001
Al	15.567	15.540	15.627	15.631	15.669
Cr	0.023	0.019	0.019	0.025	0.033
Fe3+	0.410	0.439	0.353	0.336	0.295
Fe2+	0.000	0.001	0.000	0.004	0.001
	16.000	16.000	16.000	16.000	16.000
Fe2+	3.137	2.757	2.785	2.803	2.828
Mn	0.025	0.021	0.012	0.023	0.017
Mg	4.460	4.827	4.792	4.772	4.739
Zn	0.377	0.395	0.411	0.402	0.416
	8.000	8.000	8.000	8.000	8.000
Mol% Her	36.51	31.58	32.49	32.73	33.28
Mol% Spn	55.75	60.34	59.90	59.65	59.24
Mol% Chr	0.14	0.12	0.12	0.15	0.21
Mol% Mag	2.56	2.74	2.21	2.10	1.84
Mol% Gah	4.72	4.94	5.14	5.03	5.20
Mol% Usp	0.00	0.02	0.00	0.05	0.02
Mol% Gax	0.31	0.26	0.15	0.29	0.22
Total	100.00	100.00	100.00	100.00	100.00
Fe2/(Fe2+Mg)	0.41	0.36	0.37	0.37	0.37
Mg/(Mg+Fe2)	0.59	0.64	0.63	0.63	0.63
Fe2/(Fe2+Fe3)	0.88	0.86	0.89	0.89	0.91
Fe3/R3+	0.03	0.03	0.02	0.02	0.02
Cr/R3+	0.00	0.00	0.00	0.00	0.00

Spinel

Sample No.	77SP2E	77SP2F	SH21SP3A	SH21SP3B	SH21SP3C
Analysis No.					
SiO2	0.8158	0.0181	0.0325	0.026	0.027
TiO2	0.0182	0.0039	0.0141	0	0.0108
Al2O3	60.5688	61.3427	59.3496	59.4431	59.7728
Cr2O3	0.1043	0.1323	0.1307	0.1127	0.1168
FeO*	17.1889	16.932	24.7354	24.116	21.8884
MnO	0.0857	0.092	0.4289	0.328	0.2391
MgO	14.6677	14.7045	10.6861	10.7906	11.0964
ZnO	2.5814	2.6643	0.5195	0.6092	0.5519
total	96.03	95.89	95.90	95.43	93.70
FeO	15.23	15.40	22.89	22.60	21.75
Fe2O3	2.18	1.70	2.05	1.69	0.15
TOTAL	96.25	96.06	96.10	95.59	93.72

Formulas on the basis of 24 cations/32 oxygens

Ti	0.003	0.001	0.002	0.000	0.002
Al	15.618	15.699	15.628	15.696	15.950
Cr	0.018	0.023	0.023	0.020	0.021
Fe3+	0.358	0.277	0.344	0.284	0.025
Fe2+	0.003	0.001	0.002	0.000	0.002
	16.000	16.000	16.000	16.000	16.000
Fe2+	2.784	2.797	4.275	4.234	4.117
Mn	0.016	0.017	0.081	0.062	0.046
Mg	4.783	4.759	3.559	3.603	3.745
Zn	0.417	0.427	0.086	0.101	0.092
	8.000	8.000	8.000	8.000	8.000
Mol% Her	32.41	33.08	51.10	51.02	51.15
Mol% Spn	59.79	59.49	44.48	45.04	46.81
Mol% Chr	0.11	0.14	0.14	0.12	0.13
Mol% Mag	2.24	1.73	2.15	1.78	0.16
Mol% Gah	5.21	5.34	1.07	1.26	1.15
Mol% Usp	0.04	0.01	0.03	0.00	0.02
Mol% Gax	0.20	0.21	1.01	0.78	0.57
Total	100.00	100.00	100.00	100.00	100.00
Fe2/(Fe2+Mg)	0.37	0.37	0.55	0.54	0.52
Mg/(Mg+Fe2)	0.63	0.63	0.45	0.46	0.48
Fe2/(Fe2+Fe3)	0.89	0.91	0.93	0.94	0.99
Fe3/R3+	0.02	0.02	0.02	0.02	0.00
Cr/R3+	0.00	0.00	0.00	0.00	0.00

Spinel

Sample No.	SH21SP3D	SH21SP3E	SH21SP4B	SH21SP4C	SH21SP5A
Analysis No.					
SiO2	0.2498	0.0297	0.0101	0.0235	0.0166
TiO2	0.0191	0.0326	0.0337	0.0161	0.023
Al2O3	59.0365	59.2295	58.8721	58.8521	59.0429
Cr2O3	0.1234	0.1267	0.0641	0.0076	0.1451
FeO*	23.9659	23.622	23.7042	23.4423	23.2738
MnO	0.3482	0.3635	0.2409	0.2385	0.5393
MgO	11.0249	10.6863	10.2954	10.2721	10.9736
ZnO	0.6305	0.5906	0.3978	0.4299	0.5866
total	95.40	94.68	93.62	93.28	94.60
FeO	22.08	22.49	22.99	22.86	21.82
Fe2O3	2.10	1.26	0.80	0.64	1.62
TOTAL	95.61	94.81	93.70	93.35	94.76

Formulas on the basis of 24 cations/32 oxygens

Ti	0.003	0.006	0.006	0.003	0.004
Al	15.617	15.752	15.840	15.882	15.692
Cr	0.022	0.023	0.012	0.001	0.026
Fe3+	0.354	0.214	0.137	0.111	0.274
Fe2+	0.003	0.006	0.006	0.003	0.004
	16.000	16.000	16.000	16.000	16.000
Fe2+	4.141	4.238	4.383	4.375	4.111
Mn	0.066	0.069	0.047	0.046	0.103
Mg	3.688	3.594	3.503	3.506	3.689
Zn	0.104	0.098	0.067	0.073	0.098
	8.000	8.000	8.000	8.000	8.000
Mol% Her	49.37	51.42	53.79	53.95	49.46
Mol% Spn	46.11	44.93	43.79	43.82	46.11
Mol% Chr	0.14	0.14	0.07	0.01	0.16
Mol% Mag	2.21	1.34	0.85	0.69	1.71
Mol% Gah	1.31	1.23	0.84	0.91	1.22
Mol% Usp	0.04	0.07	0.07	0.03	0.05
Mol% Gax	0.83	0.87	0.58	0.58	1.29
Total	100.00	100.00	100.00	100.00	100.00
Fe2/(Fe2+Mg)	0.53	0.54	0.56	0.56	0.53
Mg/(Mg+Fe2)	0.47	0.46	0.44	0.44	0.47
Fe2/(Fe2+Fe3)	0.92	0.95	0.97	0.98	0.94
Fe3/R3+	0.02	0.01	0.01	0.01	0.02
Cr/R3+	0.00	0.00	0.00	0.00	0.00

Spinel

Sample No.	SH21SP5C	SH14SP5B	SH14SP5C	SH14SP5D	SH14SP5E
Analysis No.					
SiO2	0.014	0.0285	1.5446	1.1797	0.031
TiO2	0	0	0	0	0.0038
Al2O3	60.1161	57.2038	55.3497	55.6705	59.0314
Cr2O3	0.0124	0.1181	0.1621	0.1662	0.1795
FeO*	18.6391	29.3422	30.8624	31.3824	24.4716
MnO	0.2519	0.0857	0.1077	0.1063	0.0288
MgO	14.0826	7.1024	7.1324	7.0204	11.3189
ZnO	0.6375	0.7602	0.6152	0.6988	1.0159
total	93.75	94.64	95.77	96.22	96.08
FeO	17.18	27.75	27.43	27.84	21.88
Fe2O3	1.62	1.77	3.81	3.94	2.88
TOTAL	93.92	94.82	96.16	96.62	96.37

Formulas on the basis of 24 cations/32 oxygens

Ti	0.000	0.000	0.000	0.000	0.001
Al	15.727	15.668	15.297	15.280	15.485
Cr	0.002	0.022	0.030	0.031	0.032
Fe3+	0.271	0.310	0.673	0.690	0.482
Fe2+	0.000	0.000	0.000	0.000	0.001
	16.000	16.000	16.000	16.000	16.000
Fe2+	3.189	5.392	5.379	5.422	4.072
Mn	0.047	0.017	0.021	0.021	0.005
Mg	4.659	2.460	2.493	2.437	3.755
Zn	0.104	0.130	0.107	0.120	0.167
	8.000	8.000	8.000	8.000	8.000
Mol% Her	38.15	65.33	62.85	63.27	47.69
Mol% Spn	58.24	30.75	31.16	30.46	46.94
Mol% Chr	0.01	0.14	0.19	0.19	0.20
Mol% Mag	1.69	1.94	4.21	4.31	3.01
Mol% Gah	1.31	1.63	1.33	1.50	2.09
Mol% Usp	0.00	0.00	0.00	0.00	0.01
Mol% Gax	0.59	0.21	0.27	0.26	0.07
Total	100.00	100.00	100.00	100.00	100.00
Fe2/(Fe2+Mg)	0.41	0.69	0.68	0.69	0.52
Mg/(Mg+Fe2)	0.59	0.31	0.32	0.31	0.48
Fe2/(Fe2+Fe3)	0.92	0.95	0.89	0.89	0.89
Fe3/R3+	0.02	0.02	0.04	0.04	0.03
Cr/R3+	0.00	0.00	0.00	0.00	0.00

Spinel

Sample No.	SH14SP5F	SH14SP5G	SH14SP5I	SH14SP5I2
Analysis No.				
SiO2	0.034	0.0337	0.0221	0.0377
TiO2	0.0115	0.0053	0.0391	0.0096
Al2O3	58.7375	58.0616	59.8219	59.17
Cr2O3	0.2056	0.1897	0.2233	0.1902
FeO*	24.235	25.1607	23.2109	22.5464
MnO	0.045	0.05	0	0.039
MgO	11.088	10.8531	11.5716	11.2638
ZnO	1.078	0.9945	0.9902	0.9028
total	95.43	95.35	95.88	94.16
FeO	21.91	22.21	21.62	21.44
Fe2O3	2.58	3.28	1.77	1.23
TOTAL	95.69	95.68	96.06	94.28
Formulas on the basis of 24 cations/32 oxygens				
Ti	0.002	0.001	0.007	0.002
Al	15.524	15.410	15.653	15.754
Cr	0.036	0.034	0.039	0.034
Fe3+	0.436	0.555	0.294	0.209
Fe2+	0.002	0.001	0.007	0.002
	16.000	16.000	16.000	16.000
Fe2+	4.107	4.182	4.008	4.049
Mn	0.009	0.010	0.000	0.007
Mg	3.706	3.643	3.829	3.793
Zn	0.178	0.165	0.162	0.151
	8.000	8.000	8.000	8.000
Mol% Her	48.36	48.59	47.94	49.08
Mol% Spn	46.33	45.54	47.87	47.41
Mol% Chr	0.23	0.21	0.24	0.21
Mol% Mag	2.72	3.47	1.84	1.30
Mol% Gah	2.23	2.07	2.03	1.88
Mol% Usp	0.02	0.01	0.08	0.02
Mol% Gax	0.11	0.12	0.00	0.09
Total	100.00	100.00	100.00	100.00
Fe2/(Fe2+Mg)	0.53	0.53	0.51	0.52
Mg/(Mg+Fe2)	0.47	0.47	0.49	0.48
Fe2/(Fe2+Fe3)	0.90	0.88	0.93	0.95
Fe3/R3+	0.03	0.03	0.02	0.01
Cr/R3+	0.00	0.00	0.00	0.00

Appendix III Sapphirine Templates

Sapphirines Sept. 30, 1997 Revised 6/9/98

Sample No.	22sapph1b-1	22sapph1b-2	22sapph1b-3	22sapph1b-4
Analysis No.				
SiO2	14.42	14.02	14.17	14.44
TiO2	0.12	0	0.17	0.05
Al2O3	59.16	60.44	59.28	59.04
Cr2O3				
FeO*	11.94	10.52	11.84	12.14
MnO	0.17	0.12	0.24	0.19
MgO	15.73	15.87	15.69	15.67
ZnO	0.06	0.04	0	0.03
CaO	0	0	0	0
Na2O	0	0	0.03	0
Subtotal	101.60	101.01	101.42	101.56
FeO	9.13	8.38	8.88	9.23
Fe2O3	3.12	2.38	3.29	3.23
TOTAL	101.85	101.21	101.75	101.85

Formulas on the basis of 14 cations/20 oxygens

Si	1.713	1.666	1.685	1.717
Al	4.287	4.334	4.315	4.283
	6.000	6.000	6.000	6.000
Al	3.995	4.129	3.993	3.989
Ti	0.012	0.000	0.017	0.005
Cr	0.000	0.000	0.000	0.000
Fe3+	0.279	0.213	0.295	0.289
Fe2+	0.907	0.832	0.883	0.918
Mn	0.017	0.012	0.024	0.019
Mg	2.785	2.810	2.781	2.777
Zn	0.005	0.004	0.000	0.003
Ca	0.000	0.000	0.000	0.000
Na	0.000	0.000	0.007	0.000
	8.000	8.000	8.000	8.000
Fe2/(Fe2+Mg)	0.25	0.23	0.24	0.25
Fe3+/(Fe3+Fe2)	0.24	0.20	0.25	0.24

Sapphirines

Sample No.	22sapph1b-5	22sapph1a-1	22sapph1a-2	22sapph1a-3
Analysis No.				
SiO2	14.52	13.94	13.88	13.94
TiO2	0.01	0.03	0.08	0.02
Al2O3	59.12	60.05	60.83	59.66
Cr2O3				
FeO*	11.68	10.6	9.79	11.05
MnO	0.24	0.21	0.19	0.18
MgO	15.42	15.55	16.09	15.58
ZnO	0.03	0	0	0
CaO	0	0	0	0
Na2O	0	0.01	0.02	0.02
Subtotal	101.02	100.39	100.88	100.45
FeO	9.58	8.71	7.87	8.62
Fe2O3	2.33	2.10	2.13	2.70
TOTAL	101.22	100.60	101.09	100.72

Formulas on the basis of 14 cations/20 oxygens

Si	1.735	1.668	1.646	1.669
Al	4.265	4.332	4.354	4.331
	6.000	6.000	6.000	6.000
Al	4.059	4.138	4.152	4.088
Ti	0.001	0.003	0.008	0.002
Cr	0.000	0.000	0.000	0.000
Fe3+	0.210	0.190	0.190	0.244
Fe2+	0.957	0.871	0.781	0.863
Mn	0.024	0.021	0.019	0.018
Mg	2.746	2.774	2.845	2.781
Zn	0.003	0.000	0.000	0.000
Ca	0.000	0.000	0.000	0.000
Na	0.000	0.002	0.005	0.005
	8.000	8.000	8.000	8.000
Fe2/(Fe2+Mg)	0.26	0.24	0.22	0.24
Fe3+/(Fe3+Fe2)	0.18	0.18	0.20	0.22

Sapphirines	May 17,1998		Revised 6/9/98	
Sample No.	SH21SAP4A	SH21SAP4B	SH21SAP4C	SH21SAP4D
Analysis No.				
SiO2	13.7447	13.8145	13.5562	13.3292
TiO2	0.0446	0.0758	0.0694	0.1189
Al2O3	55.3197	55.5144	55.5684	56.9386
Cr2O3	0.0561	0.0481	0.0097	0.0385
FeO*	11.5929	11.6965	10.2437	11.1834
MnO	0.2801	0.3736	0.1289	0.3482
MgO	14.4955	14.4849	14.2965	14.595
ZnO	0.0432	0.1381	0.026	0.0345
CaO	0.0479	0.0425	0.0509	0.0533
Na2O	0.0205	0.0205	0.006	0.0162
Subtotal	95.65	96.21	93.96	96.66
FeO	9.00	8.88	9.16	8.60
Fe2O3	2.89	3.13	1.21	2.87
TOTAL	95.89	96.38	94.05	96.91
Formulas on the basis of 14 cations/20 oxygens				
Si	1.738	1.739	1.738	1.665
Al	4.262	4.261	4.262	4.335
	6.000	6.000	6.000	6.000
Al	3.985	3.975	4.136	4.047
Ti	0.005	0.008	0.008	0.013
Cr	0.006	0.005	0.001	0.004
Fe3+	0.275	0.296	0.117	0.270
Fe2+	0.952	0.935	0.982	0.899
Mn	0.030	0.040	0.014	0.037
Mg	2.733	2.718	2.732	2.717
Zn	0.004	0.013	0.002	0.003
Ca	0.006	0.006	0.007	0.007
Na	0.005	0.005	0.001	0.004
	8.000	8.000	8.000	8.000
Fe2/(Fe2+Mg)	0.26	0.26	0.26	0.25
Fe3+/(Fe3+Fe2)	0.22	0.24	0.11	0.23

Sapphirines

Sample No.	SH21SAP5A	SH21SAP5B	SH21SAP5C
Analysis No.			
SiO2	14.0174	13.4226	13.6514
TiO2	0.1097	0.0762	0.1182
Al2O3	53.7935	55.4386	54.029
Cr2O3	0.0223	0.0401	0.0352
FeO*	13.4114	11.6344	12.5576
MnO	0.3598	0.3072	0.2848
MgO	14.3257	13.9154	14.2447
ZnO	0.0431	0.0454	0.1165
CaO	0.026	0.0121	0.0139
Na2O	0.0081	0.0046	0
Subtotal	96.12	94.90	95.05
FeO	9.66	9.59	9.15
Fe2O3	4.17	2.28	3.79
TOTAL	96.49	95.08	95.31

Formulas on the basis of 14 cations/20 oxygens

Si	1.776	1.714	1.745
Al	4.224	4.286	4.255
	6.000	6.000	6.000
Al	3.811	4.057	3.884
Ti	0.012	0.008	0.013
Cr	0.002	0.004	0.004
Fe3+	0.398	0.219	0.364
Fe2+	1.024	1.024	0.978
Mn	0.039	0.033	0.031
Mg	2.706	2.648	2.714
Zn	0.004	0.004	0.011
Ca	0.004	0.002	0.002
Na	0.002	0.001	0.000
	8.000	8.000	8.000
Fe2/(Fe2+Mg)	0.27	0.28	0.26
Fe3+/(Fe3+Fe2)	0.28	0.18	0.27

Appendix IV Garnet Templates.

Garnets	Sept. 30, 1997		Revised 6/9/98		
Sample No.	14gt2-1	14gt2-2	14gt2-3	14gt2-4	14gt2-5
Analysis No.					
SiO2	38.33	38.27	38.65	39.15	38.72
TiO2	0.05	0.06	0.08	0.08	0.2
Al2O3	22.7	22.56	22.6	22.41	22.6
FeO	29.97	30.67	29.67	29.76	31.49
MnO	1.18	1.02	1.09	1.1	1.13
MgO	8.92	8.54	9.04	9.11	7.35
CaO	1.46	1.52	1.36	1.41	1.46
ZnO	0	0.01	0	0	0
Total	102.61	102.64	102.49	103.02	102.95

Formulas on the basis of 12 oxygens

Si	2.915	2.918	2.935	2.956	2.950
Ti	0.003	0.003	0.005	0.005	0.011
Al	2.035	2.027	2.023	1.994	2.029
	2.038	2.031	2.027	1.999	2.041
Fe	1.906	1.956	1.884	1.879	2.006
Mn	0.076	0.066	0.070	0.070	0.073
Mg	1.011	0.971	1.023	1.025	0.835
Ca	0.119	0.124	0.111	0.114	0.119
	3.112	3.116	3.088	3.089	3.033
Mol% Alm	61.2	62.8	61.0	60.8	66.1
Mol% Pyr	32.5	31.1	33.1	33.2	27.5
Mol% Sps	2.4	2.1	2.3	2.3	2.4
Mol% Gro	3.8	4.0	3.6	3.7	3.9
Fe/(Fe+Mg)	0.653	0.668	0.648	0.647	0.706
Mg/(Mg+Fe)	0.347	0.332	0.352	0.353	0.294

Garnets

Sample No.	22gt3-1	22gt3-2	22gt3-3	22gt3-4	22gt3-5
Analysis No.					
SiO2	39.45	39.65	39.78	39.81	39.53
TiO2	0.04	0.02	0.1	0.04	0.22
Al2O3	22.92	22.91	22.86	22.89	22.94
FeO	26.39	26.18	27.14	25.97	26.35
MnO	2.11	2.1	2.11	2.07	2.14
MgO	11.07	10.78	10.51	11	10.87
CaO	0.94	0.95	0.93	0.93	1.04
ZnO	0.01	0.34	0	0	0
Total	102.92	102.59	103.43	102.71	103.09

Formulas on the basis of 12 oxygens

Si	2.943	2.963	2.960	2.967	2.944
Ti	0.002	0.001	0.006	0.002	0.012
Al	2.015	2.018	2.005	2.011	2.014
	2.018	2.019	2.010	2.013	2.026
Fe	1.647	1.636	1.689	1.619	1.641
Mn	0.133	0.133	0.133	0.131	0.135
Mg	1.231	1.201	1.166	1.222	1.207
Ca	0.075	0.076	0.074	0.074	0.083
	3.086	3.046	3.062	3.046	3.066
Mol% Alm	53.4	53.7	55.2	53.1	53.5
Mol% Pyr	39.9	39.4	38.1	40.1	39.4
Mol% Sps	4.3	4.4	4.3	4.3	4.4
Mol% Gro	2.4	2.5	2.4	2.4	2.7
Fe/(Fe+Mg)	0.572	0.577	0.592	0.570	0.576
Mg/(Mg+Fe)	0.428	0.423	0.408	0.430	0.424

Garnets

Sample No.	22gt3-6	22gt3-7	22gt3-8	22gt3-9	22gt3-10
Analysis No.					
SiO2	39.86	39.84	39.75	39.76	40.24
TiO2	0.31	0.18	0.04	0.27	0.41
Al2O3	23.03	23.57	22.94	22.9	22.95
FeO	26.85	26.31	26.29	26.61	26.61
MnO	2.07	2.25	2.21	2.21	2.5
MgO	10.98	10.68	10.58	10.77	10.39
CaO	0.92	0.98	0.97	0.97	1
ZnO	0	0.08	0	0	0
Total	104.02	103.81	102.78	103.49	104.10

Formulas on the basis of 12 oxygens

Si	2.944	2.942	2.967	2.952	2.970
Ti	0.017	0.010	0.002	0.015	0.023
Al	2.005	2.052	2.018	2.004	1.996
	2.022	2.062	2.020	2.019	2.019
Fe	1.659	1.625	1.641	1.652	1.642
Mn	0.130	0.141	0.140	0.139	0.156
Mg	1.209	1.176	1.177	1.192	1.143
Ca	0.073	0.078	0.078	0.077	0.079
	3.070	3.019	3.035	3.060	3.021
Mol% Alm	54.0	53.8	54.1	54.0	54.4
Mol% Pyr	39.4	38.9	38.8	38.9	37.8
Mol% Sps	4.2	4.7	4.6	4.5	5.2
Mol% Gro	2.4	2.6	2.6	2.5	2.6
Fe/(Fe+Mg)	0.578	0.580	0.582	0.581	0.590
Mg/(Mg+Fe)	0.422	0.420	0.418	0.419	0.410

Garnets	May 17,1998				Revised 6/9/98
Sample No.	77GT8A	77GT8B	77GT8C	77GT2A	77GT2B
Analysis No.					
SiO2	38.823	38.739	39.085	38.9017	38.966
TiO2	0.082	0.071	0.075	0.0155	0.0043
Al2O3	22.046	22.014	22.221	22.0177	22.1313
FeO	21.86	22.01	20.082	20.8946	21.3456
MnO	2.282	2.203	2.167	2.0761	2.0699
MgO	12.004	11.826	13.142	12.503	12.0568
CaO	1.604	1.596	1.635	1.5689	1.5207
ZnO	0.1109	0.0896	0	0.0043	0.077
Total	98.70	98.46	98.41	97.98	98.09
Si	2.975	2.978	2.977	2.987	2.992
Ti	0.005	0.004	0.004	0.001	0.000
Al	1.992	1.994	1.995	1.992	2.003
	1.996	1.999	1.999	1.993	2.003
Fe	1.401	1.415	1.279	1.342	1.371
Mn	0.148	0.143	0.140	0.135	0.135
Mg	1.371	1.355	1.492	1.431	1.380
Ca	0.132	0.131	0.133	0.129	0.125
	3.052	3.045	3.045	3.037	3.011
Mol% Alm	45.9	46.5	42.0	44.2	45.5
Mol% Pyr	44.9	44.5	49.0	47.1	45.8
Mol% Sps	4.9	4.7	4.6	4.4	4.5
Mol% Gro	4.3	4.3	4.4	4.3	4.2
Fe/(Fe+Mg)	0.505	0.511	0.462	0.484	0.498
Mg/(Mg+Fe)	0.495	0.489	0.538	0.516	0.502

Garnets

Sample No.	77GT2C	77GT2D	77GT2E	77GT2F	SH14GT5E
Analysis No.					
SiO2	38.9862	39.1806	38.9214	38.9652	37.8802
TiO2	0.0264	0.1242	0.0163	0.0164	0.0304
Al2O3	22.2083	22.1135	22.2992	22.1612	21.3263
FeO	20.9597	20.1559	19.8325	19.2447	26.4648
MnO	2.0986	2.074	2.12	2.0274	0.9094
MgO	12.3523	12.7464	13.0866	12.8953	9.2342
CaO	1.5992	1.5937	1.4925	1.5031	1.2179
ZnO	0.0235	0.0556	0.0684	0.0493	0
Total	98.23	97.99	97.77	96.81	97.06
Si	2.985	2.995	2.979	3.002	3.001
Ti	0.002	0.007	0.001	0.001	0.002
Al	2.004	1.993	2.012	2.012	1.991
	2.006	2.000	2.013	2.013	1.993
Fe	1.342	1.289	1.270	1.240	1.753
Mn	0.136	0.134	0.137	0.132	0.061
Mg	1.410	1.453	1.493	1.481	1.090
Ca	0.131	0.131	0.122	0.124	0.103
	3.020	3.006	3.022	2.977	3.008
Mol% Alm	44.5	42.9	42.0	41.6	58.3
Mol% Pyr	46.7	48.3	49.4	49.7	36.2
Mol% Sps	4.5	4.5	4.5	4.4	2.0
Mol% Gro	4.3	4.3	4.0	4.2	3.4
Fe/(Fe+Mg)	0.488	0.470	0.460	0.456	0.617
Mg/(Mg+Fe)	0.512	0.530	0.540	0.544	0.383

Garnets

Sample No.	SH14GT5F	SH14GT5G	SH14GT5H
Analysis No.			
SiO2	37.6599	37.6354	37.4148
TiO2	0.0797	0.0577	0.1003
Al2O3	21.1683	21.2571	21.13
FeO	25.912	26.6571	25.5446
MnO	0.9849	0.942	0.817
MgO	9.16	8.8208	8.245
CaO	1.1931	1.2243	1.3671
ZnO	0.0192	0	0.1408
Total	96.16	96.59	94.62
Si	3.007	3.001	3.031
Ti	0.005	0.003	0.006
Al	1.992	1.998	2.017
	1.997	2.001	2.023
Fe	1.730	1.778	1.730
Mn	0.067	0.064	0.056
Mg	1.090	1.048	0.996
Ca	0.102	0.105	0.119
	2.989	2.994	2.901
Mol% Alm	57.9	59.4	59.7
Mol% Pyr	36.5	35.0	34.3
Mol% Sps	2.2	2.1	1.9
Mol% Gro	3.4	3.5	4.1
Fe/(Fe+Mg)	0.613	0.629	0.635
Mg/(Mg+Fe)	0.387	0.371	0.365

Appendix V Orthopyroxene Templates.

Orthopyroxenes Sept. 30, 1997 Revised 6/9/98

Sample No.	77opx8good	14opx1-1	14opx1-2	14opx1-4	14opx1-5a	14opx1-5b
Analysis No.						
SiO2	46.66	45.83	46	46.87	47.92	47.36
TiO2	0.11	0.21	0.1	0.18	0.12	0.09
Al2O3	10.53	11.36	11.04	10.87	9.84	10.8
Cr2O3						
FeO*	19	23.29	23.59	23.56	24.36	23.62
MnO	0.81	0.46	0.38	0.45	0.42	0.4
MgO	22.2	19.82	19.64	19.64	19.28	19.59
ZnO	0.11	0	0	0.14	0	0
CaO	0.11	0	0.04	0.03	0	0.05
Na2O	0	0	0.02	0	0.04	0
Subtotal	99.53	100.97	100.81	101.74	101.98	101.91
FeO	15.08	19.22	19.57	20.35	22.44	21.33
Fe2O3	4.36	4.53	4.47	3.56	2.13	2.54
TOTAL	99.86	101.42	101.26	101.96	102.19	102.16
Formulas on the basis of 4 cations/6 oxygens						
Si	1.712	1.685	1.696	1.715	1.756	1.730
Al	0.288	0.315	0.304	0.285	0.244	0.270
	2.000	2.000	2.000	2.000	2.000	2.000
Al	0.167	0.177	0.175	0.184	0.181	0.195
Ti	0.003	0.007	0.003	0.006	0.004	0.003
Cr	0.000	0.000	0.000	0.000	0.000	0.000
Fe3+	0.120	0.125	0.124	0.098	0.059	0.070
Fe2+	0.463	0.591	0.603	0.623	0.688	0.652
Mn	0.025	0.014	0.012	0.014	0.013	0.012
Mg	1.214	1.086	1.079	1.071	1.053	1.067
Zn	0.003	0.000	0.000	0.004	0.000	0.000
Ca	0.004	0.000	0.002	0.001	0.000	0.002
Na	0.000	0.000	0.001	0.000	0.003	0.000
	2.000	2.000	2.000	2.000	2.000	2.000
Mol% Wo	0.00	0.00	0.00	0.00	0.00	0.00
Mol% En	50.52	44.52	44.41	44.89	45.49	45.12
Mol% Fs	19.25	24.22	24.82	26.10	29.71	27.56
Mol% CaTiTs	0.17	0.33	0.16	0.28	0.19	0.14
Mol% CrCaTs	0.00	0.00	0.00	0.00	0.00	0.00
Mol% CaTs	0.43	0.00	0.16	0.12	0.00	0.20
Mol% FeMgTs	16.11	17.70	17.40	17.60	17.80	19.48
Mol% FerriTs	12.03	12.52	12.40	9.81	5.87	6.99
Mol% Other	1.49	0.72	0.66	1.21	0.94	0.52
Total	100.00	100.00	100.00	100.00	100.00	100.00
Fe2+/(Fe2++Mg)	0.275942	0.352329	0.358551	0.367648	0.395071	0.379244
Fe3/(Fe3+Fe2)	0.206299	0.174833	0.170501	0.136121	0.078671	0.096838

Orthopyroxenes

Sample No.	21opx3-1	21opx3-1	21opx3-3	21opx3-4	21opx3-5	21opx3-7
Analysis No.						
SiO2	47.5	46.47	48.28	48.28	48.38	48.27
TiO2	0.11	0.26	0.05	0.14	0.21	0.12
Al2O3	11.15	10.5	10.64	10.51	10.78	10.94
Cr2O3						
FeO*	21.04	21.48	20.37	19.93	19.42	20.21
MnO	1.19	1.2	1.16	1.26	1.14	1.24
MgO	21.47	20.88	21.73	21.87	22.12	22.27
ZnO	0	0.03	0	0.01	0	0
CaO	0	0.06	0.03	0.03	0.01	0.03
Na2O	0	0.03	0.02	0.01	0	0
Subtotal	102.46	100.91	102.28	102.04	102.06	103.08
FeO	17.43	17.10	17.74	17.50	17.47	16.85
Fe2O3	4.01	4.87	2.92	2.70	2.17	3.73
TOTAL	102.86	101.37	102.57	102.30	102.28	103.45

Formulas on the basis of 4 cations/6 oxygens

Si	1.706	1.700	1.734	1.737	1.736	1.717
Al	0.294	0.300	0.266	0.263	0.264	0.283
	2.000	2.000	2.000	2.000	2.000	2.000
Al	0.179	0.153	0.185	0.183	0.192	0.176
Ti	0.003	0.008	0.002	0.004	0.006	0.004
Cr	0.000	0.000	0.000	0.000	0.000	0.000
Fe3+	0.108	0.134	0.079	0.073	0.059	0.100
Fe2+	0.524	0.523	0.533	0.527	0.524	0.501
Mn	0.036	0.037	0.035	0.038	0.035	0.037
Mg	1.150	1.139	1.164	1.173	1.183	1.181
Zn	0.000	0.001	0.000	0.000	0.000	0.000
Ca	0.000	0.002	0.001	0.001	0.000	0.001
Na	0.000	0.002	0.001	0.001	0.000	0.000
	2.000	2.000	2.000	2.000	2.000	2.000
Mol% Wo	0.00	0.00	0.00	0.00	0.00	0.00
Mol% En	47.63	47.23	49.18	49.86	50.47	49.37
Mol% Fs	21.70	21.70	22.53	22.39	22.36	20.95
Mol% CaTiTs	0.17	0.40	0.08	0.21	0.32	0.18
Mol% CrCaTs	0.00	0.00	0.00	0.00	0.00	0.00
Mol% CaTs	0.00	0.24	0.12	0.12	0.04	0.11
Mol% FeMgTs	17.85	14.95	18.36	18.14	19.23	17.57
Mol% FerriTs	10.84	13.40	7.90	7.31	5.86	10.00
Mol% Other	1.81	2.08	1.85	1.97	1.71	1.81
Total	100.00	100.00	100.00	100.00	100.00	100.00
Fe2+/(Fe2++Mg)	0.312973	0.314814	0.314148	0.309848	0.306995	0.297982
Fe3/(Fe3+Fe2)	0.171421	0.203924	0.129064	0.121868	0.100615	0.166299

Orthopyroxenes

Sample No.	21opx3-8	21opx3-9	21opx3-10
Analysis No.			
SiO2	48.42	47.75	49.06
TiO2	0.26	0.18	0.09
Al2O3	10.87	10.99	9.47
Cr2O3			
FeO*	20.42	20.33	20.6
MnO	1.24	1.21	1.23
MgO	21.87	21.75	22.47
ZnO	0.07	0.05	0
CaO	0.01	0.06	0.01
Na2O	0.01	0	0.01
Subtotal	103.17	102.32	102.94
FeO	17.68	17.07	17.40
Fe2O3	3.05	3.62	3.56
TOTAL	103.41	102.63	103.30

Formulas on the basis of 4 cations/6 oxygens

Si	1.725	1.714	1.751
Al	0.275	0.286	0.249
	2.000	2.000	2.000
Al	0.182	0.180	0.149
Ti	0.008	0.005	0.003
Cr	0.000	0.000	0.000
Fe3+	0.082	0.098	0.096
Fe2+	0.527	0.513	0.519
Mn	0.037	0.037	0.037
Mg	1.162	1.164	1.195
Zn	0.002	0.001	0.000
Ca	0.000	0.002	0.000
Na	0.001	0.000	0.001
	2.000	2.000	2.000
Mol% Wo	0.00	0.00	0.00
Mol% En	49.17	48.67	51.26
Mol% Fs	22.30	21.44	22.27
Mol% CaTiTs	0.39	0.27	0.14
Mol% CrCaTs	0.00	0.00	0.00
Mol% CaTs	0.04	0.23	0.04
Mol% FeMgTs	17.74	17.69	14.83
Mol% FerriTs	8.17	9.78	9.56
Mol% Other	2.20	1.92	1.91
Total	100.00	100.00	100.00
Fe2+/(Fe2++Mg)	0.311991	0.305762	0.302819
Fe3/(Fe3+Fe2)	0.134326	0.160134	0.155523

Orthopyroxenes 17-May-98 Revised 6/9/98

Sample No.	SH10OPX3A	SH10OPX3B	SH10OPX3C	SH10OPX3D	SH10OPX3E
Analysis No.					
SiO2	45.514	45.487	45.175	45.536	45.287
TiO2	0.149	0.157	0.143	0.091	0.124
Al2O3	10.128	10.035	10.055	10.099	10.162
Cr2O3	0.014	0.022	0.014	0.011	0
FeO*	23.449	23.358	23.863	23.155	22.995
MnO	0.477	0.491	0.51	0.558	0.568
MgO	18.411	18.339	18.371	18.338	18.301
ZnO	0.002	0	0.075	0.011	0.021
CaO	0.097	0.128	0.101	0.113	0.089
Na2O	0.018	0.007	0.015	0.006	0.02
Subtotal	98.26	98.02	98.32	97.92	97.57
FeO	21.06	21.17	20.50	21.09	20.82
Fe2O3	2.66	2.44	3.74	2.30	2.42
TOTAL	98.52	98.27	98.62	98.14	97.79
Formulas on the basis of 4 cations/6 oxygens					
Si	1.731	1.734	1.719	1.737	1.733
Al	0.269	0.266	0.281	0.263	0.267
	2.000	2.000	2.000	2.000	2.000
Al	0.185	0.185	0.170	0.192	0.192
Ti	0.005	0.005	0.005	0.003	0.004
Cr	0.000	0.001	0.000	0.000	0.000
Fe3+	0.076	0.070	0.107	0.066	0.070
Fe2+	0.670	0.675	0.652	0.673	0.666
Mn	0.015	0.016	0.016	0.018	0.018
Mg	1.044	1.042	1.042	1.043	1.044
Zn	0.000	0.000	0.002	0.000	0.001
Ca	0.004	0.005	0.004	0.005	0.004
Na	0.001	0.001	0.001	0.000	0.001
	2.000	2.000	2.000	2.000	2.000
Mol% Wo	0.00	0.00	0.00	0.00	0.00
Mol% En	44.29	44.39	43.75	44.35	44.31
Mol% Fs	28.42	28.74	27.39	28.61	28.28
Mol% CaTiTs	0.24	0.25	0.23	0.15	0.20
Mol% CrCaTs	0.02	0.03	0.02	0.02	0.00
Mol% CaTs	0.40	0.52	0.41	0.46	0.36
Mol% FeMgTs	18.33	18.49	16.45	19.04	18.90
Mol% FerriTs	7.60	6.99	10.70	6.60	6.97
Mol% Other	0.71	0.58	1.04	0.76	0.98
Total	100.00	100.00	100.00	100.00	100.00
Fe2+/(Fe2++Mg)	0.39089122	0.393028	0.38503	0.392142	0.389565
Fe3/(Fe3+Fe2)	0.10189301	0.093832	0.140863	0.089326	0.094694

Orthopyroxenes

Sample No.	SH10OPX3F	77OPX11A	77OPX11B	77OPX11C
Analysis No.				
SiO2	45.418	46.774	46.837	47.063
TiO2	0.069	0.118	0.108	0.099
Al2O3	9.887	10.056	10.037	9.716
Cr2O3	0.036	0	0.033	0.027
FeO*	23.425	17.326	17.281	17.268
MnO	0.625	1.046	0.989	1.004
MgO	18.293	22.361	22.449	22.547
ZnO	0.105	0.067	0.112	0.062
CaO	0.08	0.094	0.065	0.049
Na2O	0.01	0	0.004	0.015
Subtotal	97.95	97.84	97.92	97.85
FeO	20.71	14.83	14.70	14.87
Fe2O3	3.02	2.77	2.87	2.66
TOTAL	98.15	98.05	98.09	98.05

Formulas on the basis of 4 cations/6 oxygens

Si	1.735	1.739	1.740	1.749
Al	0.265	0.261	0.260	0.251
	2.000	2.000	2.000	2.000
Al	0.180	0.180	0.179	0.174
Ti	0.002	0.004	0.003	0.003
Cr	0.001	0.000	0.001	0.001
Fe3+	0.087	0.078	0.080	0.074
Fe2+	0.662	0.461	0.457	0.462
Mn	0.020	0.033	0.031	0.032
Mg	1.041	1.239	1.243	1.249
Zn	0.003	0.002	0.003	0.002
Ca	0.003	0.004	0.003	0.002
Na	0.001	0.000	0.000	0.001
	2.000	2.000	2.000	2.000
Mol% Wo	0.00	0.00	0.00	0.00
Mol% En	44.13	52.73	52.90	53.53
Mol% Fs	28.03	19.62	19.43	19.81
Mol% CaTiTs	0.11	0.19	0.17	0.16
Mol% CrCaTs	0.05	0.00	0.05	0.04
Mol% CaTs	0.33	0.37	0.26	0.20
Mol% FeMgTs	17.31	17.60	17.25	16.98
Mol% FerriTs	8.67	7.75	8.02	7.45
Mol% Other	1.37	1.74	1.92	1.85
Total	100.00	100.00	100.00	100.00
Fe2+/(Fe2++Mg)	0.388442	0.27122093	0.26865175	0.27009967
Fe3/(Fe3+Fe2)	0.115885	0.1438809	0.14943491	0.13876597

Orthopyroxenes

Sample No.	SH21OPX3A	SH21OPX3B	SH21OPX3C	SH21OPX3D
Analysis No.				
SiO2	45.4394	45.9212	45.532	45.7347
TiO2	0.0972	0.1366	0.1789	0.148
Al2O3	10.837	10.2139	10.5711	10.288
Cr2O3	0	0	0.022	0.0252
FeO*	17.9526	18.471	18.495	18.1624
MnO	1.0307	1.0362	0.9942	0.9891
MgO	20.5474	20.6096	20.2327	20.637
ZnO	0.0561	0.0108	0.0065	0.0194
CaO	0.1272	0.1029	0.0602	0.1185
Na2O	0.0103	0.014	0.0033	0.0037
Subtotal	96.10	96.52	96.10	96.13
FeO	16.40	17.04	17.44	16.83
Fe2O3	1.72	1.59	1.17	1.48
TOTAL	96.21	96.67	96.21	96.26

Formulas on the basis of 4 cations/6 oxygens

Si	1.731	1.745	1.739	1.743
Al	0.269	0.255	0.261	0.257
	2.000	2.000	2.000	2.000
Al	0.217	0.202	0.215	0.205
Ti	0.003	0.004	0.006	0.005
Cr	0.000	0.000	0.001	0.001
Fe3+	0.049	0.046	0.034	0.043
Fe2+	0.523	0.541	0.557	0.536
Mn	0.033	0.033	0.032	0.032
Mg	1.167	1.167	1.152	1.173
Zn	0.002	0.000	0.000	0.001
Ca	0.005	0.004	0.002	0.005
Na	0.001	0.001	0.000	0.000
	2.000	2.000	2.000	2.000
Mol% Wo	0.00	0.00	0.00	0.00
Mol% En	49.26	49.96	49.24	50.17
Mol% Fs	22.06	23.17	23.82	22.95
Mol% CaTiTs	0.16	0.22	0.29	0.24
Mol% CrCaTs	0.00	0.00	0.03	0.04
Mol% CaTs	0.52	0.42	0.25	0.48
Mol% FeMgTs	21.35	20.07	21.48	20.40
Mol% FerriTs	4.94	4.56	3.36	4.25
Mol% Other	1.72	1.61	1.54	1.46
Total	100.00	100.00	100.00	100.00
Fe2+/(Fe2++Mg)	0.30933	0.31682948	0.32601048	0.31389554
Fe3/(Fe3+Fe2)	0.08631825	0.07766309	0.05682584	0.07342152

Orthopyroxenes

Sample No.	SH21OPX3E	SH14OPX5B	SH14OPX5C	SH14OPX5D
Analysis No.				
SiO2	45.571	44.7544	44.6872	45.5861
TiO2	0.1785	0.1412	0.1466	0.1148
Al2O3	10.5051	10.4922	10.7315	9.7258
Cr2O3	0.0661	0	0.0124	0
FeO*	18.2738	22.4066	22.6728	22.3401
MnO	1.0873	0.1918	0.2133	0.1943
MgO	20.3408	18.3602	18.2938	18.8054
ZnO	0.0646	0.0429	0.0279	0
CaO	0.0983	0.0787	0.0737	0.0634
Na2O	0.0003	0.0284	0	0.011
Subtotal	96.19	96.50	96.86	96.84
FeO	17.01	20.39	20.59	20.78
Fe2O3	1.40	2.24	2.32	1.74
TOTAL	96.26	96.68	97.06	97.02

Formulas on the basis of 4 cations/6 oxygens

Si	1.739	1.727	1.719	1.751
Al	0.261	0.273	0.281	0.249
	2.000	2.000	2.000	2.000
Al	0.211	0.204	0.206	0.192
Ti	0.006	0.005	0.005	0.004
Cr	0.002	0.000	0.000	0.000
Fe3+	0.040	0.065	0.067	0.050
Fe2+	0.543	0.658	0.662	0.668
Mn	0.035	0.006	0.007	0.006
Mg	1.157	1.056	1.049	1.077
Zn	0.002	0.001	0.001	0.000
Ca	0.004	0.003	0.003	0.003
Na	0.000	0.002	0.000	0.001
	2.000	2.000	2.000	2.000
Mol% Wo	0.00	0.00	0.00	0.00
Mol% En	49.42	44.66	44.14	46.40
Mol% Fs	23.19	27.82	27.87	28.76
Mol% CaTiTs	0.29	0.23	0.24	0.19
Mol% CrCaTs	0.10	0.00	0.02	0.00
Mol% CaTs	0.40	0.33	0.30	0.26
Mol% FeMgTs	20.75	19.91	20.40	19.09
Mol% FerriTs	4.02	6.51	6.70	5.03
Mol% Other	1.83	0.55	0.31	0.27
Total	100.00	100.00	100.00	100.00
Fe2+/(Fe2++Mg)	0.31939666	0.38387593	0.38704072	0.38264073
Fe3/(Fe3+Fe2)	0.06891478	0.09000685	0.09189142	0.07003916

VITA

Amy Mechel Johnson was born on December 31, 1972 in Fairmont, WV. At age eleven she moved with her family to Lewisburg, WV, the place she will always call home. In May, 1995 she graduated from Concord College, Athens, WV with a Bachelor of Science degree in Comprehensive Chemistry. The following August she completed the requirements for a minor in Geology at the same college. During her study at Virginia Tech she took six weeks to study abroad at the University of Reykjavík, Iceland during their 1997 Summer Program in association with the University of Minnesota. Her future plans include moving to the Pacific Northwest, one of the few places in the US where she could find volcanoes and glaciers.